LANDSCAPE-BASED HYDROLOGICAL MODELLING

UNDERSTANDING THE INFLUENCE OF CLIMATE, TOPOGRAPHY, AND VEGETATION ON CATCHMENT HYDROLOGY

LANDSCAPE-BASED HYDROLOGICAL MODELLING

UNDERSTANDING THE INFLUENCE OF CLIMATE, TOPOGRAPHY, AND VEGETATION ON CATCHMENT HYDROLOGY

Proefschrift

ter verkrijging van de graad van doctor
aan de Technische Universiteit Delft,
op gezag van de Rector Magnificus prof. ir. K. C. A. M. Luyben,
voorzitter van het College voor Promoties,
in het openbaar te verdedigen op maandag 15 juni 2015 om 10:00 uur

door

Hongkai GAO

Master of Sciences in Physical Geography (Cold and Arid Environmental and Engineering Research Institute), Chinese Academy of Sciences.
geboren te Henan, China.

Dit proefschrift is goedgekeurd door de promotor:

Prof. dr. ir. H. H. G. Savenije

Copromotor: Dr. M. Hrachowitz

Samenstelling promotiecommissie:

Rector Magnificus,	voorzitter
Prof. dr. ir. H. H. G. Savenije,	Technische Universiteit Delft, promotor
Prof. dr. V. Andréassian,	Irstea, France
Prof. dr. W. G. M. Bastiaanssen,	UNESCO-IHE & Technische Universiteit Delft
Prof. dr. S. Uhlenbrook,	UNESCO-IHE & Technische Universiteit Delft
Prof. dr. Z. Su,	Universiteit Twente
Prof. dr. M. Bierkens,	Universiteit Utrecht
Dr. F. Fenicia,	Eawag, Switzerland
Prof. dr. ir. N. C. van de Giesen,	Technische Universiteit Delft, reservelid

Keywords: root zone storage capacity, FLEX-Topo, model transferablity, parameter regionalization, glacier and snow hydrology, Heihe River, Ping River, Urumqi River

Printed by: Ipskamp Drukkers

Front & Back: Designed by Lei Fu.

Copyright © 2015 by H. Gao

ISBN 978-94-6259-724-2

An electronic version of this dissertation is available at
http://repository.tudelft.nl/.

To my beloved family

PREFACE

When I started my academic career as a master student in the Chinese Academy of Sciences, my grandfather asked me two questions: what are you going to research? How can we use your research results? Actually, I was doing some research related to climate change and glacier hydrology, which is far from having direct practical implications. After I did answer, I could see my grandpa's confusion and disappointment from his face. These two questions illustrate the reservations of people outside hydrology. It was very hard to convince an old man, who had suffered the famine in Mao's time, to accept the idea of investing huge amounts of money and efforts to produce nothing visible except for paper.

After seven years of research, I hope I can partly answer my grandpa's two questions, and convince myself and probably make it clearer to the public what I did and why I did it.

What did I do? In this thesis, a new rainfall-runoff model has been developed. This modelling framework is based on landscape information. In previous studies, models were either too simple to include catchment heterogeneity, or too complicated to be validated, leading to large model uncertainty. Our model is a middle way to include the appropriate level of heterogeneity, simultaneously avoiding to get lost in the non-homogenous data ocean. We found that climate, topography and vegetation have a dominant influence on hydrological processes. After properly accounting this information, we could transfer a hydrological model from one catchment to another without recalibration.

Why did I do that? Improving our understanding of water balance and fluxes at catchment scale is the target of this thesis. It is not necessary to stress the importance of water for human beings and ecosystems. Too much water (flood), lack of water (drought), or poor water quality (pollution) are all linked to serious disasters. A hydrological model is an indispensable tool to forecast rainfall-runoff in practice. From engineering point of view, we need a hydrological model to forecast floods or droughts, to do water resources management, and to predict hydrography in ungauged basins. From a scientific point of view, it is not sufficient to calibrate model parameters to fit hydrographs. Parameter calibration cannot generate new knowledge or help us to understand hydrological processes. Scientifically, models represent our integrated and systematic knowledge of catchment hydrology. How we simulate hydrological processes and create a model is highly related to our point of view. For example, if we intend to study the galaxy, we should use a telescope. Contrarily, if we want to study an atom, a microscope is more useful than a telescope, for sure. Similarly, if a catchment is the object of our study, we should view the catchment as a giant and not as an ant [Savenije, 2009]. Landscapes, from a giant point of view, are the proper scale to study catchments. Viewing and modelling a catchment's hydrological processes from a different angle is the motivation and innovation of this study.

What and why are two most fundamental questions, which I always asked myself during my PhD research. I would say this thesis is only the start of my career to pursue the answers to these two basic questions, not the end. And I am convinced that this is not a bad start, because I feel I am on the right track.

Hongkai GAO
Delft, March 2015

CONTENTS

1

INTRODUCTION

Always ask the basic questions.

Hubert Savenije

1.1. LANDSCAPE AND CATCHMENT HYDROLOGY

Landscape refers to the visible features of an area of land (New Oxford American Dictionary). Natural landscapes are defined on the basis of climate, topography, vegetation and geology [Mücher et al., 2010]. Combinations and variations of fundamental landscape elements constitute the diverse land surface, which crucially influence surface water hydrology, groundwater hydrology, and their interaction [Winter, 2001]. Investigating hydrology (referred to as catchment hydrology hereafter) in the context of landscapes enable us to understand water movement over and through different terrain against of other earth sciences.

1.1.1. CLIMATE AND HYDROLOGY

Climate, to some extent, determines catchment hydrology. Firstly and most importantly, as the start of rainfall(snow/ice melt)-runoff processes, the quantity, tempo-spatial distribution and phase of precipitation have a primary impact on catchment hydrology [Beven, 2012].

Secondly, climate determines the accessible energy for evaporation, which consumes most part (60-65%) of terrestrial precipitation [Bengtsson, 2010; Seneviratne et al., 2010]. The surface net radiation is mainly partitioned into sensible heat and latent heat fluxes. Latent heat, in the form of evaporation, consumes 50-60% of net radiation globally [Seneviratne et al., 2013]. Therefore, coupling the global energy and water cycle is the frontier in climate and hydrologic studies [Trenberth et al., 2009], e.g. the GEWEX (Global Energy and Water Exchanges) project.

To systematically understand the interaction between climate and hydrology, Budyko and Miller [1974] proposed an empirical relationship describing the interaction between

water and energy at catchment scale, which can be used to estimate actual evaporation based on precipitation and energy input [Fuh, 1981]. It shows that a catchment's climate condition (E_0/P), primarily determines actual evaporation (E_a), and runoff (Q), although depending on landscape characteristics such as vegetation and topography as well [Zhang et al., 2001]. We can even draw the conclusion that hydrology is a product of climate from global and continental scale in long time series, or safely address that climate is the primary determining factor for hydrology.

1.1.2. TOPOGRAPHY AND HYDROLOGY

In most cases, the boundary of a catchment is delineated by surface topography, simply because a catchment is the area collecting rainfall. In addition, the local micrometeorology, especially the energy and precipitation, is highly influenced by topography [Barry, 2013]. Therefore, the dependence of precipitation and energy on topography, as essential forcing data of catchment hydrology, is not negligible. Moreover, topography determines the flow gradient and momentum, and hence water movement and drainage [Freeze and Harlan, 1969]. Besides, topography determines the distribution pattern of a drainage system [Costa-Cabral and Burges, 1994], which strongly influences runoff generation and flow convergence [Rodríguez-Iturbe and Valdés, 1979]. Furthermore, topography determines the different runoff generation mechanisms at different locations [Savenije, 2010]. Significant differences in hydrological function, for example between riparian area and hillslope, is well documented by a wide range of experimental studies [e.g. McGlynn and McDonnell, 2003; Seibert et al., 2003; Molenat et al., 2008; Jencso et al., 2009; Detty and McGuire, 2010]. Additionally, the distribution of other landscape components, such as vegetation and soil, are interrelated with topography [Tromp-van Meerveld and McDonnell, 2006; Savenije, 2010; Gao et al., 2014a]. Therefore, topography could be an integrated indicator for other landscape factors.

1.1.3. VEGETATION AND HYDROLOGY

Interception and transpiration, both of which are primarily determined by vegetation cover, are the two most substantial types of evaporation. Interception accounts for a large proportion of evaporation, even above 50% in arid regions [Savenije, 2004]. Transpiration dominates global terrestrial evaporation [Jasechko et al., 2013], although with large uncertainty [Coenders-Gerrits et al., 2014]. Since 65% of terrestrial precipitation returns to the atmosphere by evaporation [Seneviratne et al., 2010], this indicates that vegetation plays a crucial role in the hydrological cycle. Vegetation has also great influences on runoff generation. The macro-pores generated by root channels and other biologically induced macropores are key to preferential flow, which is one of the dominant runoff generation mechanisms [Beven and Germann, 1982; Uhlenbrook, 2006]. Also, vegetation plays an essential role in soil formation, and hence infiltration capacity [Dunne et al., 1991]. Vegetation even impacts on groundwater fluctuation in arid/semi-arid regions [Wang and Pozdniakov, 2014]. In the long-term water balance, vegetation characteristics influence the Budyko curve, more specifically a denser vegetation cover corresponds with higher evaporation efficiency (E_a/E_0) in the same climate condition [Yang et al., 2009].

1.1.4. OTHER FACTORS AFFECTING HYDROLOGY

There are clearly other factors that may influence the hydrological behaviour of a catchment. For example, Fenicia et al. [2014] advocated that geology was mainly responsible for the contrasting behaviour of three neighbouring catchments in Luxembourg. Geology intensely impacts on aquifer characteristics and hence hydrograph recession [Tague and Grant, 2004]. However, it is relatively easier to derive the aquifer information from hydrography [Troch et al., 2013]. Therefore, we retained this research for further researches.

Soil texture (proportion of sand silt and clay) is regarded as important input information for numerous hydrological models. For instance, a physical-based model, such as SHE [Abbott and Refsgaard, 1996], derives the soil porosity and hydraulic conductivity from soil texture [Saxton et al., 1986]. It then calculates the water movement based on Darcy's law and Richard's equation [Freeze and Harlan, 1969]. However, numerous studies criticized the arbitrary upscaling of physical laws from soil column scale to hillslope and catchment scale [Beven, 2002]. Alternatively, conceptual models, such as SWAT [Arnold and Fohrer, 2005], link soil texture with root zone storage capacity. However, we argue that the root zone storage capacity and its spatial distribution, which strongly impact runoff generation and evaporation, is primarily determined by the precipitation pattern (climate) and the water demand of ecosystems (climate and phenology), and independent of soil texture [Gao et al., 2014b]. Therefore, we did not explicitly include the influence of soils on model structure and model parameters in this thesis.

1.2. WHY A LANDSCAPE-BASED MODEL?

A model reflects the modeler's knowledge and understanding of hydrological processes [Beven, 2001; Savenije, 2009; Fenicia et al., 2011]. From this point of view, all models are conceptual models. The concepts of catchment hydrology are highly relevant to the perspective of modelers. From the ants' point of view, ants see tremendous heterogeneity. In contrast, from outer space, astronauts may view a catchment as a point. Our proposed landscape-based model is viewing a catchment at meso-scale as a giant. In this case, we do not need to take all detailed heterogeneity into account, but retain the most remarkable patterns of heterogeneity.

Zoom out from the soil column (compare with a distributed model)

What will a giant see in a catchment? The detailed soil texture? Probably not. A giant most probably sees the landscapes. Traditional physical-based distributed models apply partial differential equations [Freeze and Harlan, 1969] to describe the water movement based on pressure gradients obtained by topography and conductivity derived from soil texture. In practical implementation, a study catchment is discretized into different cells, where the water movement is calculated between these cells. Distributed models can give us detailed information, but as previously mentioned, it has been criticized for arbitrary upscaling and the high computational costs. More importantly, this type of models loses the pattern inherent in landscapes at catchment scale [Sivapalan, 2005].

Landscape heterogeneity (compare with a lumped model)

Lumped models partition rainfall into infiltration and runoff based on conceptualized soil moisture condition. Lumped models are simple and have low computational cost. However, the simulated results are lumped and impossible to be mapped back,

which hinders its further detailed validation. This also hampers our understanding of catchment hydrological processes. And more importantly, without considering heterogeneity, we cannot upscale or transfer a model structure and its optimized parameters to other catchments, even neighborhood catchments [Blöschl et al., 2013; Hrachowitz et al., 2013b]. Therefore, recalibrating a lumped model based on rainfall-runoff data before implementing is always necessary.

Landscape-based model is a middle way [Savenije, 2010].

Climate, vegetation, topography and geology are essential components of natural landscapes [Mücher et al., 2010]. Different combinations of different components generate different landscapes. A landscape-based model is a middle way between simple lumped models, and complicated distributed models. It can represent the most remarkable catchment heterogeneity, while retaining the hydrological pattern at catchment scale. Moreover, it is easier to incorporate expert knowledge into this type of model, which makes the model robust and consistent [Gharari et al., 2014; Hrachowitz et al., 2014]. Finally, landscape-based models are helpful to bridge the gap between modelers and experimentalists [Seibert and McDonnell, 2002].

Landscapes are easily observable

Additionally, landscapes are easy to be observed in a field survey. Remote sensing is another approach of observing catchments as a giant. With the development of remote sensing techniques, we can observe various kinds of hydrology related information [Bastiaanssen et al., 2012; Duan and Bastiaanssen, 2013], such as landscapes (topography, vegetation, water body, snow and ice), precipitation, energy budget components, groundwater storage variation, and surface soil moisture. These data sets are crucial complementary information for calibrating and validating our simulated hydrology related output [Tang et al., 2009; Winsemius et al., 2009].

Practical usage (landscape change)

Influenced by human behavior and climate change, landscapes are experiencing significant disturbance, such as wildfires, deforestation, reforestation and land use change [Hansen et al., 2013]. These landscape changes affect catchment hydrological behavior and water resources [Montanari et al., 2013]. Therefore, in practice there is an urgent need to develop landscape-based hydrological models to predict the possible influences of landscape changes on hydrological processes to support the decision making on water resources and land use [Savenije et al., 2014].

1.3. WHY FLEX-TOPO?

Although the interconnection between landscapes and hydrology has been studied and documented before, systematical introduction of involving this type of information in a hydrological model is still underexploited. Previous semi-distributed model attempted to take heterogeneity into account as well. Various approaches were applied to discretize catchments, such as the Fundamental Hydrologic Landscape Unit (FHLU) [Winter, 2001], the Representative Elementary Watershed (REW) [Reggiani et al., 2000; Zhang and Savenije, 2005], Hydrological Response Units (HRUs, i.e. SWAT) [Flügel, 1996; Arnold and Fohrer, 2005], topography and landscapes [Beven and Kirkby, 1979; Beven, 2001]. However, with too much available information (such as soil, vegetation and slope information in SWAT), the HRU type models have 'degenerated to a GIS-clipping exercise' in

many case studies [Zehe et al., 2014]. Real hydrological processes were not fully considered and reflected in a model structure.

Comparing with other types of semi-distributed models, the innovations of the landscape-based FLEX-Topo model are:

1 The hypothesis of the FLEX-Topo model is the landscapes are a result of co-evolution of climate, topography, vegetation and geology. Therefore, it is possible to use one or two factors as integrated indicators to represent the catchment heterogeneity, instead of taking all heterogeneity into account;

2 Topography determines dominant runoff generation mechanism in different locations, especially the relative elevation (the height above the nearest drainage, HAND). Different runoff generation mechanisms are represented by different model structures, such as saturated overland flow in riparian areas and subsurface storm flow on hillslopes;

3 The root zone storage capacity ($S_{u,max}$), an essential parameter to partition precipitation into infiltration, transpiration, and runoff, rather than being linked to soil texture in other models, is hypothesized and validated to be mainly impacted by climate and vegetation. This finding simplifies the regionalization of this parameter. More importantly, it makes this parameter part of a living organism, while may change with land cover and climate change.

4 Different landscapes are modelled in parallel, only connected by groundwater and the drainage network. This parallel model structure does not only simplify our simulation, it is also very likely closer to reality. Specifically, there is no doubt that saturated overland flow is the dominant runoff generation mechanism on wetlands. Likewise the saturated area on wetlands does not expand into hillslope and trigger runoff generation on hillslopes. Contrarily, runoff generation on hillslopes is determined by local connectivity, independent of wetland soil moisture. On plateaus, the rainfall mainly infiltrates and recharges the groundwater, which is isolated from the other two landscapes. Parallel modelling allows the introduction of parameter constraints between landscape classes. Based on hydrological realism and expert knowledge, additional parameter constraints, related to the comparison between landscapes elements, reduced the degree of freedom during calibration.

5 The number of parameters in FLEX-Topo is rigorously restricted to reduce parameter equifinality.

1.4. OUTLINE OF THE THESIS

In this chapter, we briefly introduced the background of landscape-based modelling, and the outline of this thesis. The main results of the present thesis is divided into five parts:

The Second Chapter presents how climate controls the root zone storage capacity at catchment scale. The theory was tested in over 300 catchments in Thailand and the United Sates.

The Third Chapter focuses on testing the realism of the landscape-based hydrological model (FLEX-Topo) in the upper Heihe River basin, in China, to understand the influence of topography on hydrological processes and natural vegetation cover.

The Fourth Chapter demonstrates the powerful transferability of hydrological models after considering vegetation or topographic information in the upper Ping River basin in Thailand.

In the Fifth Chapter, we extend the FLEX-Topo modelling framework to a highly glacierized catchment in northwest China. Topography and glacier cover information have been included to simulate snow and glacier melt.

In the Sixth Chapter, we summarize the main results from this thesis and provide some perspective for further research.

2

CLIMATE CONTROLS HOW ECOSYSTEMS SIZE THE ROOT ZONE STORAGE CAPACITY AT CATCHMENT SCALE

The root zone moisture storage capacity (S_R) of terrestrial ecosystems is a buffer providing vegetation continuous access to water and a critical factor controlling land-atmospheric moisture exchange, hydrological response and biogeochemical processes. However, it is impossible to observe directly at catchment scale. Here, using data from 300 diverse catchments, it was tested that, treating the root zone as a reservoir, the mass curve technique (MCT), an engineering method for reservoir design, can be used to estimate catchment-scale S_R from effective rainfall and plant transpiration. Supporting the initial hypothesis, it was found that MCT-derived S_R coincided with model-derived estimates. These estimates of parameter S_R can be used to constrain hydrological, climate and land surface models. Further, the study provides evidence that ecosystems dynamically design their root systems to bridge droughts with return periods of 10-40 years, controlled by climate and linked to aridity index, inter-storm duration, seasonality and runoff ratio.

This chapter is based on:
Gao, H., Hrachowitz, M., Schymanski, S. J., Fenicia, F., Sriwongsitanon, N., and Savenije, H. H. G.: Climate controls how ecosystems size the root zone storage capacity at catchment scale, Geophysical Research Letters, 10.1002/2014GL061668, 2014.

2.1. INTRODUCTION

The critical influence of vegetation on the water cycle was realized early [Bates, 1921; Horton, 1933] and is by now, together with its wider implications [Seneviratne et al., 2013], well acknowledged [Jenerette et al., 2012; Rodriguez-Iturbe, 2000; Thompson et al., 2011]. It is also understood that water and vegetation interact in a co-evolutionary system towards establishing equilibrium conditions between vegetation and moisture availability in water-limited environments [Donohue et al., 2007; Eagleson, 1978, 1982]. In other words, ecosystems tend to avoid water shortage [Eagleson, 1982; Schenk, 2008] and the associated negative effect on plants' carbon assimilation rates [Porporato et al., 2004]. There is empirical and theoretical evidence that they do so by designing root systems that allow for the most efficient extraction of water from the substrate, thereby meeting the canopy water demand (or transpiration) while minimizing their costs in terms of carbon expenditure for root growth and maintenance [Milly, 1994; Schymanski et al., 2008; Troch et al., 2009].

In spite of a generally good understanding of how ecosystems and hydrology are interlinked, little is known about the detailed mechanisms controlling these connections, leaving many factors involved difficult to quantify. This is in particular true for the water holding capacity, or the plant available water storage capacity in the root zone (S_R), which is a key parameter for ecosystem function [Milly, 1994; Rodriguez-Iturbe et al., 2007; Sayama et al., 2011]. It was suggested previously that changes in S_R directly affect runoff [Donohue et al., 2012], transpiration rates [Milly, 1994] as well as, through its influence on transpiration and thus on latent heat exchange, land surface temperatures [De Laat and Maurellis, 2006; Legates et al., 2010; Seneviratne et al., 2013] and thus the fundamental hydrological response characteristics of natural systems [Kleidon, 2004; Laio et al., 2001; Porporato et al., 2004]. In spite of the understanding that soils, and thus also S_R, are manifestations of the combined and co-evolving influences of climate, biota and geology [van Breemen, 1993; Phillips, 2009], S_R was in the past mostly estimated from soil characteristics or rooting depths [Saxton and Rawls, 2006; Huang et al., 2013], disregarding the importance of climate. Thus an approach to quantify S_R accounting for feedback among the system components, will facilitate a better understanding of how much sub-surface water can be accessed by root systems and is key for efficiently constraining hydrological and ecological predictions.

2.2. HYPOTHESIS

Both, ecosystems and humans, need continuous access to water, requiring a buffer to balance the high variability of hydrological fluxes in the natural system. Where humans design reservoirs to store water to do so, ecosystems dimension their root zones. A classical engineering method for designing the size of reservoirs is the mass curve technique (MCT; Figure 2.1) and refinements thereof [Hazen, 1914; Klemeš, 1997; Rippl, 1883]. Using this technique, the reservoir size is estimated as a function of water demand, water input and the length of dry periods. These factors show a striking resemblance with those that have been reported to control S_R: potential evaporation, precipitation, interstorm duration and seasonality [Gentine et al., 2012; Milly, 1994]. Given these similarities and treating the root zone as a reservoir, we tested the hypothesis that the MCT

can be used to estimate S_R at the catchment scale, independently of point-scale root or soil observations, exclusively based on climate data (inflow and water demand) and to thereby establish a direct and quantifiable link between climate, ecosystem and hydrology. Note that a catchment can consist of several ecosystems. Hereafter, however, S_R of an ecosystem describes the integrated value of S_R for all ecosystems in a catchment.

2.3. METHODS

2.3.1. ESTIMATION OF ROOT ZONE STORAGE CAPACITY (S_R)

MASS CURVE TECHNIQUE (MCT)

The MCT is a method to estimate the reservoir storage based on the relationship between cumulative inflow and water demand (Figure 2.1a). To estimate S_R (Figure 2.1b) firstly the average annual plant water demand E_{ta} is determined from $E_{ta} = P_e - Q$, with $P_e = P - E_i$, where P_e is the cumulative inflow, P is precipitation, E_i is interception and Q is runoff. Then water demand in dry seasons (E_{td}) is estimated using a linear relationship between E_{ta}/E_{td} and the ratio of annual average to dry season average Normalized Difference Vegetation Index, i.e. $NDVI_a/NDVI_d$, assuming that transpiration is linearly related to the vegetation index and incoming radiation while being constrained by soil moisture [Wang et al., 2007]. Finally, P_e is plotted together with E_{td}. The required S_R for each year is estimated based on the periods where the rate of water demand exceeds inflow (Figure 2.1). In other words, the vertical distance between the tangents to the accumulated P_e, parallel to E_{td}, at the beginning and the end of dry seasons yields the estimated S_R of that year (Figure 2.1b).

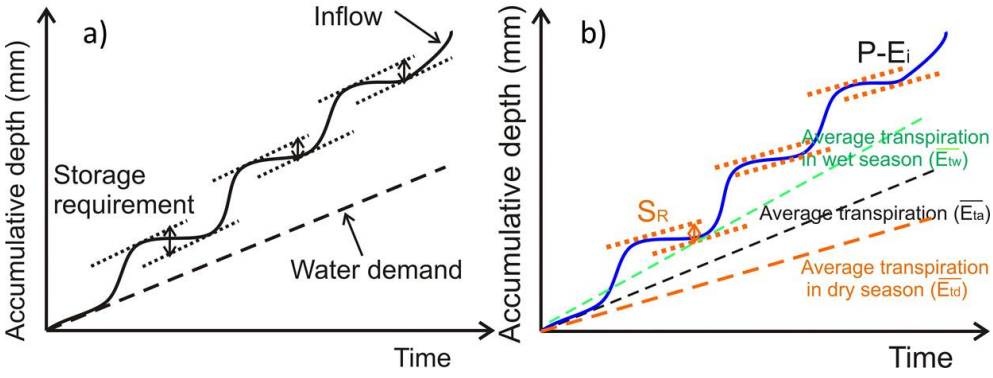

Figure 2.1: a) Mass Curve Technique (MCT) diagram, used to design the required storage of reservoirs to meet a given water demand. The inflow is accumulated in time and the storage requirement for each year is defined by the vertical distance between the tangents at the start and at the end of each dry season, where the tangent slope is determined by the water demand. When the slope of the inflow curve is steeper than the slope of the demand line, storage is increasing, when the slope is less steep, demand is depleting storage; b) application of the MCT to determine root zone storage capacity S_R ($\overline{E_{ta}}$: long-term mean transpiration; $\overline{E_{tw}}$: long-term mean wet season transpiration; $\overline{E_{td}}$: long-term mean dry season transpiration). The mean dry season determines the water demand.

FREQUENCY ANALYSIS

The Gumbel distribution [Gumbel, 1935], frequently used for estimating hydrological extremes, was used to standardize the frequency of drought occurrence (Figure 2.5). Here, Gumbel uses the reduced variate y as a function of the return period T of annual S_R estimates ($y = -\ln(-\ln(1-1/T))$). Being a linear relationship, this allows the estimation of the S_R required to overcome droughts with certain return periods, such as droughts with return periods of 10, 20 and 40 years (S_{R10y}, S_{R20y}, S_{R40y}).

2.3.2. ROOT ZONE STORAGE CAPACITY FROM HYDROLOGICAL MODELS ($S_{U,MAX}$)

To test the MCT-derived values of S_R for plausibility, a conceptual hydrological model was used to independently estimate the root zone storage capacity. It was developed based on the FLEX framework [Fenicia et al., 2008b]. As for most hydrological models its core is a dynamic buffer that moderates flows and retains tension water for plant use, essentially reflecting S_R [Zhao and Liu, 1995; Fenicia et al., 2008b]. Here, the tension water storage capacity function of the Xinanjiang model [Zhao and Liu, 1995], controlled by parameter $S_{u,max}$ was adopted. The MOSCEM-UA [Vrugt et al., 2003] algorithm was used for a multi-objective model calibration, based on the Kling-Gupta efficiency (I_{KGE}) [Gupta et al., 2009] of flow, logarithmic flow and the flow duration curve. All pareto-optimal parameter sets were retained as feasible and used for further analysis (in Figure 2.5 2.6g only the median values of $S_{u,max}$ are shown for clarity). The description of the model is available in Table 2.1 and the caption of Figure 2.2. The MCT-derived S_R was then evaluated against the model-derived values of $S_{u,max}$.

Table 2.1: Water balance equations and constitutive equations for each reservoir in the FLEX model. See caption of Figure 2.2 for explanation.

Reservoirs	Water balance equations	Constructive equations
Interception	$\frac{dS_i}{dt} = P_l - E_i - P_{tf}$ (2.1)	$E_i = \begin{cases} E_p;\ S_i > 0 \\ 0;\ S_i = 0 \end{cases}$ (2.2) $P_{tf} = \begin{cases} 0;\ S_i < S_{i,max} \\ P_r;\ S_i = S_{i,max} \end{cases}$ (2.3)
Unsaturated reservoir	$\frac{dS_u}{dt} = P_e(1 - C_r) - E_a$ (2.4)	$E_a = (E_0 - E_i)\min\left(\frac{S_u}{S_{u,max}C_e}, 1\right)$ (2.5) $C_r = 1 - \left(1 - \frac{S_u}{S_{u,max}(1+\beta)}\right)^{\beta}$ (2.6) $R_u = P_e C_r$ (2.7)
Splitter and lag function		$R_f = R_u D$; (2.8) $R_s = R_u(1 - D)$ (2.9) $R_{fl}(t) = \sum_{i=1}^{T_{lag}} c(i) \cdot R_f(t - i + 1)$ (2.10) $c(i) = i / \sum_{u=1}^{T_{lag}} u$ (2.11)
Fast reservoir	$\frac{dS_f}{dt} = R_{fl} - Q_f$ (2.12)	$Q_f = S_f / K_f$ (2.13)
Slow reservoir	$\frac{dS_s}{dt} = R_s - Q_s$ (2.14)	$Q_s = S_s / K_s$ (2.15)

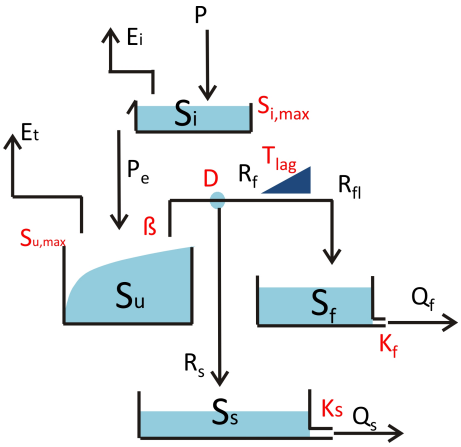

Figure 2.2: FLEX hydrological model structure. There are four reservoirs - the interception reservoir S_i (mm), the unsaturated reservoir S_u (mm), the fast response reservoir S_f (mm) and the slow response reservoir S_s (mm). Related water balance and constitutive equations are given in Table 2.1. Rainfall P (mm d^{-1}) is first partitioned between interception evaporation E_i (mm d^{-1}) and effective rainfall P_e (mm d^{-1}) based on a threshold $S_{i,max}$ (mm). Effective rainfall is partitioned between water retention in the soil and yield runoff R (mm d^{-1}), based on Su, the root zone storage capacity $S_{u,max}$ (mm) and a shape parameter β (-). Plant transpiration E_t (mm d^{-1}) is calculated based on potential evaporation E_0 (mm d^{-1}), a soil moisture threshold parameter C_e (-) and the relative soil moisture ($S_u/S_{u,max}$). The generated runoff is further partitioned between a fast component R_f (mm d^{-1}) and a slow component R_s (mm d^{-1}) through a separator D (-). A lag function is applied to simulate the lag time T_{lag} (d) between peak flow and storm event. Finally, two linear reservoirs with different time constants K_f (d) and K_s (d) are used to calculate the fast and slow runoff. The total runoff Q_m (mm d^{-1}) is the sum of the fast component Q_f (mm d^{-1}) and the slow component Q_s (mm d^{-1}).

2.4. DATA SETS

For an initial analysis, data from 6 catchments in Thailand, with catchment areas between 452 and 3858 km^2, were used (Figure 2.3; Table 2.2). These catchments are characterized by tropical savanna climate (Köppen-Geiger group Aw) with average annual precipitation and runoff of 1174 mm yr^{-1} and 268 mm yr^{-1}. Land use is dominated by evergreen and deciduous forest (Figure 2.3d). Further, data from 323 in the United States catchments, with areas between 67 and 10329 km^2, data records > 30 years and limited anthropogenic influence, available through the Model Parameter Estimation Experiment [Schaake et al., 2006] were used. MOPEX catchments with more than 20% of precipitation falling as snow were excluded from the analysis since neither the MCT nor the model account for snow dynamics. Likewise, catchments in very arid climates (I_A>2, $I_A = E_0/P$, E_0 is potential evaporation) were excluded as vegetation in such regions may favor different survival strategies such as increased water storage in the plants themselves. Catchment average precipitation was calculated with inverse distance weighting. Potential evaporation was estimated using the Hargreaves equation [Hargreaves and Samani, 1982]. The interception threshold E_i to estimate P_e was set to 2mm d^{-1}. Catchment average annual and dry season mean NDVI values were obtained from the MODIS13Q1 product (2002-2012; LP DAAC) by using the average of all cells within the

catchment over the required period.

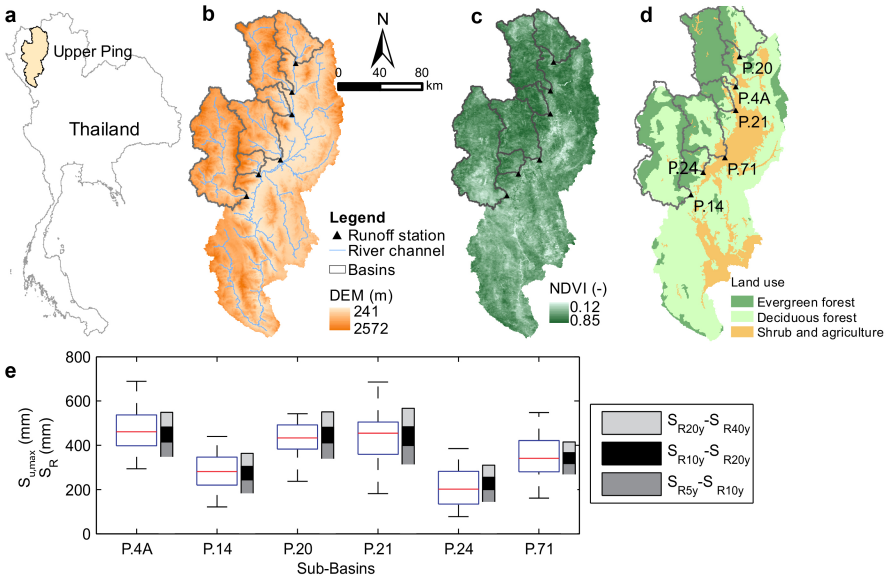

Figure 2.3: Upper Ping River catchment maps: (a) Context; (b) elevation; (c) average annual NDVI; (d) land use. (e) compares the values of MCT-derived S_R for different return periods (grey boxes) with the range of feasible calibrated values of $S_{u,max}$ from the hydrological model (red lines indicate the medians, boxes the 25/75th and whiskers the 5/95th quantiles).

Table 2.2: Basic information of the 6 sub-basins of the Upper Ping River basin

Catchment	Area (km^2)	Observation (period)	Average rainfall (mm/yr)	Average runoff (mm/yr)
P.4A	1902	1995-2005	1142	187
P.14	3853	1995-2005	1128	258
P.20	1355	1995-2005	1023	277
P.21	515	1995-2005	1029	229
P.24A	452	1995-2005	1043	290
P.71	1798	1996-2005	1088	161

Table 2.3: Simplified eco-region classification
[a] Simplified eco-region classification of the study catchments in the US, based on the CEC Level II Eco-regions together with the associated Köppen-Geiger climate groups and the predominant vegetation type in the study catchments. For clarity in the presentation, functionally similar regions were grouped together according to climate and vegetation considerations. Class 1 combines relatively low elevation regions with humid continental climates and deciduous forests, while Class 2 represents humid sub-tropical and oceanic climates at higher elevations. Class 3 combines the humid plains regions dominated by mixed forests. Classes 4 and 5 represent prairies, where Class 5 combines more arid prairie regions, with increasing influence of short grass prairie. Class 6 represents humid, mountainous regions with marked seasonality.
[b] Class 7 represents tropical forest (Thailand), characterized by relatively dry conditions and marked seasonality.

Class[a]	Name	CEC Level II Eco-regions	Köppen-Geiger climate groups	Predominant vegetation
1	Mixed Forest Region	5.2 Mixed wood shield 5.3 Atlantic highlands	Dfa, Dfb	Deciduous forest
2	Mountain Forest Region	8.1 Mixed wood plains 8.4 Ozark, Ouachita-Appalachian forests	Cfa, Cfb	Deciduous forest
3	Plains	8.2 Central USA plains 8.3 Southeastern USA plains 8.5 Mississippi alluvial and southeast USA coastal plains	Cfa, Dfa	Mixed forest
4	Temperate Prairies	9.2 Temperate prairies	Cfa, Dfa	Mixed grass prairie
5	Semi-arid Prairies	9.3 West-Central semi-arid prairies 9.4 South-Central semi-arid prairies	Bsk, Cfa, Dfa	Short and mixed grass prairie
6	Seasonal Western Region	6.2 Western Cordillera 7.1 Marine West coast forest	Csb	Coniferous forest, shrubland
7[b]	Tropical Forest	n.a.	Aw	Evergreen and deciduous forest

2.5. RESULTS AND DISCUSSIONS

Depending on dry season characteristics in individual years (Figure 2.4), the 6 Thai study catchments exhibited considerable fluctuations in MCT-derived S_R needed in the individual years to satisfy dry period plant water demand, with overall values across all 6 catchments from 100 mm to 450 mm (Figure 2.3e, 2.5). In the individual catchments the range between the minimum and the maximum values for annual S_R was on average 200 mm. To generalize these results, the required S_R for drought return periods of 5, 10, 20, 40, 60 and 100 years were estimated using the Gumbel distribution (Figure 2.5).

Calibrating the hydrological model to stream flow observations for these 6 study catchments showed that the ranges of calibrated $S_{u,max}$ correspond surprisingly well with the values of MCT-derived S_R (Figure 2.3e). In fact, values of S_R required to cover canopy water demand for droughts with return periods from 10 to 20 years coincided with the median of calibrated $S_{u,max}$ in each catchment, with some vegetation-related variation: the results suggest that catchments with higher values of annual catchment average NDVI (P.4A, NDVI = 0.69; P.21, NDVI = 0.70) and thus higher canopy water demand develop larger S_{R20y} of 447mm and 439 mm, respectively, than those with lower canopy water demand (P.14, NDVI = 0.64, S_{R20y} = 280mm; P.24, NDVI = 0.66, S_{R20y} = 219mm). In other words, ecosystems in these catchments have developed root zone that allow them to overcome droughts with return periods of 10-20 years. These results suggest that plants "design" their root-accessible water storage according to a cost minimization strategy [Milly, 1994], i.e. to meet canopy water demand with minimal carbon allocation to roots. It could be observed in these 6 catchments that ecosystems develop storage capacities S_R that are mainly controlled by atmospheric moisture supply and canopy demand dynamics, which supports earlier studies that documented the importance of canopy water demand and environmental conditions for S_R [Field et al., 1992; Milly, 1994; Gentine et al., 2012] and the hypothesis that ecosystems adapt their root

zones [Schenk, 2006] by lateral or vertical growth [Schenk and Jackson, 2002] to access the necessary soil water volume.

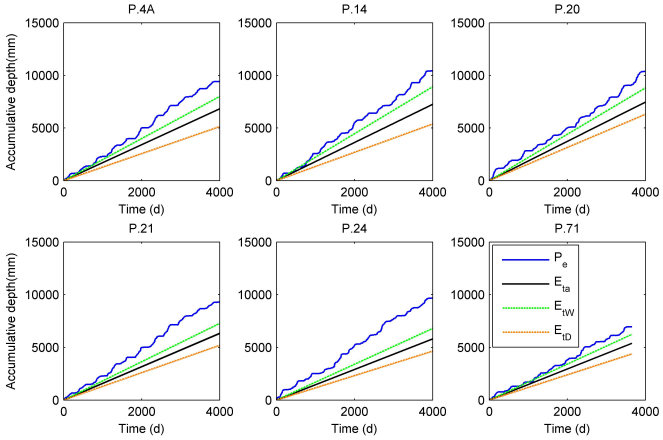

Figure 2.4: MCT plots for the 6 study catchments in Thailand, characterized by different water demand conditions ($\overline{E_{ta}}$: long-term mean water demand; $\overline{E_{tw}}$: long-term mean water demand in wet seasons; $\overline{E_{td}}$: long-term mean water demand in dry seasons)

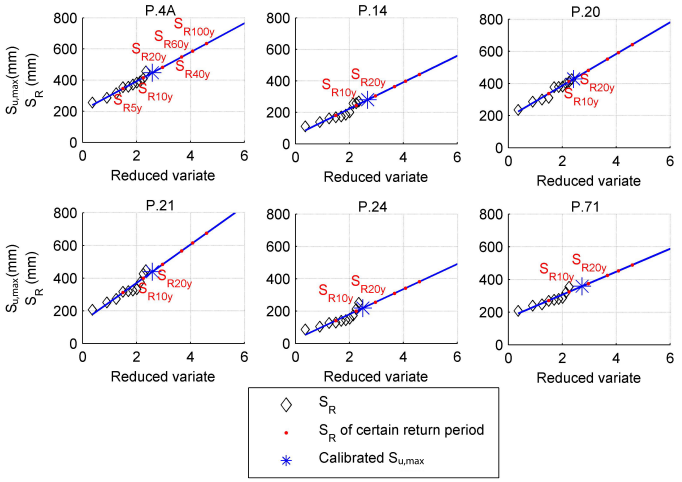

Figure 2.5: Root zone storage capacities S_R related to different drought return periods as estimated using the Gumbel distribution for the 6 study catchments in Thailand. Black diamonds indicate the annual S_R obtained by the MCT; red dots indicate different return periods of S_R; the blue stars indicate the medians of feasible $S_{u,max}$, based on all pareto-optimal values from the hydrological model.

The hypothesis of climate and canopy water demand being dominant controls on S_R and the existence of a link between S_R and $S_{u,max}$ was further tested by applying the same methodology as above to additional 323 very diverse catchments across the US. Based on all 329 study catchments (Thailand and US), statistically highly significant relationships between calibrated $S_{u,max}$ and MCT-derived S_R for drought return periods of 10-40 years (R^2_{10y} = 0.61, R^2_{20y}= 0.75, R^2_{40y}= 0.71; $p < 0.001$; Figure 2.6a-c) suggest that across the contrasting environmental conditions in these catchments, ecosystems design their S_R according to similar, simple, first order principles. Figure 2g displays the full range of $S_{R10y} - S_{R40y}$, compared to $S_{u,max}$ values for all study catchments, showing that the majority of catchments' $S_{u,max}$ plots within the $S_{R10y} - S_{R40y}$ range.

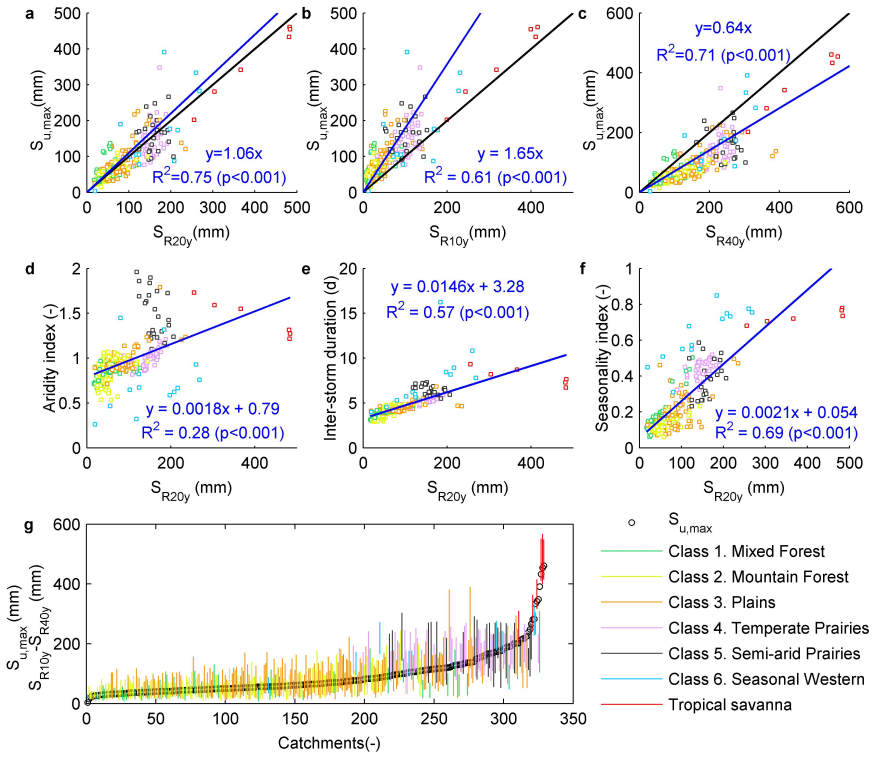

Figure 2.6: Relationships between S_R, $S_{u,max}$ and climate indices for the 329 study catchments. (a) $S_{u,max}$ vs. S_{R20y} (storage capacity with 20 years return periods); (b) $S_{u,max}$ vs. S_{R10y}; (c) $S_{u,max}$ vs. S_{R40y}; (d) S_{R20y} vs. aridity index (I_A); (e) S_{R20y} vs. inter-storm duration (I_{ISD}); (f) S_{R20y} vs. seasonality index (I_S); (g) $S_{u,max}$ (black circles) and ranges of S_R between 10 and 40 year return periods (S_{R10y}-S_{R40y}), sorted by increasing $S_{u,max}$. Colors indicate ecoregion classes, based on simplified CEC Level II ecoregions.

2.5.1. LINKS BETWEEN CLIMATE, VEGETATION AND S_R

The results indicate that at the catchment scale the plant available storage capacity is controlled by catchment wetness characteristics: when plotting S_{R20y} for the individual catchments against their respective aridity indices (I_A) ($R^2 = 0.28$; $p < 0.001$) or the mean inter-storm durations (I_{ISD}), a proxy for dry period durations ($R^2 = 0.57$; $p < 0.001$), it was found that the lowest S_R (< 100mm) are required in wet climates (Figure 2.6d) with shortest inter-storm durations (Figure 2.6e), while larger S_R are required in regions with higher aridity and longer dry period durations. Another determining factor for S_R was found to be the seasonality of precipitation. The higher the rainfall seasonality index ($\frac{1}{\overline{P_a}} \sum_{m=1}^{m=12} |\overline{P_m} - \frac{\overline{P_a}}{12}|$, where ($\overline{P_m}$)is the mean rainfall of month m, and ($\overline{P_a}$) is the mean annual rainfall), the larger a S_R is required ($R^2 = 0.69$; $p < 0.001$; Figure 2.6f). Stepwise multiple linear regression further showed that combining the three predictors I_S, I_A and I_{ISD} can explain 79% of the variance in S_{R20y} ($S_{R20y} = 218 I_S + 64 I_A + 5 I_{ISD} - 51$; $R^2_{adj} = 0.79$; $p < 0.001$; variance inflation factor < 4). Furthermore, the US study catchments were classified according to the CEC North American Level II ecoregions (Table 2.3; Figure 2.7a) [Wiken et al., 2011], with the 6 tropical catchments in Thailand constituting one additional class. Note that the CEC classification was simplified for clarity of the presentation, without overall impact on the interpretation. The classification indicates that, for example, in semi-arid Prairies (Table 2.3; Figure 2.7) dominated by seasonal short and mix-grass Prairie vegetation, S_{R20y} is around 150-200 mm, which is below the values of ~ 200-500 mm that would be expected for ecosystems with comparable aridity indices (I_A ~ 1-2) but dominated by evergreen plants as indicated by the regression line in Figure 2.6d. By going dormant during the dry season, thereby minimizing transpiration, such ecosystems only need to access sufficient moisture to reach maturity during the growing season. In contrast, the results also suggest that ecosystems in environments with marked seasonality and out of phase precipitation and energy supply, such as West-coast ecoregions (Table 2.3; Figure 2.7), require higher S_R than ecosystems with higher aridity indices in other climates (Figure 2.6d) to ensure sufficient access to water throughout the prolonged dry periods (Figure 2.6e). The here suggested concept of S_R is conceptually different from rooting depth, as it accounts for the volume of water accessible to roots and thus rather reflects the average root density in a catchment. It was however observed that patterns of S_R are broadly corresponding with observed rooting depths in previous studies. For example, some observations by Schenk and Jackson [2002] include that Tropical Savanna ecosystems are characterized by, on average, deepest rooting depths, with a median value of 1.2 m. Similarly, they report elevated root depths (0.8-2m) in Mediterranean climates as well as low and comparable root depths in temperate forests and grasslands. Our results (Figure 2.8) likewise suggest that the largest S_R are required in Tropical Savanna systems (~ 400 mm) and, although wetter than Mediterranean climates, in the Seasonal Western Region (~ 100-200 mm), while forests and grasslands (Classes 1-3) exhibit low and comparable S_R requirements.

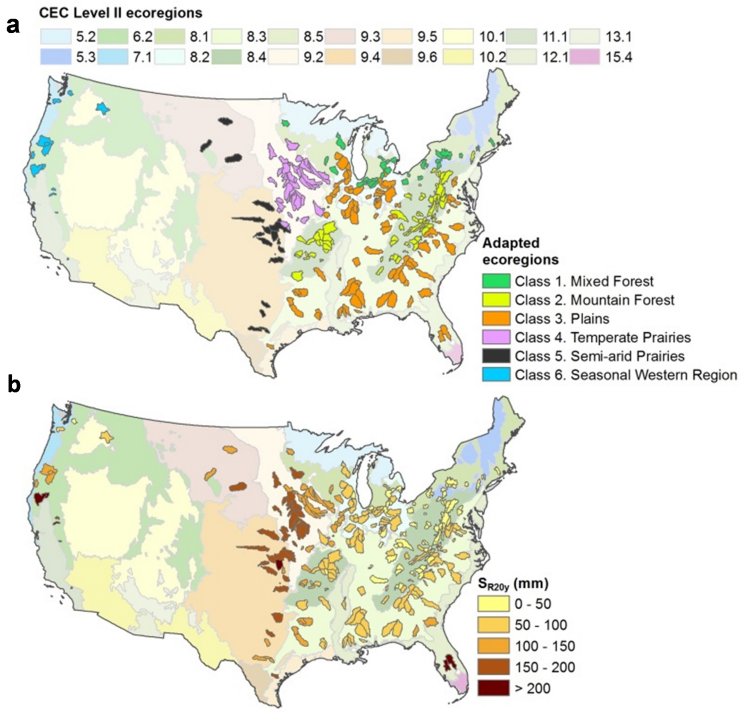

Figure 2.7: CEC North American Level II ecoregions in the US overlain by (a) the MOPEX study catchments classified based on the simplified CEC North American Level II ecoregions and (b) the S_{R20y} for the MOPEX study catchments. The horizontal color bar applies to the background in both figures, the individual vertical color bars apply to the catchments in the respective sub-panels.

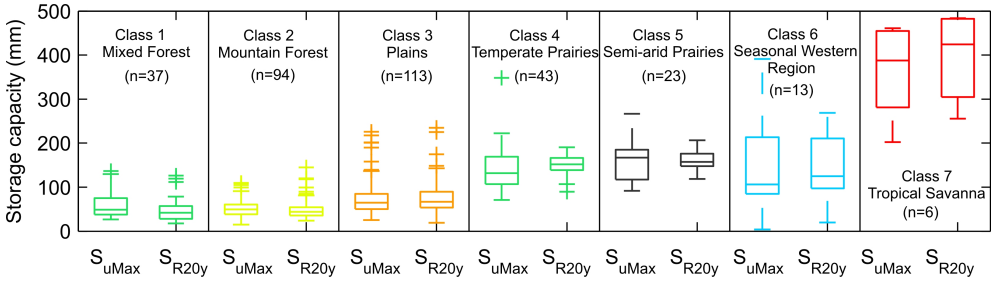

Figure 2.8: Distributions of $S_{u,max}$ and S_{R20y} in the 7 simplified ecoregion classes of the 329 study catchments.

2.5.2. IMPLICATIONS FOR THE HYDROLOGICAL RESPONSE AND BEYOND

Following these results, not only a spatial pattern of S_{R20y} across the US emerges, following the precipitation and evaporative energy supply gradients (Figure 2.7b), but it could also be shown that the long-term annual catchment runoff coefficient ($C_r = Q/P$)

exhibits a significant, negative correlation with S_{R20y} (R^2 = 0.48; $p < 0.001$; Figure 2.9). This suggests that flow partitioning into runoff and evaporative fluxes, as shown in the Budyko framework [Budyko and Miller, 1974], is strongly controlled by S_R [Gentine et al., 2012]. While humid catchments are characterized by low S_R and high C_r, vegetation in more arid catchments requires a higher S_R to store more water, resulting in lower C_r and thus in proportionally higher plant transpiration. This does not only underline the importance of S_R for understanding the hydrological response but it also emphasizes the role of co-evolution of vegetation and hydrology. Furthermore, the positive correlation between S_{R20y} and rainfall seasonality implies a certain buffering of seasonality effects on the runoff ratio, resulting in only small deviations of catchments from the Budyko curve despite differences in climatic seasonality [Williams et al., 2012].

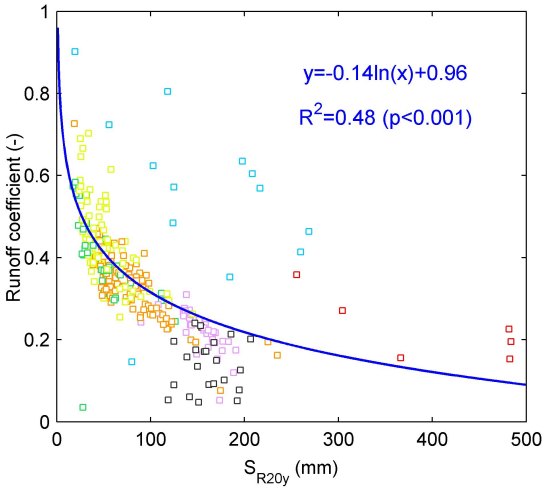

Figure 2.9: Relationship between S_{R20y} and the mean annual runoff coefficient for the 329 study catchments.

Limitations of MCT method include its dependence on the availability of water inflow and demand data. This restricts the possibility to estimate S_R for individual ecosystems or a grid-based spatial distribution within a catchment. Further, S_R estimates are currently based on constant water demand estimates and may benefit from allowing for seasonal variations. Additional research is also required to determine at which scales the method is applicable.

The root zone storage is the core of hydrological models as it controls the partitioning of available water for plant use and flow generation. The estimation of this parameter from independently observed data can reduce the number of calibration parameters and the associated parameter uncertainty in hydrological models, in particular for predictions in ungauged basins [Blöschl et al., 2013; Hrachowitz et al., 2013b]. Similarly, estimates of S_R, as a controlling factor of soil moisture, are potentially useful for a range

of geophysical applications: (1) in ecology, estimates of S_R may be valuable for understanding factors controlling primary production and growth as well as ecosystem development and survival strategies [Kolb et al., 1990; Briggs and Knapp, 1995; Breshears and Barnes, 1999]. (2) In land surface schemes and climate models [Dirmeyer, 2006; Niu et al., 2011; Seneviratne et al., 2013], estimates of S_R can help define land-atmosphere exchange processes of water and energy, thereby potentially improving the models' predictive ability. (3) S_R also plays a key role in biogeochemical studies. Controlling soil moisture dynamics and it establishes the physico-chemical environment for cycling of nutrients and solutes, such as nitrogen [Pastor and Post, 1986; Agehara and Warncke, 2005] or carbon [Howard and Howard, 1993; Kurc and Small, 2007]. Linking transport, plant uptake and chemical processes, S_R estimates may improve the understanding of these processes and their representation in models. (4) Through its link to vegetation and its influence on soil saturation and overland flow generation, S_R estimates may also prove beneficial for the understanding and quantification of erosion and mass movement processes [Seeger et al., 2004; Ray and Jacobs, 2007].

The dependency of S_R on climate and ecosystems/land cover further entails that S_R cannot be treated as static as it varies depending on changes in any of these. This potentially offers a simple way to account, to some extent, for a temporally evolving system, which is a step from Newtonian towards Darwinian modelling strategies [Harman and Troch, 2014; Harte, 2002; Hrachowitz et al., 2013b; Kumar and Ruddell, 2010].

2.6. CONCLUSIONS

Using data for more than 300 diverse catchments in Thailand and the US, the presented results support the hypothesis that, at catchment scale, ecosystems dynamically and optimally adjust their root systems to their environment [Milly, 1994; Kleidon and Heimann, 1998] in a way that the plant available water storage capacity is controlled by the precipitation regime, canopy water demand and land cover. It was shown that many ecosystems develop root systems that can tap sufficient water to overcome droughts with 10-40 year return periods but no more than that, as it is increasingly expensive in terms of carbon allocation to roots. It was shown that the root zone storage capacity can be calculated, independent of point-scale observations, using a simple, water-balance based method. The results strongly highlight the importance of the dynamic co-evolution of climate, ecosystems and hydrology. With this approach we have established a climate and land cover driven technique to estimate the storage capacity of the root zone at catchment scale, a crucial parameter of the water cycle at the interface of hydrological, ecological and atmospheric sciences.

3

THE INFLUENCE OF TOPOGRAPHY ON HYDROLOGICAL PROCESSES IN THE UPPER HEIHE RIVER, IN CHINA

Although elevation data are globally available and used in many existing hydrological models, their information content is still underexploited. Topography is closely related to geology, soil, climate and land cover. As a result, it may reflect the dominant hydrological processes in a catchment. In this study, we evaluated this hypothesis through four progressively more complex conceptual rainfall-runoff models. The first model ($FLEX^L$) is lumped, and it does not make use of elevation data. The second model ($FLEX^D$) is semi-distributed with different parameter sets for different units. This model uses elevation data indirectly, taking spatially variable drivers into account. The third model ($FLEX^{T0}$), also semi-distributed, makes explicit use of topography information. The structure of $FLEX^{T0}$ consists of four parallel components representing the distinct hydrological function of different landscape elements. These elements were determined based on a topography-based landscape classification approach. The fourth model ($FLEX^T$) has the same model structure and parameterization as $FLEX^{T0}$ but uses realism constraints on parameters and fluxes. All models have been calibrated and validated at the catchment outlet. Additionally, the models were evaluated at two sub-catchments. It was found that $FLEX^{T0}$ and $FLEX^T$ perform better than the other models in nested sub-catchment validation and they are therefore better spatially transferable. Among these two models, $FLEX^T$ performs better than $FLEX^{T0}$ in transferability. This supports the following hypotheses: (1) topog-

This chapter is based on:
Gao, H., Hrachowitz, M., Fenicia, F., Gharari, S., and Savenije, H. H. G.: Testing the realism of a topography-driven model (flex-topo) in the nested catchments of the upper heihe, china, Hydrology and Earth System Sciences, 18, 1895-1915, 10.5194/hess-18-1895-2014, 2014.

raphy can be used as an integrated indicator to distinguish between landscape elements with different hydrological functions; (2) FLEX^{T0} and FLEX^{T} are much better equipped to represent the heterogeneity of hydrological functions than a lumped or semi-distributed model, and hence they have a more realistic model structure and parameterization; (3) the soft data used to constrain the model parameters and fluxes in FLEX^{T} are useful for improving model transferability. Most of the precipitation on the forested hillslopes evaporates, thus generating relatively little runoff.

3.1. INTRODUCTION

Topography plays an important role in controlling hydrological processes at catchment scale [Savenije, 2010]. It may not only be a good first-order indicator of how water is routed through and released from a catchment [Knudsen et al., 1986], it also has considerable influence on the dominant hydrological processes in different parts of a catchment, which could be used to define hydrologically different response units [Savenije, 2010]. As an indicator for hydrological behaviour, topography is also linked to geology, soil characteristics, land cover and climate through co-evolution [Sivapalan, 2009; Savenije, 2010]. Thus, information on other features can to some extent be inferred from topography. However, the information provided by topography is generally underexploited in hydrological models although it is, explicitly or implicitly, incorporated in many models [e.g. Beven and Kirkby, 1979; Knudsen et al., 1986; Uhlenbrook et al., 2004].

As a typical lumped topography-driven model, TOPMODEL [Beven and Kirkby, 1979] uses the topographic wetness index (TWI) [Beven and Kirkby, 1979], which is a proxy for the probability of saturation of each point in a catchment, to consider the influence of topography on the occurrence of saturated overland flow (SOF). Similarly, the Xinanjiang model [Zhao, 1992] implicitly considers the influence of topography in its soil moisture function, as the curve of its tension water capacity distribution can be interpreted as topographic heterogeneity. Conceptually, both models implicitly reflect the variable contributing area (VCA) concept. Although the topography-aided VCA representation is present in many models, experimental evidence has shown that its underlying assumptions may not always hold [Western et al., 1999; Spence and Woo, 2003; Tromp-van Meerveld and McDonnell, 2006]. In view of these limitations, and in spite of their often demonstrated suitability, there is an urgent need to explore new and potentially more generally applicable ways to incorporate topographic information in conceptual hydrological models.

Other types of topographically driven hydrological models are distributed physically based models, which use topography essentially to define flow gradients and flow paths of water [Refsgaard and Knudsen, 1996]. The limitations of this kind of "bottom-up" model approach include the increased computational cost, and maybe more importantly, the unaccounted scale effects [Abbott and Refsgaard, 1996; Beven, 2013; Hrachowitz et al., 2013a]. Knudsen et al. [1986] developed a semi-distributed, physically based model, which divides the whole catchment into several distinct hydrological response units defined by the catchment characteristics such as meteorological conditions, topography, vegetation and soil types. Although this type of model was shown to work well in case studies, approaches like this suffer from their intensive data requirement and complex model structure, similar to modelling approaches based on the dominant runoff process concept [Grayson and Blöschl, 2001; Scherrer and Naef, 2003]. The main problem with physically based models appears to be that by breaking up catchments into small interacting cells, patterns present in the landscape are broken up as well. The question is how to make use of landscape diversity, and the related hydrological processes, while maintaining the larger scale patterns and without introducing excessive complexity.

The recently suggested topography-driven conceptual modelling approach (FLEX-

Topo) [Savenije, 2010], which attempts to exploit topographic signatures to design conceptual model structures as a means to find the simplest way to represent the complexity and heterogeneity of hydrological processes, forms a middle way between parsimonious lumped and complex distributed models, and represents the subject of this study. In the framework of FLEX-Topo, topographic information is regarded as the main indicator of landscape classes and dominant hydrological processes. A valuable key for hydrologically meaningful landscape classification is the recently introduced metric HAND (Height Above the Nearest Drainage) [Rennó et al., 2008; Nobre et al., 2011; Gharari et al., 2011], which is a direct reflection of hydraulic head to the nearest drain. Consequently, within a flexible modelling framework [Fenicia et al., 2008b, 2011], different model structures can be developed to represent the different dominant hydrological processes in different landscape classes. Note that FLEX-Topo is not another conceptual model but rather a modelling framework to make more exhaustive use of topographic information in hydrological models and it can in principal be applied to any type of conceptual model.

Model transferability is one of the important indicators in testing model realism [Klemeš, 1986]. Although many hydrological models, both lumped and distributed, frequently perform well in calibration, transferring them and their parameter sets into other catchments, or even into nested sub-catchments, remains problematic [Pokhrel and Gupta, 2011]. There are several reasons for this: uncertainty in the data, insufficient information provided by the hydrograph or an unsuitable model structure which does not represent the dominant hydrological processes or their spatial heterogeneity sufficiently well [Gupta et al., 2008]. Various techniques to improve model transferability have been suggested in the past [Seibert and McDonnell, 2002; Uhlenbrook and Leibundgut, 2002; Khu et al., 2008; Hrachowitz et al., 2013b; Euser et al., 2013; Gharari et al., 2013], and it became clear that successful transferability critically depends on appropriate methods to link catchment characteristics to model structures and parameters or in other words to link catchment form to hydrological function [Gupta et al., 2008].

In this study, the FLEX-Topo modelling strategy [Savenije, 2010] is applied and tested with a tailor-made hydrological model for a cold, large river basin in north-west China. A lumped conceptual model with lumped input data ($FLEX^L$) and a semi-distributed model with semi-distributed input data and the different parameters for different units ($FLEX^D$) are used as benchmarks to assess the additional value of topography-driven semi-distributed modelling ($FLEX^{T0}$) and the value of soft data in constraining model behaviour ($FLEX^T$). The models are used as tools for testing different hypotheses within a flexible modelling framework [Fenicia et al., 2008b, 2011]. The objectives of this study are thus (1) to develop a topography-driven semi-distributed conceptual hydrological model ($FLEX^T$, $FLEX^{T0}$), based on topography-driven landscape classification and our understanding of the catchments, and to compare it to model set-ups with less process heterogeneity ($FLEX^L$, $FLEX^D$) and (2) to assess the differences in transferability of both model structures and parameters of the tested models to two uncalibrated nested sub-catchments in the study basin, thereby evaluating the predictive power and the realism of the individual model set-ups.

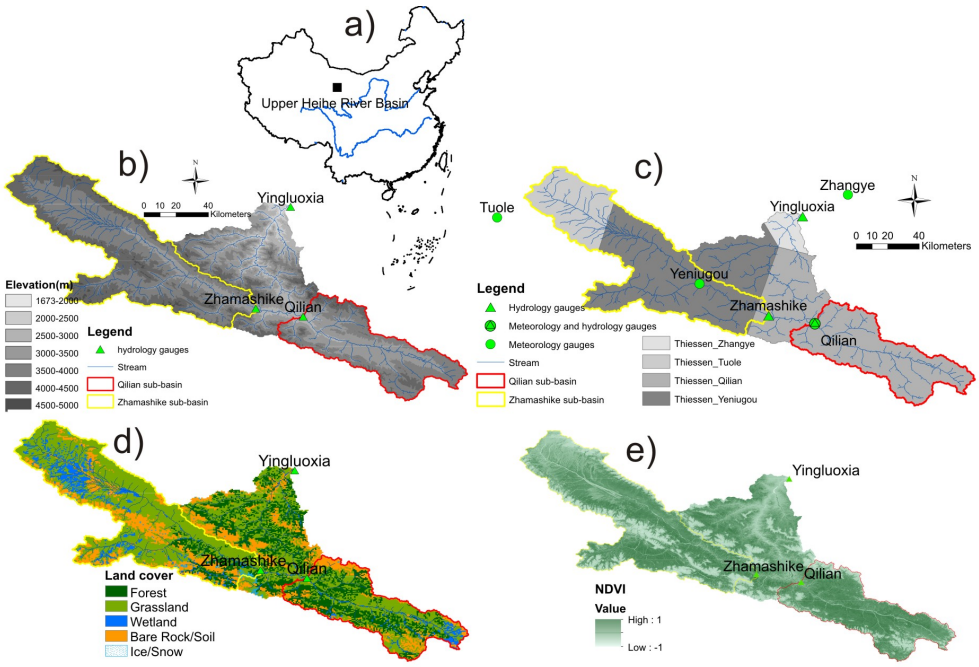

Figure 3.1: (a) location of the Upper Heihe in China; (b) DEM of the Upper Heihe with its runoff gauging stations, meteorological stations, streams and the outline of two sub-catchments; (c) meteorological stations and associated Thiessen polygons, the different grayscale indicates different long term annual average precipitation (the darker the more precipitation: Zhangye is 131 (mm/a); Tuole is 293 (mm/a); Qilian is 394 (mm/a); Yeniugou is 413(mm/a)); (d) land cover map of the Upper Heihe; (e) averaged NDVI map in the summer of 2002.

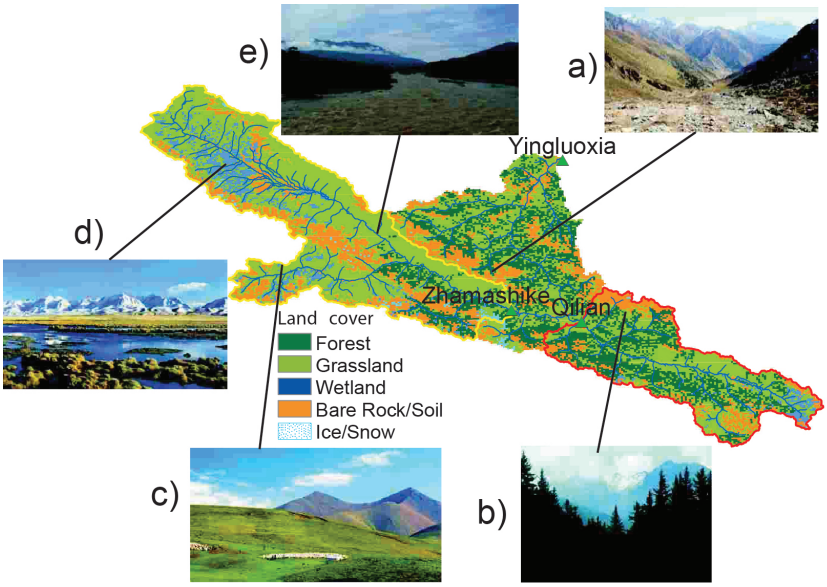

Figure 3.2: Characteristic landscapes in different locations in the Upper Heihe. **(a)** shows the bare-soil/rock-covered hillslope; **(b)** shows the forest-covered hillslope; **(c)** shows the grass-covered hillslope; **(d)** shows the wetland and terrace; **(e)** shows the muddy river.

3.2. STUDY SITE

The Upper Heihe River basin (referred to as Upper Heihe) is part of the second largest inland river in China which, from its source in the Qilian Mountains, drains into two lakes in the Gobi Desert. The Upper Heihe is located in the south-west of Qilian Mountain in north-western China (Figure 3.1a). It is gauged by the gauging station at Yingluoxia, with a catchment area of 10 000 km^2. Two sub-catchments are gauged separately by Zhamashike and Qilian (Figure 3.1b). The elevation of the Upper Heihe ranges from 1700 to 4900 m (Figure 3.1b). The mountainous headwaters, which are the main runoff-producing region and relatively undisturbed by human activities, are characterized by a cold desert climate. Long-term average annual precipitation and potential evaporation are about 430 and 520 mm a^{-1}. Over 80 % of the annual precipitation falls from May to September. Snow normally occurs in winter but with a limited snow depth, averaging between 4 and 7 mm a^{-1} of snow water equivalent for the whole catchment [Wang et al., 2010]. The Thiessen polygons of four meteorological stations in and around the Upper Heihe are shown in Figure 3.1c. The soil types are mostly mountain straw and grassland soil, cold desert, chernozemic soil and chestnut-coloured soil. Land cover in the Upper Heihe is composed of forest (20 %), grassland (52 %), bare rock or bare soil (19 %) and wetland (8 %), as well as ice and permanent snow (0.8 %) (Figure 3.1d).

The Upper Heihe has been the subject of intensive research since the 1980s [Li et al., 2009]. A number of hydrological models have been previously applied in this cold mountainous watershed [Kang et al., 2002; Xia et al., 2003; Chen et al., 2003; Zhou et al., 2008; Jia et al., 2009; Li et al., 2011; Zang et al., 2012]. Because of limited water resources and

Table 3.1: Summary of four the meteorological stations in and close to the Upper Heihe.

Meteorology Station	Elevation (m)	Latitude (°)	Longitude (°)	area ratio (%)	P (mm/a)	T (°C)	E_0 (mm/a)
Zhangye	1484	38.93	100.43	4	131	7.1	804
Yeniugou	3320	38.42	99.58	43	413	-3.2	392
Qilian	2788	38.18	100.25	40	394	0.8	513
Tuole	3368	38.80	98.42	13	293	-3.0	421

Table 3.2: Catchment characteristics of the entire Upper Heihe and two sub-catchments, Qilian and Zhamashike.

Runoff Station	Latitude (°)	Longitude (°)	Average Elevation (m)	Area (km^2)	Discharge (mm/a)
Yingluoxia (Upper Heihe)	38.80	100.17	3661	10,009	145
Qilian (East tributary)	38.19	100.24	3535	2,924	142
Zhamashike (West tributary)	38.23	99.98	3990	5,526	124

the increasing water demand of industry and agriculture, the conflict between human demand and ecological demand in the lowland parts of the Heihe River has become more and more severe. As the main runoff-producing region for the Heihe River, the Upper Heihe is thus essential for the water management of the whole river system.

3.2.1. THE LANDSCAPES AND THE PERCEPTUAL MODEL OF THE UPPER HEIHE

Figure3.1 illustrates different characteristic landscape elements in the Upper Heihe which were used to guide model development. Five characteristic landscapes can be identified in the Upper Heihe: bare-rock mountain peaks, forested hillslopes, grassland hillslopes, terraces and wetlands. Typically, above a certain elevation, the landscape is covered by bare soil/rock (Figure 3.2a) or permanent ice/snow. At lower elevations, north-facing hillslopes tend to be covered by forest (Figure 3.2b), while the bottom of hillslopes and south-facing hillslopes are, in contrast, dominantly covered by grass (Figure 3.2c). Terraces, which are irregularly flooded in wet periods and have comparably low terrain slopes, are mostly located between channels and hillslopes, and are typically covered by grassland (Figure 3.2d). Wetlands consist of meadows and open water, located in the bottom of the valleys (Figure 3.2d).

In this study, we separate landscapes based on their different hydrologic function. A wetland is a landscape element where groundwater come to the surface and where there is direct contact between the groundwater and the terrain. A hillslope is a landscape element that has sufficient slope for preferential flow to occur parallel to the surface. A plateau is a landscape element with a high HAND but insufficient slope to generate lateral preferential flow. Instead preferential flow in vertical, recharging groundwater. Lateral flow may occur when precipitation intensity exceeds the infiltration capacity. Terraces are landscape element with modest HAND and modest slope which can function

as wetland, hillslope or plateau depending on the moisture state.

This information was the basis for the development of a perceptual model of the Upper Heihe, which synthesizes our understanding of catchment hydrological behaviour. Typically, on bare soil/rock, interception can be considered negligible due to the absence of significant vegetation cover. The bare-soil/rock landscape at high elevations is further characterized by a thin soil layer, underlain by partly weathered bedrock, with higher permeable debris slopes at lower elevations. On the rock and the thin soil, the dominant lateral runoff processes are Hortonian overland flow (HOF) and SOF. Part of the localized overland flow may re-infiltrate, thereby feeding the debris slope and groundwater, while the rest of surface runoff, characterized by elevated sediment loads, is routed into streams. The picture of turbid water in a channel (Figure 3.2e), illustrates the presence of soil erosion, which is likely to be caused by HOF and SOF in the bare-soil/rock hillslopes. On the grass- and forest-covered hillslopes, subsurface storm flow (SSF) is considered to be the dominant hydrological process as a result of the presence of efficient subsurface drainage networks that were created by biological and geological activity, significantly influencing the hillslope runoff yield mechanism [Beven, 2013]. It can be expected that the forest-covered hillslopes are characterized by higher interception capacities and transpiration rates than the grassland hillslopes due to the larger leaf area index (LAI) and deeper root zone. Typically, the dominant hydrological process of wetlands and terraces is SOF due to the shallow groundwater levels and related limited additional storage capacity. For the same reason, evaporative fluxes in the wetlands can be assumed to be energy rather than moisture constrained and thus close to potential rates. Further, given the short distance to the channel network, the lag times for runoff generation in wetlands can be considered negligible on a daily timescale.

3.3. DATA

3.3.1. DATA SET

Meteorological data were available on a daily basis from four stations in and around the Upper Heihe (1959–1978), while daily runoff data were available for the main outlet of the basin at Yingluoxia (1959–1978) and two nested sub-catchments, Qilian (1967–1978) and Zhamashike (1959–1978). The meteorological data, as the forcing data of the hydrological models, included daily precipitation and daily mean air temperature. Because only data from four meteorological stations were available, the Thiessen polygon method (Figure 3.1c) was applied to spatially extrapolate precipitation and temperature. A summary of meteorological data is given in Table 3.1. The basic information of the three basins is listed in Table 3.2. Potential evaporation was estimated by the Hamon equation [Hamon, 1961], which is based on daily average temperature.

The 90 m × 90 m digital elevation model (DEM) of the study site (Figure 3.1b) was obtained from http://srtm.csi.cgiar.org/ and used to derive the local topographic indices HAND, slope and aspect. The normalized difference vegetation index (NDVI) map (Figure 3.1e) was derived from cloud-free Landsat Thematic Mapper (TM) maps in the summer of 2002, which were obtained from US Geological Survey EarthExplorer (http://earthexplorer.usgs.gov/). The land cover map (Figure 3.1d) was made available by the Environmental and Ecological Science Data Center for West China. The

pictures shown in Figure 3.2 as soft data were downloaded from Google Earth.

3.3.2. DISTRIBUTION OF FORCING DATA

The elevation of the Upper Heihe ranges from 1674 to 4918 m with only four meteorological stations in or around the catchment, covering an area of 10 000 km^2. In addition, the meteorological stations in the Upper Heihe River are all located at relatively low elevations in the valley bottoms, which are easily accessible for maintenance but potentially unrepresentative [Klemeš, 1990]. Precipitation and temperature data were thus adjusted using empirical relationships.

The entire catchment was thus first discretized into four parts by the Thiessen polygon method. Each Thiessen polygon was then further stratified into seven elevation zones with steps of 500 m. Annual precipitation (Equation 3.1) was assumed to increase linearly with elevation increase, according to empirical relationships for the region obtained from literature [Wang, 2009]:

$$P_{aj} = P_a + (h_j - h_0)\, C_{pa} \tag{3.1}$$

where P_a (mm a^{-1}) is the annual observed precipitation, P_{aj} (mm a^{-1}) is the annual extrapolated precipitation in elevation h_j (m), h_0 (m) is the elevation of the meteorological station and $C_{pa} = 0.115$ mm (m a)$^{-1}$ [Wang, 2009] is the precipitation lapse rate. However, Equation (3.1) is only suitable for annual precipitation extrapolation, but not suitable for daily precipitation because there are many days without precipitation within one year. Daily elevation-adjusted precipitation was therefore derived from Equation (3.1) with the following expression:

$$P_j = P\frac{P_{aj}}{P_a} = P\frac{P_a + (h_j - h_0)\, C_{pa}}{P_a} = P\left(1 + \frac{C_{pa}}{P_a}(h_j - h_0)\right), \tag{3.2}$$

where P (mm d^{-1}) is the observed daily precipitation and P_j (mm d^{-1}) is the daily extrapolated precipitation in elevation.

Equation (3.3) is used to extrapolate the daily mean temperature:

$$T_j = T - C_t (h_j - h_0). \tag{3.3}$$

T (°C) is the observed daily mean temperature; T_j (°C) is the elevation-corrected daily mean temperature; C_t (°C m^{-1}) is the environmental temperature lapse rate, which is set to 0.006 °C m^{-1} [Gao et al., 2012]. The potential evaporation was estimated in each elevation zone using the elevation-corrected temperature.

3.4. MODELLING APPROACH

In this study four conceptual models of different complexity were designed and tested: a lumped model (FLEX^{L}); a model with a semi-distributed model structure, consisting of four structurally identical, parallel components with different parameter sets for each component (FLEX^{D}); a topography-driven semi-distributed model without soft data (FLEX^{T0}); and FLEX^{T} with the same model structure as FLEX^{T0} but constrained by expert knowledge. All models are a combination of reservoirs, lag functions and connection elements

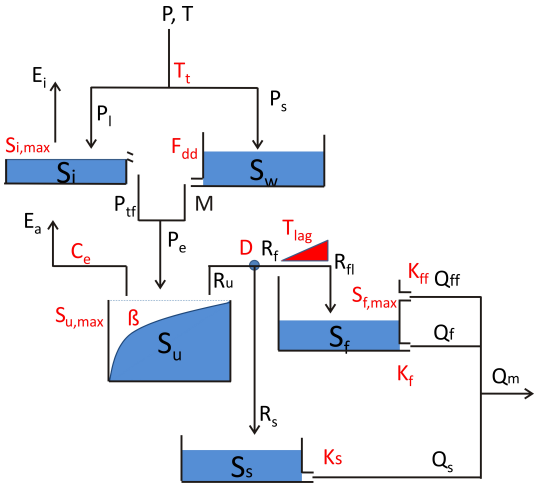

Figure 3.3: The lumped model structure FLEX^L.

linked in various ways to represent different hydrological functions constructed with the flexible modelling framework SUPERFLEX [Fenicia et al., 2011].

3.4.1. LUMPED MODEL (FLEX^L)

The lumped model (FLEX^L) (Figure 3.3) has a similar structure to earlier applications of the FLEX model [Fenicia et al., 2008b], and it comprises five reservoirs: a snow reservoir (S_w), an interception reservoir (S_i), an unsaturated reservoir (S_u), a fast-response reservoir (S_f) and a slow-response reservoir (S_s). A lag function represents the lag time between storm and flood peak. The elevation-corrected Thiessen-polygon-averaged precipitation, temperature and potential evaporation are used as forcing data. Note that this model structure was developed based on the perceptual model of the basin: the snow cover in winter shown in Figure 3.2d indicates the necessity of the snow reservoir; the forest cover in Figure 3.2b indicates the necessity of the interception reservoir; the unsaturated reservoir is important to separate the precipitation into runoff and unsaturated reservoir storage; the response reservoirs (S_f, S_s) are included to represent the fast and slow-response in hydrological models. The equations are shown in Table 3.3. On the other hand, including the elevation correction of precipitation and temperature in this lumped model is also based on our knowledge of the large catchment area and elevation differences.

SNOW AND INTERCEPTION ROUTINE

Precipitation can be stored in snow or interception reservoirs before the water enters the unsaturated reservoir. Basically, the snow routine plays an important role in winter and spring while interception becomes more important in summer and autumn. Here it is assumed that interception happens during rainfall events when the daily air temperature is above the threshold temperature (T_t; the units of the parameters are listed in

Table 3.3: Water balance and constitutive equations used in FLEX^{L}.

Reservoirs	Water balance equations	Constructive equations
Snow	$\frac{dS_w}{dt} = P_s - M$ (3.4)	$M = \begin{cases} F_{dd}(T - T_t) & \text{if } T > T_t \\ 0 & \text{if } T \le T_t \end{cases}$ (3.5)
Interception	$\frac{dS_i}{dt} = P_l - E_i - P_{tf}$ (3.6)	$E_i = \begin{cases} E_0;\ S_i > 0 \\ 0;\ S_i = 0 \end{cases}$ (3.7)
		$P_{tf} = \begin{cases} 0;\ S_i < S_{i,max} \\ P_r;\ S_i = S_{i,max} \end{cases}$ (3.8)
Unsaturated reservoir	$\frac{dS_u}{dt} = P_e(1 - C_r) - E_a$ (3.9)	$E_a = (E_0 - E_i)\min\left(\frac{S_u}{S_{u,max}C_e}, 1\right)$ (3.10)
		$C_r = 1 - \left(1 - \frac{S_u}{S_{u,max}(1+\beta)}\right)^{\beta}$ (3.11)
		$R_u = P_e C_r$ (3.12)
Splitter and lag function		$R_f = R_u D$; (3.13) $R_s = R_u(1 - D)$ (3.14)
		$R_{fl}(t) = \sum_{i=1}^{T_{lag}} c(i) \cdot R_f(t - i + 1)$ (3.15)
		$c(i) = i / \sum_{u=1}^{T_{lag}} u$ (3.16)
Fast reservoir	$\frac{dS_f}{dt} = R_{fl} - Q_{ff} - Q_f$ (3.17)	$Q_{ff} = \max(0, S_f - S_{f,max})/K_{ff}$ (3.18)
		$Q_f = S_f/K_f$ (3.19)
Slow reservoir	$\frac{dS_s}{dt} = R_s - Q_s$ (3.20)	$Q_s = S_s/K_s$ (3.21)

Tables 3.5 and 3.6) and there is no snow cover, i.e. typically in summer. When the average daily temperature is below T_t, precipitation is stored as snow cover, which normally occurs in winter. When there is snow cover and the temperature is above T_t, the effective precipitation (P_e ; hereinafter the unit of fluxes is mm d^{-1}) is equal to the sum of rainfall (P) and snowmelt (M), conditions normally prevailing in early spring and early autumn. Note that snowmelt water is conceptualized to directly infiltrate into the soil, thus effectively bypassing the interception store. In other words, interception and snowmelt never happen simultaneously. Their respective activation is controlled by air temperature, precipitation and the presence of snow cover.

The snow routine was designed as a simple degree-day model as successfully applied in many conceptual models [Seibert, 1997; Uhlenbrook et al., 2004; Kavetski and Kuczera, 2007; Hrachowitz et al., 2013b; Gao et al., 2012]. As shown in Equation (3.4) and (3.5), M is the snowmelt, S_w (the unit of storage is mm) is the storage of snow reservoir, dt (d) is the discretized time step and F_{dd} is the degree day factor, which defines the melted water per day per Celsius degree above T_t.

The interception evaporation E_i was calculated by potential evaporation (E_0) and the storage of interception reservoir (S_i), with a daily maximum storage capacity ($S_{i,max}$) (Equation 3.6, 3.7, 3.8).

SOIL ROUTINE

The soil routine, which is the core of hydrological models used in this study, determines the amount of runoff generation. In this study, we applied the widely used beta function

of the Xinanjiang model [Zhao, 1992] to compute the runoff coefficient for each time step as a function of the relative soil moisture. In Equation (3.11), C_r (−) indicates the runoff coefficient, S_u is the soil moisture content, $S_{u,max}$ is the maximum soil moisture capacity in the root zone and β is the parameter describing the spatial process heterogeneity in the study catchment. In Equation (3.12), P_e indicates the effective rainfall and snowmelt into the soil routine; R_u represents the generated flow during rainfall events. In Equation (3.13), R_f indicates the flow into the fast-response routine; D is a splitter to separate recharge from preferential flow. In Equation (3.14), R_s indicates the flow into the groundwater reservoir. In Equation (3.10) S_u, $S_{u,max}$ and potential evaporation (E_0) were used to determine actual evaporation E_a; C_e indicates the fraction of $S_{u,max}$ above which the actual evaporation is equal to potential evaporation, here set to 0.5 as previously suggested by Savenije [1997]; otherwise E_a is constrained by the water available in S_u.

RESPONSE ROUTINE

Equations (3.15) and (3.16) were used to describe the lag time between storm and peak flow. $R_f(t-i+1)$ is the generated fast runoff in the unsaturated zone at time $t-i+1$, T_{lag} is a parameter which represents the time lag between storm and fast runoff generation, $c(i)$ is the weight of the flow in $i-1$ days before and $R_{fl}(t)$ is the discharge into the fast-response reservoir after convolution.

The linear-response reservoirs, representing a linear relationship between storage and release, are applied to conceptualize the discharge from the surface runoff reservoir, fast-response reservoirs and slow-response reservoirs. In Equation (3.18), Q_{ff} is the surface runoff, with timescale K_{ff}, active when the storage of the fast-response reservoir exceeds the threshold $S_{f,max}$. In Equations (3.19) and (3.21), Q_f and Q_s represent the fast and slow runoff; S_f and S_s represent the storage state of the fast and the groundwater reservoirs; K_f and K_s are the timescales of the fast and slow runoff, respectively, while Q_m is the total modelled runoff from the three individual components.

3.4.2. MODEL WITH SEMI-DISTRIBUTED FORCING DATA (FLEX^D)

In order to test the influence of model complexity on model performance and model transferability, another benchmark model (FLEX^D) based on FLEX^L was developed. The four parallel model structures of FLEX^D are identical to FLEX^L, but they are run with independent parameter sets (Figure 3.4) and semi-distributed input data (see Section 3.3.2), resulting in distributed accounting of the four Thiessen polygons and the seven elevation bands in the study area (Figure 3.4). In total, there are 48 parameters for these four Thiessen polygons.

3.4.3. TOPOGRAPHY-DRIVEN, SEMI-DISTRIBUTED MODELS (FLEX^{T0} AND FLEX^T)

Based on the perceptual model of the Upper Heihe (see Section "The landscapes and the perceptual model of the Upper Heihe"), the hypotheses that different observable landscape units are associated with different dominant hydrological processes was tested by incorporating these units into hydrological models.

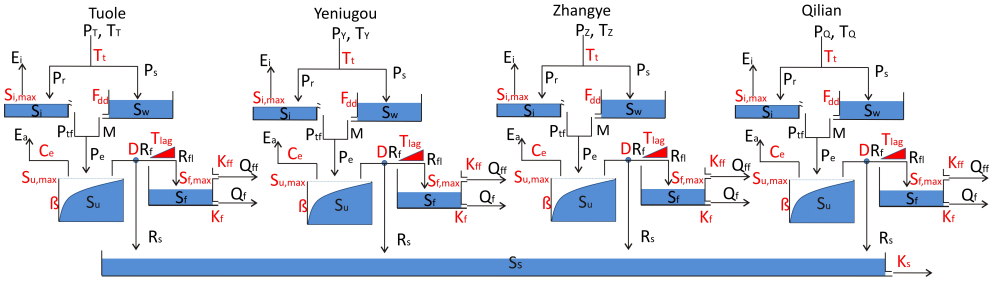

Figure 3.4: The semi-distributed model structure FLEX^{D}, consisting of four parallel components, representing one Thiessen polygon each. Each of the parallel components is characterized by an individual parameters set.

LANDSCAPE CLASSIFICATION

In this study, HAND [Rennó et al., 2008; Nobre et al., 2011; Gharari et al., 2011], elevation, slope and aspect (Figure 3.5) were used for deriving a hydrologically meaningful landscape classification. The stream initiation threshold for estimating HAND was set to 20 cells (0.16 km^2), which was selected to maintain a close correspondence between the derived stream network and that of the topographic map. The HAND threshold value for distinction between wetland and other landscapes was set at 5 m, similar to what was used in earlier studies [Gharari et al., 2011]. If HAND is larger than 5 m, but the local slope is less than 0.1, the landscape element defines terrace as a landscape unit that connects hillslopes with wetlands. The most dominant landscape in the Upper Heihe, however, is the hillslope, which has been further separated into three subclasses according to HAND, absolute elevation, aspect and vegetation cover (Figure 3.5). Thus, hillslopes above 3800 m and with HAND > 80 m, typically characterized by bare soil/rock, have been accordingly defined as bare-soil/rock hillslopes. At elevations between 3200 and 3600 m and aspect between 225 and 135°, or at elevations below 3200 m and aspect between 270 and 90°, hillslopes in the Upper Heihe are generally forested [Jin et al., 2008] and thus have been defined as forest hillslopes. The remaining hillslopes were defined as grassland hillslopes. From the classification map (Figure 3.6b), it can be seen that the landscape classification is similar to the independently obtained land cover map (Figure 3.6a) except for the area of wetland, due to different definitions between the land cover map and our classification. Note that wetland and terrace landscape classes have been combined (Figure 3.6b), because the area proportion of wetlands varies over time, while terraces may be flooded at times, which can be described by the VCA concept. This combination is unlikely to reduce realism and makes the model simpler. Consequently, the NDVI map has been averaged in accordance with this classification (Figure 3.6c).

FLEX^{T0} AND FLEX^{T} MODEL STRUCTURES

Based on the landscape classification and the perceptual models for each landscape, different model structures to represent the different dominant hydrological processes were assigned to the four individual landscape classes (Table 3.4). The four model structures ran in parallel, except for the groundwater reservoir (Figure 3.7). The snowmelt process was considered in all landscapes using the same method as described in Section 3.4.4.

In the bare-soil/rock class, HOF ($R_{H,B}$), caused by the comparatively low infiltration

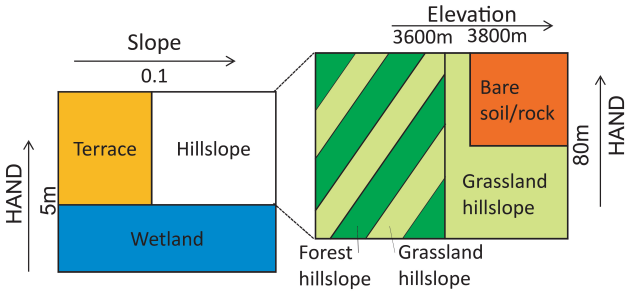

Figure 3.5: Summary of the landscapes classification criteria. The numbers (5 m, 80 m, 3600 m and 0.1) are the criteria for different landscape classes, e.g. < 5 m for wetland and > 5 m for terrace and hillslope.

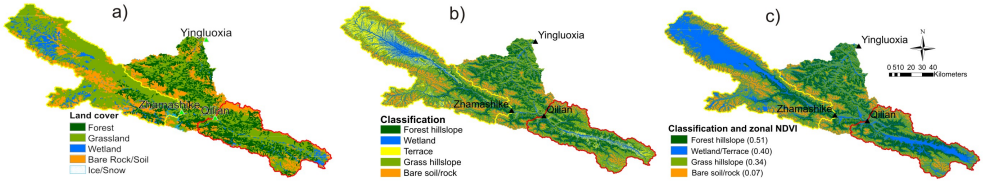

Figure 3.6: Comparison of land cover **(a)**, landscape classification maps **(b, c)** and the NDVI in each land cover **(c)**.

capacity compared to vegetation-covered soils on hillslopes, is controlled by a threshold parameter (P_t) (Equation 3.22). HOF only occurs when the daily effective precipitation ($P_{e,B}$) is larger than P_t:

$$R_{H,B}=\max\left(P_{e,B}-P_t, 0\right). \tag{3.22}$$

SOF ($R_{S,B}$), caused by limited storage capacity of the rather shallow soils at high elevations, happens when the amount of water in the unsaturated reservoir exceeds the storage capacity ($S_{u,max,B}$). Deep percolation from bare soil/rock into groundwater ($R_{p,B}$) is controlled by the relative soil moisture ($S_{u,B}/S_{u,max,B}$) and maximum percolation ($P_{erc,B}$):

$$R_{p,B}=P_{erc,B}\frac{S_{u,B}}{S_{u,max,B}}. \tag{3.23}$$

The actual evaporation ($E_{a,B}$) is estimated by potential evaporation ($E_{0,B}$) and relative soil moisture ($S_{uB}/S_{u,max,B}$), which is the same as the calculation of $R_{p,B}$ by $P_{erc,B}$ and $S_{u,B}/S_{u,max,B}$ in Equation (3.23). The generated surface runoff on the bare soil/rock is separated into the water re-infiltrating ($R_{r,B}$) while flowing on the higher permeable debris slopes and the water directly routed to the channel ($R_{f,B}$) by a separator (D_B). As in FLEX^D, the lag times are characterized by different lengths in the individual components. The response process of the surface runoff is controlled by a linear reservoir.

The grassland and forest hillslopes have the same model structure as FLEX^L, due to their similar runoff-producing mechanisms, but are characterized by different pa-

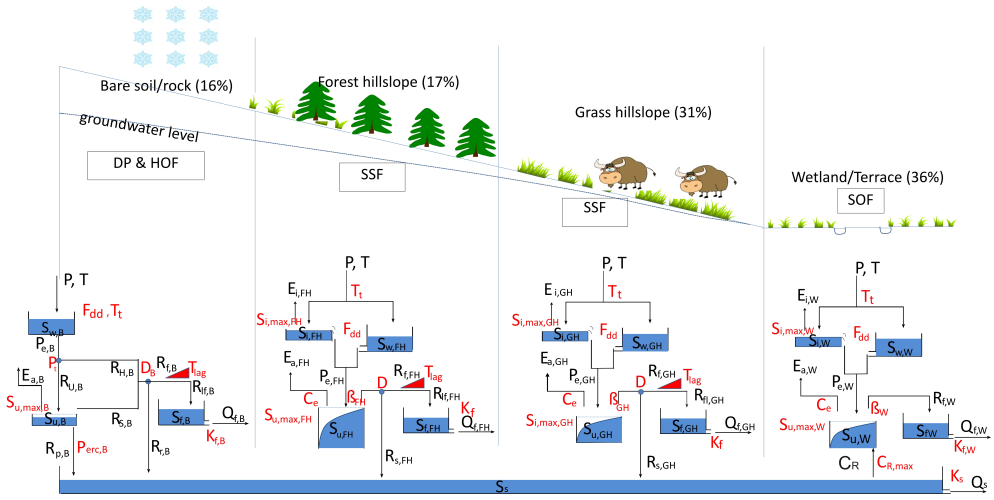

Figure 3.7: Perceptual model and parallel model structures of FLEX^{T} for the Upper Heihe.

Table 3.4: Proportion of different landscape units in the study catchments.

	Wetland/ terrace (%)	Grassland hillslope (%)	Forest hillslope (%)	Bare soil/rock (%)
Heihe	36	31	17	16
Qilian	33	28	25	14
Zhamashike	46	33	6	15

rameter values for interception ($S_{i,max,GH}$ and $S_{i,max,FH}$) and unsaturated zone processes ($S_{u,max,GH}$, $S_{u,max,FH}$ and β_{GH}, β_{FH}), reflecting different land cover and root zone depth. The lag times of grassland and forest hillslopes are the same as in the bare-soil/rock landscape elements. The generated runoff from grassland and forest hillslopes is represented by $Q_{f,GH}$ and $Q_{f,FH}$. In the wetland/terrace landscape element, SOF ($Q_{f,W}$) is conceptualized as the dominant hydrological process due to the shallow groundwater and resulting limited storage capacity. Additionally capillary rise (C_R) is represented by a parameter ($C_{R,max}$) indicating a constant amount of capillary rise. The calculation method of effective rainfall and actual transpiration is the same as for grassland and forest hillslopes. The lag time of storm runoff in wetland is neglected due to the, on average, comparatively close distance of wetlands/terraces to the channel. The groundwater (Q_s) was assumed to be generated from one single aquifer in the catchment and represented by a lumped linear reservoir. In total FLEX^{T} requires 25 parameters. The final simulated runoff is equal to the sum of runoffs from all landscape elements according to their areal proportions (Figure 3.7).

Table 3.5: Uniform prior parameter distributions of the FLEX^{L} and FLEX^{D} models.

Parameter	Range	Parameters	Range
F_{dd} (mm/(d °C^{-1}))	(1, 8)	K_s (d)	90
T_t (°C)	(−2.5, 2.5)	$S_{f,max}$ (mm)	(10, 200)
$S_{i,max}$ (mm d^{-1})	(0.1, 5)	K_{ff} (d)	(1, 5)
$S_{u,max}$ (mm)	(50, 1000)	K_f (d)	(1, 20)
β (−)	(0.1, 5)	T_{lag} (d)	(0, 5)
D (−)	(0, 1)	C_e (−)	0.5

3.4.4. MODEL CALIBRATION

OBJECTIVE FUNCTIONS

To allow for the model to adequately reproduce different aspects of the hydrological response, i.e. high flow, low flow and the flow duration curve, and thereby increase model realism, a multi-objective calibration strategy was adopted in this study, using the Nash–Sutcliffe efficiency (NSE) [Nash and Sutcliffe, 1970] of the hydrographs (I_{NS}) to evaluate the model performance during high flow, the NSE of the flow duration curve (I_{NSF}) to evaluate the simulated flow frequency and the NSE of the logarithmic flow (I_{NSL}) which emphasizes the lower part of the hydrograph.

CALIBRATION METHOD

The groundwater recession parameter (K_s) is not treated as a free calibration parameter but it was rather obtained directly from the observed hydrograph using a master recession curve approach (MRC) [Fenicia et al., 2006]. Therefore, K_s was fixed at 90 (d) to avoid its interference with other processes. Together with fixing C_e this results in 10, 40 and 23 free calibration parameters for FLEX^{L}, FLEX^{D} and FLEX$^{T0/T}$, respectively.

The MOSCEM-UA (Multi-Objective Shuffled Complex Evolution Metropolis-University of Arizona) algorithm [Vrugt et al., 2003] was used as the calibration algorithm to find the Pareto-optimal fronts of the three objective functions. There are three parameters to be set for MOSCEM-UA: the maximum number of iterations, the number of complexes and the number of random samples that is used to initialize each complex. For the FLEX^{L} model the number of iterations was set to 50 000, the number of complexes to 10 and the number of random samples to 1000. To account for increase model complexity, these MOSCEM-UA parameters of the FLEX^{D} were set to 50 000, 40 and 3200; those of FLEX^{T} to 50 000, 23 and 2300. The uniform prior parameter distributions of FLEX^{L} and FLEX^{D} are listed in Table 3.5 and the ones of FLEX^{T0} and FLEX^{T} are given in Table 3.6.

CONSTRAINTS ON PARAMETERS AND FLUXES IN FLEX^{T}

Guided by our perceptual understanding of the study catchment in the Section on “The landscapes and the perceptual model of the Upper Heihe” and the NDVI map (Figure 3.6c), a set of realism constraints for model parameters and simulated fluxes was developed, similar to what was recently suggested by Gharari et al. [2014]. Parameter sets and model simulations that do not respect these constraints were regarded as non-behavioural parameters and rejected during calibration. The motivation is that by reducing unre-

Table 3.6: Uniform prior parameter distributions of the FLEX^{T0} and FLEX^{T} model.

Parameters in all 3 models	Range	Parameters for bare soil/rock	Range	Parameter for forest hillslope	Range	Parameter for grass hillslope	Range	Parameter for wetland	Range
F_{dd} (mm/(d °C^{-1}))	(1, 8)	$S_{u,max,B}$ (mm)	(5, 500)	$S_{i,max,FH}$ (mm d^{-1})	(1, 10)	$S_{i,max,GH}$ (mm d^{-1})	(0, 10)	$S_{i,max,W}$ (mm d^{-1})	(0.1, 10)
T_t (°C)	(−2.5, 2.5)	$P_{max,B}$ (mm d^{-1})	(0.1, 10)	$S_{u,max,FH}$ (mm)	(100, 1000)	$S_{u,max,GH}$ (mm)	(50, 1000)	$S_{u,max,W}$ (mm)	(5, 1000)
P_t (mm d^{-1})	(5, 35)	D_B (−)	(0, 1)	β_{FH} (−)	(0.1, 5)	β_{GH} (−)	(0.1, 5)	β_W (−)	(0.1, 5)
K_f (d)	(1, 20)	K_{ff} (d)	(2, 50)					$C_{R,max}$ (mm d^{-1})	(0.01, 2)
K_s (d)	90							K_r (d)	(1, 9)
D (−)	(0, 1)								
T_{lagT} (d)	(0, 5)								
T_{lagY} (d)	(0, 5)								
T_{lagQ} (d)	(0, 5)								

Table 3.7: The soft data to constrain the automatic calibration.

Soft parameter constraint based on perceptual realism	Soft performance constraint based on NDVI map
$S_{i,max,FH} > S_{i,max,GH}$	$E_{i,FH} + E_{a,FH} > E_{i,GH} + E_{a,GH}$
$S_{i,max,FH} > S_{i,max,W}$	$E_{i,W} + E_{a,W} > E_{i,GH} + E_{a,GH}$
$S_{u,max,FH} > S_{u,max,GH} > S_{u,max,W}$	$E_{i,GH} + E_{a,GH} > E_{a,B}$
$S_{u,max,FH} > S_{u,max,GH} > S_{u,max,B}$	$E_{a,FH} > E_{a,GH}$
$K_s > K_f > K_{ff}$	
$K_s > K_f > K_r$	

alistic parameter combinations, the predictive uncertainty of a model may reduce, although the performance during calibration may be slightly decreased. More specifically, the parameters related to interception evaporation and transpiration were constrained based on expert knowledge (Table 3.7). It was assumed that the interception threshold in the forest class ($S_{i,max,FH}$) needs to be larger than in the grassland ($S_{i,max,GH}$) and wetland/terrace classes ($S_{i,max,W}$) due to the increased interception capacity of forests. In addition, the root zone depth of forest hillslopes ($S_{u,max,FH}$) should be deeper than in grassland ($S_{u,max,GH}$). Furthermore, the root zone depth of wetland/terrace ($S_{u,max,W}$) and bare soil/rock ($S_{u,max,B}$) are assumed to be shallower than those of hillslopes. The timescale of groundwater (K_s) was assumed to be the highest due to its slow recession process, while the timescales of SOF in the wetland/terrace class (K_r) and the surface runoff in the bare-soil/rock hillslope class (K_{ff}) were defined to be the shortest, with the timescale of SSF (K_f) on forest and grassland hillslope assumed to be in-between. Additional soft performance constraints were introduced to avoid unreasonable trade-offs among fluxes in different landscapes (Table 3.7). It is assumed that the combined annual average evaporation and transpiration in forest ($E_{i,FH} + E_{a,FH}$ – the unit is mm a^{-1}) should be larger than in grassland ($E_{i,GH} + E_{a,GH}$) due to the higher vegetation cover

Table 3.8: The averaged results of all the points on the Pareto front of three objective functions of the three models FLEX^{L}, FLEX^{D}, FLEX^{T0} and FLEX^{T} in calibration, split-sample and nested sub-catchments validation.

	Calibration			Split-sample validation			Zhamashike validation			Qilian validation		
	I_{NS}	I_{NSF}	I_{NSL}	I_{NS}	I_{NSF}	I_{NSL}	I_{NS}	I_{NSF}	I_{NSL}	I_{NS}	I_{NSF}	I_{NSL}
FLEX^{L}	0.82	0.99	0.87	0.79	0.95	0.78	0.54	0.79	0.56	0.56	0.87	0.59
FLEX^{D}	0.81	0.99	0.84	0.80	0.96	0.83	0.56	0.82	0.60	0.38	0.67	0.44
FLEX^{T0}	0.82	0.99	0.88	0.80	0.97	0.84	0.60	0.89	0.70	0.68	0.90	0.71
FLEX^{T}	0.80	0.98	0.84	0.78	0.95	0.82	0.65	0.92	0.74	0.71	0.96	0.75

in forests (see the NDVI map in Figure 3.6c). Similarly, the annual average evaporative fluxes from wetland/terrace ($E_{i,W}$ + $E_{a,W}$) are assumed to be higher than from the grassland as the latter are more moisture constrained. The evaporative water loss from the bare-soil/rock class ($E_{a,B}$) is the lowest, due to its sparse vegetation cover, limited near-surface storage and lowest temperatures. Furthermore, transpiration in forest ($E_{a,FH}$) should be expected to be higher than in grassland ($E_{a,GH}$) because more water is used for biomass production and deeper roots allow access to a larger pool of water.

3.4.5. MODEL EVALUATION

Model evaluation is usually limited to calibration followed by split-sample validation [Klemeš, 1986]. Frequently, split-sample validation can result in satisfactory model performance as the model is trained by data from the same location in the preceding calibration period. On the basis of successful split-sample validation, models and their parameterizations are then often considered acceptable for predicting the rainfall-runoff response at the given study site. It has in the past, however, been observed that many models with adequate split-sample performance failed to reproduce hydrographs even in the nested sub-basins of the calibrated basin [e.g. Pokhrel and Gupta, 2011]. In this study, we therefore applied the calibrated models of different complexity and degrees of input data distribution together with their calibrated parameter sets to two nested catchments to test the models' transferability and thus the ability to reproduce the hydrological response in catchments they have not explicitly been trained for. This kind of nested sub-catchment validation can, even if it is not an entirely independent validation in the sense of a proxy-basin test [Klemeš, 1986], give crucial information on the process realism and the related predictive power of a model. In this study the hydrological data at the main outfall Yingluoxia (1959–1968) were used for model calibration. Subsequently the model was tested by a split-sample test at the main outfall (1969–1978) and its two nested stations: Qilian (1967–1978) and Zhamashike (1959–1978).

3.5. RESULTS

3.5.1. RESULTS OF FLEX^{L} AND FLEX^{D}

Table 3.8, as well as Figure 3.8a and 3.9a, illustrate that FLEX^{L} performed quite well in the calibration period with respect to both the hydrograph and the flow duration curve (FDC). In spite of a somewhat reduced performance, the lumped model was also able to reproduce the major features of the catchment response in the split-sample valida-

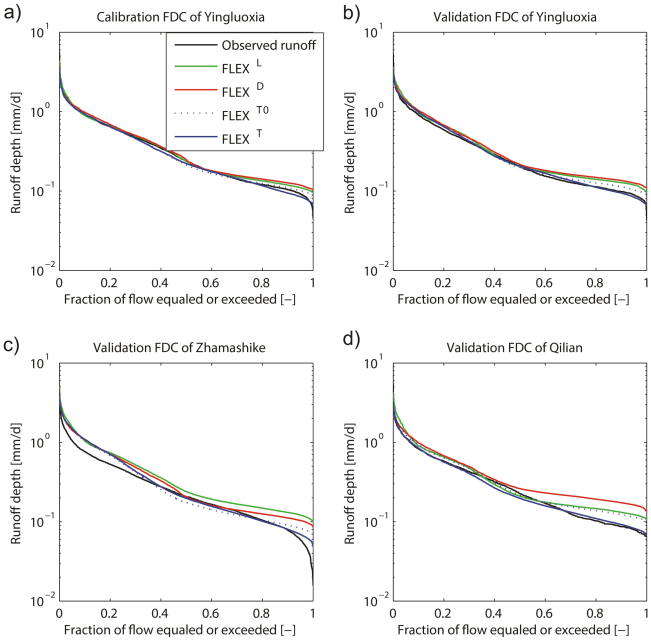

Figure 3.8: Calibration **(a)** and validation results for the flow duration curve of four models ($FLEX^L$ (lumped model), $FLEX^D$ (semi-distributed model with different parameter sets for different Thiessen polygons), $FLEX^{T0}$ (FLEX-Topo model without constraints) and $FLEX^T$ (FLEX-Topo model with constraints)) for the entire Upper Heihe **(b)** and the two tested sub-catchments **(c, d)**. The curves make use of the average value of the parameter sets on the Pareto-optimal front.

tion (Table 3.8, Figures. 3.8b and 3.9b). Testing the model's potential in an uncalibrated part of the catchment as if the uncalibrated parts were ungauged basins (Sivapalan et al., 2003; Hrachowitz et al., 2013b), the performance of $FLEX^L$ was far from satisfactory (Table 3.8, Figures. 3.8c and d, 3.9c and d). The validation hydrographs in two tested sub-catchments, which are in the same period as the split-sample validation, are shown in Figure 3.9c and d. One interesting observation is that the large precipitation event at the end of the warm season in 1970 did not generate a flood peak in all three catchments, a characteristic that cannot be adequately reproduced by $FLEX^L$ (Figure 3.9b–d). Similarly, the sub-catchment FDCs (Figure 3.8b–d) indicate that $FLEX^L$, while in general mimicking the FDC of the entire catchment well, poorly represents the low flow characteristics of the two sub-catchments.

In the next step the influence of distributing the model forcing and complexity on the model performance was tested using the $FLEX^D$ model set-up (Figure 3.4). It was found that although the modelled hydrograph and FDC reflect the observed response dynamics similarly well to $FLEX^L$ (Figures. 3.8a and 3.9a), the objective functions indicate a slightly poorer calibration performance (Table 3.8), in spite of two additional

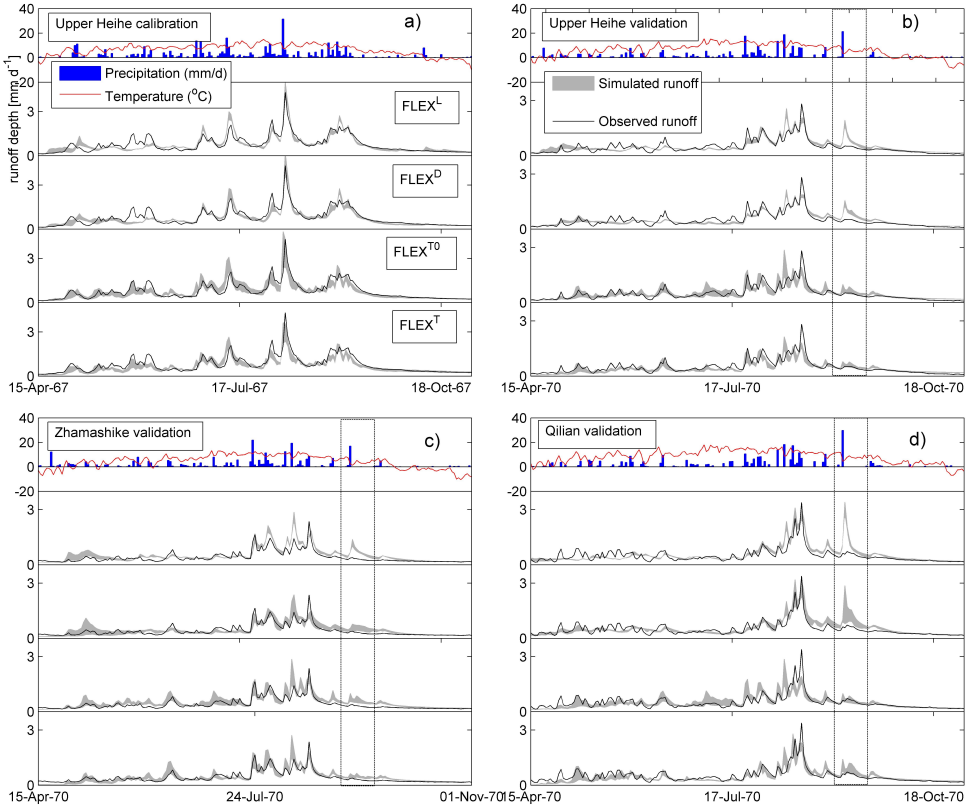

Figure 3.9: Comparison between observed values (black line) and the envelope of all modelled Pareto-optimal hydrographs (grey shaded area) of four models – FLEX^{L} (lumped model), FLEX^{D} (semi-distributed model with different parameter sets for different Thiessen polygons), FLEX^{T0} (FLEX-Topo model without constraints) and FLEX^{T} (FLEX-Topo model with constraints) – in the calibration period **(a)**, split-sample validation **(b)** and sub-catchments validation **(c, d)**. Precipitation (blue bars) and temperature (red line) are also shown. The dashed box indicates the September 1970 storm event.

parameters in each parallel model component accounting for differences in channel routing lag times. In this study, the reason is potentially related to the uncertainty in the precipitation–elevation relationship and the inappropriate soil moisture distribution dictated by the Thiessen polygons. In the split-sample and Qilian sub-catchment validation (Table 3.8, Figure 3.8b and d), FLEX^{D} does not add value to the results of the lumped FLEX^{L} model which is mostly related to the adverse effects of increased equifinality. However, the validation results in Zhamashike improve with FLEX^{D}, with increased NSE values for both FDC and the hydrograph (Table 3.8), although base flow is still not reproduced well (Figure 3.8c). This indicates that at least for the Zhamashike sub-catchment the distributed precipitation is more representative than catchment-averaged precipitation or that the results are more sensitive to the heterogeneity of precipitation and temperature input than in the Qilian sub-catchment. In addition, hydrograph inspec-

Table 3.9: The simulated results of FLEX^{T}.

Bare soil/rock (18 %)		Forest hillslope (17 %)		Grassland hillslope (31 %)		Wetland/terrace (36 %)	
P (mm a^{-1})	481	P (mm a^{-1})	431	P (mm a^{-1})	431	P (mm a^{-1})	410
$E_{a,B}$ (mm a^{-1})	174	$E_{i,FH}$ (mm a^{-1})	125	$E_{i,GH}$ (mm a^{-1})	58	$E_{i,W}$ (mm a^{-1})	87
$R_{p,B}$ (mm a^{-1})	115	$E_{a,FH}$ (mm a^{-1})	257	$E_{a,GH}$ (mm a^{-1})	205	$E_{a,W}$ (mm a^{-1})	220
$R_{f,B}$ (mm a^{-1})	107	$R_{s,FH}$ (mm a^{-1})	15	$R_{s,GH}$ (mm a^{-1})	63	C_{R} (mm a^{-1})	21
$Q_{f,B}$ (mm a^{-1})	77	$Q_{f,FH}$ (mm a^{-1})	26	$Q_{f,GH}$ (mm a^{-1})	101	$Q_{f,W}$ (mm a^{-1})	122

tion revealed that the mismatch of observed and modelled runoff, generated by the large precipitation event at the end of the warm season, was not captured well by the FLEX^{D} either (Figure 3.9b–d), although there was a slight improvement (see the reasons in Section 3.6.1). The results of FLEX^{D} indicate that increased model complexity alone, without deeper consideration of the underlying processes, does not result in a better model transferability.

3.5.2. RESULTS OF FLEX^{T0} AND FLEX^{T}

From Table 3.8 and Figures. 3.8 and 3.9, it can be seen that the FLEX^{T0} set-up (i.e. no constraints) results in a similar performance to FLEX^{L} and FLEX^{D} in calibration and validation, but outperforms the latter two when tested in the two sub-catchments. After adding the constraints, we found that the performance of FLEX^{T} in calibration and split-sample validation, as expected (because of the reduced degrees of freedom) and as indicated by the objective functions (Table 3.8), is slightly lower than the performance of other models. However, in sub-catchment validation, the performance of FLEX^{T} is significantly better than the other models. This indicates that both the model structure and the constraints on parameters and fluxes in FLEX^{T} improve model transferability.

In Table 3.9, the fluxes modelled by FLEX^{T}, which are the average values of all the results obtained by the parameter sets on the Pareto-optimal fronts, of each landscape class for the entire catchment are given. The water balances of the individual landscape units illustrate clearly the distinct dominant hydrological functions of these individual units as a priori defined by the modeller's perception of the system. Specifically, the precipitation on bare soil/rock is 481 mm a^{-1} (18 % proportion of the entire catchment precipitation), 174 mm a^{-1} (6 %) evaporates and 115 mm a^{-1} (4 %) infiltrates into cracks and eventually percolates to the groundwater. Overland flow produces 74 mm a^{-1} (3 %), while 112 mm a^{-1} (4 %) is generated as subsurface flow on shallow soil. A total of 107 mm a^{-1} (4 %) of the locally generated overland flows re-infiltrates into groundwater (107 mm a^{-1} (4 %)) due to the high permeability of debris slopes at the foot of the mountains while the remaining water (77 mm a^{-1} (3 %)) is routed to the stream network

with considerable sediment loads. Precipitation on the forest hillslopes is 431 mm a^{-1} (17 %), 125 mm a^{-1} (5 %) of which is intercepted by and evaporates from canopy and forest floor; 257 mm a^{-1} (10 %) is modelled as transpiration, while only 26 mm a^{-1} (1 %) and 15 mm a^{-1} (0.6 %), respectively, contribute to fast runoff and groundwater recharge, highlighting the dominant evaporation function of this landscape class. The precipitation on the grassland hillslopes is 431 mm a (31 %), of which 58 mm a^{-1} (4 %) is intercepted, 205 mm a^{-1} (15 %) is transpired, 101 mm a^{-1} (7 %) generates fast runoff and 63 mm a^{-1} (5 %) recharges the groundwater. For the wetland/terrace, precipitation is 410 mm a^{-1} (34 %) and in addition around 21 mm a^{-1} (1.7 %) is contributed from groundwater as capillary rise. 87 mm a^{-1} (7 %) is intercepted; 220 mm a^{-1} (19 %) is consumed by transpiration and 122 mm a^{-1} (10 %) contributes to the fast runoff. These results underline the importance of wetlands and terraces for peak flow generation. Finally, the groundwater discharge is 51 mm a^{-1} (12 %), which accounts for 37 % of the total runoff. In total, the modelled runoff depth is 143 mm a^{-1}, which is close to the observed runoff (141 mm a^{-1}). For the simulated total evaporation, it is interesting to find that the ratio between forest and wetland is 1.24, which is close to their NDVI ratio (1.27). Similarly, the ratio between water loss to atmosphere in wetland and grassland is 1.21, which is also close to their NDVI ratio (1.20). These results support the hypothesis that allowing for hydrologically meaningful process heterogeneity in models while imposing realism constraints can produce flux dynamics that are adequate reflections of reality, increasing our confidence that these models give "the right answers for the right reasons" [Kirchner, 2006].

Figure 8 shows significant improvement in the reproduction of the FDCs by $FLEX^{T0}$ and $FLEX^{T}$. FDCs are an emergent catchment property [cf. Sivapalan, 2006] and therefore a critical characteristic of system function which a model should be capable to reproduce [Westerberg et al., 2011]. In particular, the increased skill of $FLEX^{T}$ to reproduce the FDCs indicates that the flexibility introduced by considering changing proportions of hydrologically distinct landscape elements for different catchments and applying realism constraints in $FLEX^{T}$ has the potential to substantially increase the predictive power for flow characteristics, especially the low flows (Figure 3.8, Table 3.8). The importance of the expert-knowledge-based constraints imposed on $FLEX^{T}$ is illustrated by its increased ability to reproduce the FDCs as compared to $FLEX^{T0}$.The importance of accounting for an adequate level of hydrologically meaningful process heterogeneity is further illustrated by Figure 3.9, which shows the envelopes of observed and modelled hydrographs (based on all the parameter sets on the Pareto-optimal front) of three model structures, in calibration, split-sample validation and sub-catchment validation. The intense precipitation event in September 1970, which was observed at all four precipitation gauges and thus not a local event, did not generate a significant peak at any of the flow-gauging stations in this study. However, neither $FLEX^{L}$ nor $FLEX^{D}$ were able to accommodate this lack of response. Only the increased process heterogeneity in the $FLEX^{T0}$ and $FLEX^{T}$ models allowed an adequate representation of this event. For a closer analysis, the modelled hydrograph components from the different landscape elements are shown in Figure 3.10. It can be seen that the response to storm events is generally dominated by the flows generated in wetlands/terraces. Connectivity of hillslopes and bare-soil/rock landscapes however, is typically established with some delay and the

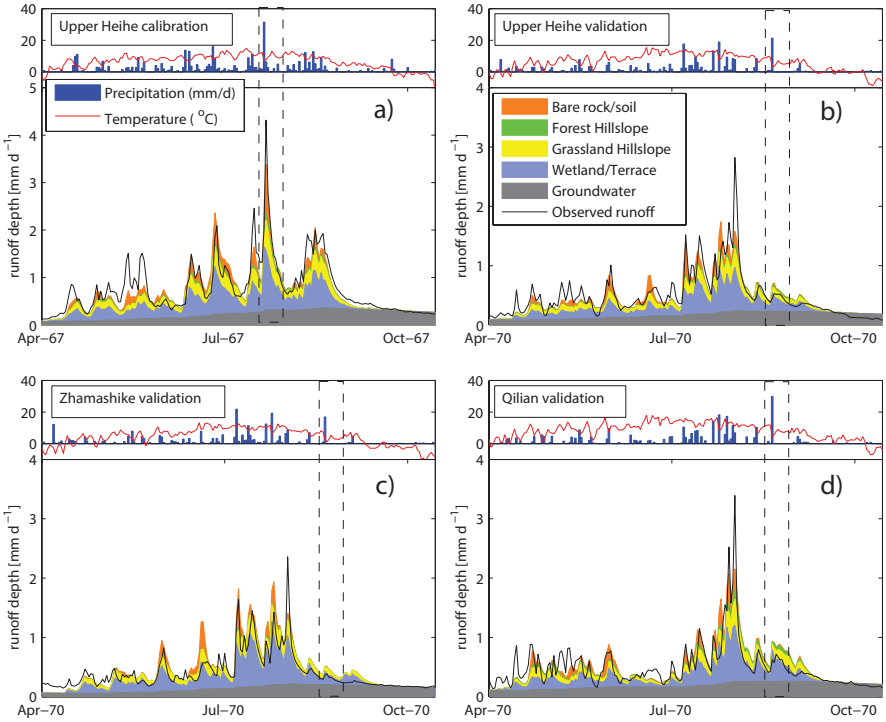

Figure 3.10: The hydrograph components of the calibration **(a)**, split-sample validation **(b)** and sub-catchments validation **(c, d)**, of the FLEX^{T} model (using the average value of the parameter sets on the Pareto-optimal front).

magnitude of their contributions to stream flow, in particular during relatively dry periods, are significantly lower than that of wetlands/terraces (Figure 3.10a). This is well illustrated for the September 1970 event shown in the dashed box in Figure 3.10b–d: while to some degree all the landscapes eventually contributed to the runoff, the wetland/terrace responded directly to the storm whereas the limited response of hillslopes and bare soil/rock contributed to the peak flow later.

3.6. DISCUSSION

3.6.1. WHY DID FLEX^{T} PERFORM BETTER THAN FLEX^{L} AND FLEX^{D}?

Some clarification can be achieved by comparing the observed precipitation duration curves (PDC) and FDCs. From Figure 3.11a it can be concluded that the entire Upper Heihe receives the lowest catchment-average precipitation input both in the original forcing data and the elevation-corrected precipitation, while being characterized by the largest runoff yield (Figure 3.11b). The Qilian sub-catchment, in contrast, receives the largest amount of precipitation, but with lower runoff yield. The Zhamashike sub-

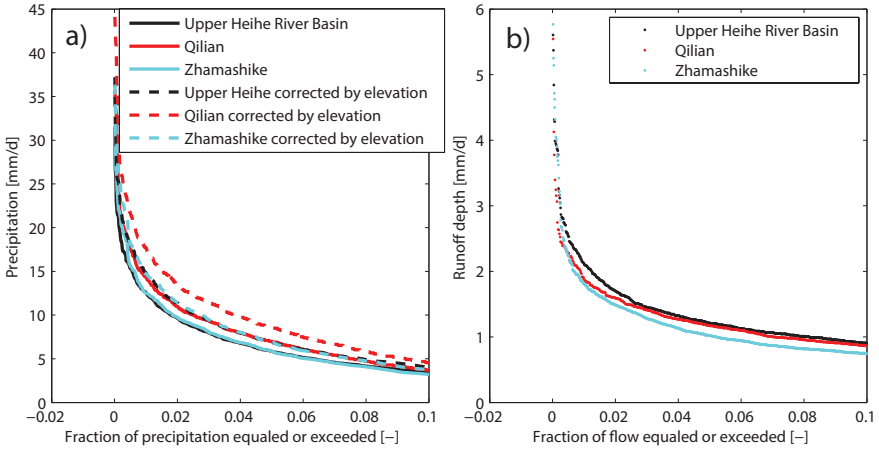

Figure 3.11: The comparison of three observed precipitation duration curves **(a)** and flow duration curves **(b)**.

catchment is characterized by similar precipitation input as the entire Upper Heihe, but exhibits much higher peak flows and lower base flows than both the entire catchment and the Qilian sub-catchment. These distinct catchment hydrological functions are difficult to reconcile in one lumped model, representing a specific rainfall-runoff relationship. Moving to a different catchment or maybe only even to a sub-catchment is likely to change the relative proportions of landscapes, thus leading to a misrepresentation of the lumped process heterogeneity and thus reduced model performance in the new catchment. A semidistributed approach like FLEX^{T}, in contrast to FLEX^{L} and FLEX^{D}, offers more flexibility in adapting the model to the ensemble of processes in a more realistic way other than the lumped ones trained by adjusting it to the hydrograph, which most likely oversimplifies the catchment heterogeneity. This underlines the increased importance and benefit of more detailed, yet flexible expert-knowledge-guided process representations compared to focusing on mere parameter calibration of lumped models.

The potential reason for overestimating the runoff in the Zhamashike sub-catchment for FLEX^{L} and FLEX^{D} (Figure 3.8c) is that these two models do not adequately represent the increased importance of evaporation from wetland/terrace. Similarly, the reason for overestimating flow in the Qilian sub-catchment (Figure 3.8d) is that these two models cannot accommodate the increased evaporation of forests as much of the Upper Heihe, for which the models were calibrated, is covered by grassland hillslope and bare soil/rock, characterized by lower evaporation rates than the other landscapes. On the other hand, both FLEX^{L} and FLEX^{D} overestimate the baseflow (Figure 3.8c and d). This can potentially be linked to neglecting capillary rise in the wetland/terrace, which influences both the baseflow and the evaporation of this landscape element. When capillary rise in FLEX^{T} is considered, the groundwater feeds the unsaturated reservoir in the wetland, which not only reduces the base flow but also increases the amount of water available for transpiration and eventually evaporation. This hydrological process is especially important in the Zhamashike sub-basin, where higher peak flows and lower

base flow happen simultaneously.

The results support the potential of FLEX^{T} and its parameterization to be spatially and scalewise better transferable than lumped model structures, such as FLEX^{L} or semi-distributed models such as FLEX^{D}, which do not explicitly allow for changing proportions of landscape units with distinct hydrological function (see Section 3.5.2). In summary, the FLEX^{T} model set-up, informed by topography, divided the catchments into four topographic subunits, representing different dominant hydrological process ensembles. This kind of modelling strategy allowed enough flexibility to capture the different functional behaviours of the three study catchments simultaneously (Table 3.8, Figures. 3.9–3.11).

SPECIFIC RAINFALL/SNOWFALL-RUNOFF EVENTS

Some modelled events, such as the rainfall/snowfall–runoff event in Figure 3.10a, also illustrate that FLEX^{T} is generating internal flow dynamics that better reflect the modeller's perception of the catchment processes. It can be seen that FLEX^{T} could reproduce the instantaneous response of the wetlands to the storm and the delayed and limited response of other landscapes. As discussed above, another interesting event was observed in September 1970. During that storm the highest daily precipitation of the available record was observed, while, however, producing only a relatively insignificant runoff peak, both in the Upper Heihe and its sub-catchments (Figure 3.9). Both FLEX^{L} and FLEX^{D} failed to adequately reproduce this event and modelled a much larger peak flow. Significant precipitation measurement error can be excluded, as the event was observed in similar magnitudes at all gauges available for this study. The failure of FLEX^{L} and FLEX^{D} to adequately respond to this event can be linked to several reasons. Firstly, the lumped accounting of the snowmelt in FLEX^{L} can partly be the reason because the lumped model does not consider the change of temperature and then the type of precipitation with elevation. The lumped model treats the precipitation as rainfall in the entire catchment when the average daily air temperature is above the rain/snow temperature threshold. However, there could be snowfall in high elevation zones, when the catchment average temperature is slightly above the threshold temperature. Likewise, there could be rainfall in lower elevation zones when the catchment average temperature is below the threshold. The temperature record (Figure 3.9) clearly shows the low average air temperature on the same day as the large precipitation event. This could partly explain the limited runoff response to this specific storm event, as the modelled results obtained from FLEX^{D} are somewhat closer to the observed response than the results of FLEX^{L} (Figure 3.9b and d).

However, FLEX^{D} could not mimic the event in a satisfactory way and hence the failure of FLEX^{D} to adequately represent the event can be attributed to an oversimplified model structure. This is supported by the results of FLEX^{T}. From Figure 3.10 it can be seen that the modelled flow generated by this storm event mostly originated in the wetlands, and a smaller proportion originated in grassland hillslopes. Contribution from forest hillslopes and bare-soil/rock hillslopes is negligible. The catchment average temperature on that day is close to the threshold temperature (Figure 3.10). Thus, at lower elevations, which are mainly characterized by wetland/terrace, grassland and forest hillslopes, the precipitation was in the form of rainfall. The temperature and precipitation records show that the preceding days were dry and warm (Figure 3.10), translating

into comparatively elevated evaporation and, linked to that, relatively high soil moisture deficits. In addition, the deep root zone on the forest hillslopes provides considerable storage capacity in the soil before discharge is generated. At a higher elevation, which is mainly characterized by bare soil/rock and grassland hillslopes, the precipitation was in a solid state, subsequently stored as snowpack. When the temperature increased again in the following days, the snow melted gradually. However, due to the slow melt rates and the dry antecedent conditions, the snowmelt water was almost completely infiltrated into the groundwater and did not contribute to the storm flow, even when the temperature increased several days later (Figure 3.10b–d). Therefore, there is apparently enough information, not only in landscapes but also in the observed discharge, to parameterize the FLEX^{T} model. In summary, FLEX^{T} allowed the low and high elevation areas to reduce the storm flow for this specific event by different mechanisms, resulting in a very limited response to the event, in close agreement with the observed response.

REALISM TESTING OF FLEX^{T} MODEL

The FLEX^{T} model is based on landscape classification, which is an observable prior to enhance model realism. Subsequently, based on our knowledge and understanding of different dominant hydrological processes in different landscapes, we assigned suitable hydrological process representations to these landscapes to highlight landscape heterogeneity. Significant differences in hydrological function, for example between wetland and hillslope, are well documented by a wide range of experimental studies [e.g. McGlynn and McDonnell, 2003; Seibert et al., 2003; Molenat et al., 2008; Jencso et al., 2009; Detty and McGuire, 2010]. The consideration of landscape heterogeneity, reflected in runoff generation mechanisms and differences in water budgets, makes the FLEX^{T} model perform better than FLEX^{L} and FLEX^{D}, reproducing hydrographs (Figure 3.9) but also FDCs (Figure 3.8), as emergent catchment properties. The suggested model hypotheses were not only tested for temporal transferability between calibration and validation periods, but also for spatial transferability to sub-catchments. This successful transferability (Table 3.8; Figures. 3.8 and 3.9) is strong supporting evidence for the hypothesis that landscape carries crucial information on hydrological function and it illustrates that, by allowing for increased process heterogeneity in models, their degree of realism, i.e. their skill to adequately represent critical features in response dynamics, increases. More convincingly, the benchmark model (FLEX^{D}) with a higher number of parameters (40 free parameters) did not improve transferability, even with nearly twice the number of parameters as in FLEX^{T} (23 free parameters). However, note that here "realism" is not primarily and necessarily linked to an improved fit of the hydrograph. It is rather linked to the incorporation of more knowledge available from observation and experiments, thereby allowing the development of models whose internal and external dynamics correspond with this information, which in turn increases model realism.

Note that this paper aims to test the realism of models, meaning that it investigates to which degree a more realistic representation has been achieved, but it does not intend to claim that the developed model is realistic in absolute terms. In that respect it emphasizes that model realism should always be seen in relation to uncertainties arising from data error as well as from the choice of constitutive functions and parameters. In this paper, a detailed analysis of the influence of these uncertainties was omitted as this

was beyond the scope of this research. Further, some of the hypotheses of the proposed model structure could not be tested individually for lack of available data. They will be further investigated during future research, using additional information. Thirdly, at this point, the interpretation is only valid in the study catchment and subsequent studies will have to test this hypothesis further in other regions in order to evaluate the generality of these findings.

3.6.2. TRANSLATING TOPOGRAPHY INFORMATION INTO HYDROLOGICAL MODELS

It is intriguing to find that the landscape classification based on topography information (HAND, slope, elevation and aspect) closely reflects the patterns and shapes of the land cover map (Figure 3.6a and b). In other words, it clearly illustrates that topography has great influence on the energy and water availability and the evolution of vegetation cover. Certain types of vegetation cover evolve under specific topographic conditions. Elevation greatly influences the amount of precipitation and available energy. HAND and slope are two important factors defining water retention and drainage. Aspect influences the energy balance and precipitation. Normally, the south-facing hillslopes receive more solar energy. Thus, the potential evaporation on the south-facing hillslopes is larger than on north-facing ones, while aspect influences the distribution of forest and grassland in arid/semi-arid regions.

Topography does not only directly influence the groundwater level and the occurrence of saturation overland flow, but it also controls the soil and vegetation cover in certain geological and climatic condition, and consequently the dominant hydrological processes [Savenije, 2010]. The presented modelling approach can therefore be seen as a step towards making more efficient use of topographic information for use in conceptual hydrological models. The successfully linked topographic information, land cover classification and hydrological model structure supports the hypothesis that topographic information can be used to distinguish landscape elements with different hydrological functions [Wagener et al., 2007; Savenije, 2010].

3.6.3. THE VALUE OF SOFT DATA IN HYDROLOGICAL MODELLING ($FLEX^{T0}$ VS. $FLEX^{T}$)

Hydrological modelling should also be seen as an art [Savenije, 2009]. To ensure that models better reflect our understanding of reality we should make use of our experience and creativity. In addition to available data, hydrologists often have extensive, yet sometimes only semi-quantitative expert knowledge about specific study sites. However, this “soft” knowledge is with some exceptions [e.g. Seibert and McDonnell, 2002, 2013], regularly underexploited in hydrological modelling. In general four types of soft data can be valuable for hydrological modelling. The first one is our explicit or inferred knowledge of the hydrological processes occurring in reality. For example, in this study, streams in high elevation tributaries, characterized by a dominance of relatively erodible bare soil/rock, exhibit relatively high levels of turbidity (Figure 3.2e), thus indicating the importance of soil erosion, which in turn supports the existence of Hortonian surface runoff in these locations. Another type of “soft” data is the expert knowledge on mean-

ingful acceptable prior parameter ranges, such as the maximum storage of the unsaturated reservoir at the catchment scale ($S_{u,max}$), which is closely linked to rooting depth and soil structure and strongly depends on the ecosystem. The third kind of valuable "soft" data is the understanding of the relative magnitude of specific parameters in different landscapes [Gharari et al., 2014], providing further constraints on model parameters, and eliminating unrealistic parameter combinations. For example, in this study it was argued that forest canopy, undergrowth and litter on forested hillslopes can intercept more precipitation ($S_{i,max,FH}$) than grass-dominated hillslopes ($S_{i,max,GH}$) (Table 3.7). Fourthly, simulation results can be constrained by "soft" data, such as NDVI maps indicating inequalities between forest and grassland transpiration (Table 3.7). Making use of these four types of soft data, a landscape driven model, FLEX^{T}, based on our understanding of the hydrological processes in the Upper Heihe, was developed and constrained. Although the use of these additional constraints resulted in a slightly reduced calibration performance of FLEX^{T} as compared to the FLEX^{T0} set-up, the more successful sub-catchments validation illustrated the value of soft data and clearly indicated that the efficient use of soft data allows for a more realistic representation of catchment heterogeneity, leading to higher predictive power.

3.6.4. THE ROLE OF FOREST IN THE UPPER HEIHE

Since forest is an important land cover in the Upper Heihe and many other catchments, the hydrological impact of forest is essential for understanding the catchment water cycle [Andréassian, 2004; Lyon et al., 2012], but also for an efficient implementation of water resource management policies. The role of forest on the catchment scale is subject of ongoing discussion in ecohydrology [Moore and Wondzell, 2005; Sriwongsitanon et al., 2011].

Various earlier studies found very diverse conclusions [Bosch and Hewlett, 1982; Robinson et al., 1991; Sahin and Hall, 1996; Andréassian, 2004; Moore and Wondzell, 2005]. In this study, the FLEX^{T} model generated little runoff in forested hillslopes in the Upper Heihe, with most of the rainfall on the forest being intercepted and transpired. In addition, these results are supported by other studies in this catchment based on remote sensing information [Tian et al., 2013], statistical analysis [Wang et al., 2011], paired catchment analysis in this region [Huang et al., 2003; Qin et al., 2011] and the simulation of an ecohydrological model [Yu et al., 2009]. Also, field observations and experimental studies in the Upper Heihe (B. Ye, personal communication, 2012) gave evidence of limited runoff from forests. This phenomenon is most likely linked to the climatic conditions in the Upper Heihe. Since the precipitation in this region reaches on average only 430 mm a^{-1}, with a maximum observed daily catchment average precipitation of below 45 mm d^{-1} (corrected by elevation), with ample storage available in the root zone, the forest hillslopes in the Upper Heihe remain largely below the moisture content necessary to establish connectivity conditions necessary to significantly contribute to storm flow.

3.7. CONCLUSIONS

We compared four model structures on the Upper Heihe in China: a lumped model ($FLEX^{L}$), a semi-distributed model with different parameter sets for different Thiessen polygons ($FLEX^{D}$), a conceptual model whose model structure is determined based on hypotheses of how topography influences hydrological processes ($FLEX^{T0}$), and $FLEX^{T}$, which is based on $FLEX^{T0}$ but constrained by soft data. $FLEX^{T0}$ and $FLEX^{T}$ perform in almost the same way as the two previous models in calibration and split-sample validation, but much better when validated in two sub-catchments. The increased performance of $FLEX^{T0}$ and $FLEX^{T}$ with respect to $FLEX^{L}$ and $FLEX^{D}$ in the sub-catchments, in particular with respect to the flow duration curves and for some specific events, indicates the following: (1) the topography-driven model, using landscapes classification as prior information and describing different dominant hydrological mechanisms in different landscapes, reflects the catchment heterogeneity in a more realistic way; (2) the natural land cover may be identified by topographic information to some extent, because the topography greatly influences the local energy and water budget; (3) the better performance of $FLEX^{T}$ compared to $FLEX^{T0}$ indicates further that the use of realism constraints guided by soft data reduced unrealistic compensation between fluxes and increased model transferability. In summary, making use of topography-derived data as prior information to guide model development is a promising avenue.

4

THE INFLUENCE OF TOPOGRAPHY AND VEGETATION ON MODEL TRANSFERABILITY IN THE UPPER PING RIVER, IN THAILAND

Understanding which catchment characteristics dominate hydrologic response, and how to take them into account in hydrological models remains an unresolved challenge. Thus, hydrological models often perform poorly when transferred to other catchments. In this study, we investigated whether accounting for topography and vegetation in conceptual models improves model transferability. We applied a stepwise modelling approach where vegetation and topography was incorporated through various approaches. The study area comprises 6 catchments of the upper Ping River basin, in Thailand. First, our benchmark was represented by a lumped model (FLEX^{L}). We then considered a modified version (FLEX^{LV}) that used vegetation information (NDVI). We also considered an alternative version (FLEX^{LM}), where vegetation information was based on hydroclimatological data. We then considered 2 distributed models, discretizing landscapes by topography. The FLEX^{T} was based on topography alone to account for landscape heterogeneity. While the FLEX^{TM} includes both topography and vegetation information. Each model was calibrated on one catchment, and then transferred with its optimized parameter sets to the other five catchments. We found that all five models performed similarly well during calibration. This indicates that all models have ability to fit the hydrographs of the 6 catchments. However, in transferability, a more stringent test, the performance of the FLEX^{L} reduced dramatically. We attributed the better performance of the other four models to the consideration of

This chapter is based on:
Gao, H., Hrachowitz, J., Sriwongsitanon, N., Fenicia, F., Gharari, S., and Savenije, H. H. G.: Towards understanding the influence of vegetation and topography on model transferability, Water Resources Research, 2015 (submitted).

vegetation and topography, which varied considerably between catchments. Co-evolution between topography, vegetation, soil and hydrology may be the reason for successful model transferability when topography and vegetation information is used.

4.1. INTRODUCTION

Spatial transferability of model structure and model parameters (hereafter referred to as model transferability) is an important quality criterion for hydrological modelling. The ability to regionalize or transfer models was an important objective and challenge of the IAHS decade on Predictions in Ungauged Basins (PUB) [Sivapalan, 2003; Hrachowitz et al., 2013b], model upscaling [Sivapalan and Kalma, 1995; Blöschl, 2001], and model consistency [Martinez and Gupta, 2011; Euser et al., 2014]. It is not uncommon that we have to recalibrate parameters or even develop new models to describe hydrological processes in different catchments, even if they are nearby. Spatial model transferability is considered a more convincing test than temporal transferability, i.e. split-sample validation [Refsgaard et al., 2014] and differential split-sample test [Hartmann and Bárdossy, 2005; Refsgaard et al., 2014]. A more robust proxy site transferability test would yield more confidence in model results and also help to increase the understanding of hydrological processes at play [Fenicia et al., 2008b]. Model transferability tests would move from location-based calibration-validation towards a stress test under a wide range of catchment conditions with diverse land surfaces and variable climate conditions. From a single study site simulation, at best, one can learn about the processes in a single catchment, but from catchment comparison one can derive more generic model concepts [Blöschl et al., 2013; Gupta et al., 2014]. Finally, it would support the inclusion of more realism in hydrological models [Gao et al., 2014a].

To deal with this challenge, one among a wide range of strategies is to assume that catchments with similar characteristics demonstrate similar behaviour, and to classify entire catchments based on their characteristics [Bárdossy, 2007]. Differences in terms of topography, topology, soils, vegetation and geology, however, make catchments unique, and hinder the application of such classification schemes, because a sufficiently high number of classes would have to be defined to account for a sufficient degree of variability [Andréassian et al., 2009].

An alternative approach is the concept of hydrological response units (HRUs), which instead of defining hydrological similarity at the scale of entire catchments, considers a smaller area [Flügel, 1996]. Previous studies applied this concept to develop models such as the Soil and Water Assessment Tool (SWAT), where HRUs are mainly based on soil type and vegetation [Arnold et al., 1995], or Dynamic TOPMODEL [Beven, 2001], which is mainly based on topographic information.

The lack of suitable data for detailed HRU definition, together with equifinality problems due to increased model complexity, frequently hinders application of such modelling strategies in practice. It is therefore critical to systematically analyse the individual effects of different sources of information such as of topography, topology, soils, vegetation and geology, to develop an understanding on how much and which information is necessary to meaningfully define HRUs and which of these factors are first order controls on model transferability.

The co-evolution of topography, vegetation, soil texture, climate and geology, suggests that these factors are correlated. We may therefore not need to consider all these aspects in our models [Savenije, 2010; Troch et al., 2013], as information of one of these aspects could in principle be derived from others. This hypothesis can be used to incorporate catchment heterogeneity into a hydrological model in a simple and parsimonious

way, hence keeping models as simple as possible, thereby keeping data requirements as well as parameter equifinality low. Based on this assumption, Savenije [2010] proposed a topography-driven modelling approach (FLEX-Topo), where only topography and land cover information is considered for the derivation of HRUs to be used in a model.

Gharari et al. [2014] found that, if adequately constrained by expert knowledge, the relatively complex FLEX-Topo can be quite robust compared to a standard lumped model even without calibration. Similarly, a recent study by Hrachowitz et al. [2014] highlighted the value of increased process complexity introduced by HRUs to adequately reproduce a wide range of hydrological signatures and thus the system integrated response characteristics of a catchment. [Gao et al., 2014a] showed that FLEX-Topo, which includes topography and land cover information, performed substantially better than a lumped model where this information was not considered.

A further way to improve model transferability is parameter regionalization [Hundecha and Bárdossy, 2004; Laaha and Blöschl, 2006; Blöschl et al., 2013]. For example, Merz and Blöschl [2004] looked for spatial regionalized patterns of parameters in the HBV model for over 300 catchments in Austria. To improve model transferability, [Samaniego et al., 2010; Kumar et al., 2013], proposed a multi-scale parameterization regionalization (MPR) method, linking model parameters with land surface characteristics at the finest spatial resolution available by transfer functions, and then upscaling model parameters to the scale of interest.

The aim of this study is to investigate how topography and land cover information can improve model transferability and how their influence can be appropriately conceptualized. Our hypothesis is that topography and vegetation are dominant controls on the hydrological behaviour of the study catchments. In order to test this hypothesis we use a suite of increasingly complex conceptual model set-ups, where the hypothesized effects of topography and vegetation on hydrological behaviour are progressively incorporated. More specifically, our hypotheses are formulated as follows: (1) topography controls model structure and the processes at play. We shall test this hypothesis by distributing the model structure according to topography. (2) Vegetation controls the partitioning of fluxes and their parameter values. This hypothesis will be tested by distributing the root zone storage capacity according to vegetation characteristics. (3) Model transferability improves if we take these aspects into account. This will be tested by applying the calibrated models in different catchments. There are clearly other possible factors that may influence the hydrological behaviour of a catchment. For example, Fenicia et al. [2014] advocated that geology was mainly responsible for the contrasting behaviour of 3 neighbouring catchments in Luxembourg. In the river basins studied in this paper, however, we assume geology not to be a major control and we retain geological influence on model structure and parameter values for further research.

The paper is structured as follows. The study site and data section presents the basic information of six catchments in the upper Ping River basin and the data used. In the model set-up section, we describe five model structures: a lumped model ($FLEX^{L}$), a lumped model using vegetation information ($FLEX^{LV}$, $FLEX^{LM}$), a distributed topography driven model ($FLEX^{T}$), and the distributed topography-driven model using vegetation information ($FLEX^{TM}$). The model evaluation section presents the objective functions we used to quantify model performance, the automatic calibration algorithm, and

the procedure of the designed virtual experiment of model transferability. The results section presents the calibrated and transferred results and the performance of the five models in their capacity to reproduce: the hydrograph, the flow duration curve (FDC), the components of the hydrograph and the evaporation from different landscapes. The discussion section presents an interpretation of the performance of these model set ups, and the conclusion section summarizes the key findings.

4.2. STUDY SITE AND DATA

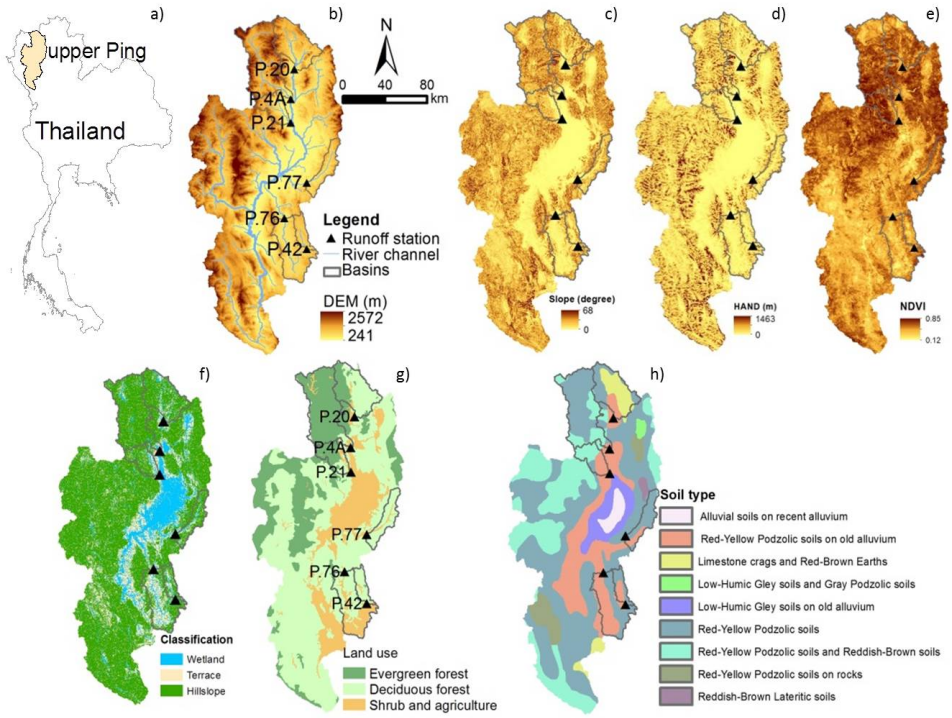

Figure 4.1: a) the location of the Upper Ping River basin (UPRB) in Thailand; b) the DEM of the UPRB, with the six study catchments and runoff stations; c) the slope map of the UPRB; d) the HAND (Height Above the Nearest Drainage) map of the UPRB; e) the dry seasonal NDVI (Normalized Difference Vegetation Index) map of the UPRB; f) landscapes classification map of the UPRB based on HAND and slope; g) the land use map of the UPRB; h) the soil type map of the UPRB.

4.2.1. STUDY SITE INTRODUCTION

The Ping River is one of the main tributaries of the Chao Phraya, which drains more than one-third of Thailand and is the country's largest river basin [Sriwongsitanon et al., 2011]. The study catchments are six sub-catchments of the Upper Ping River basin (UPRB; Figure 4.1), with areas ranging from 315 to 1902 km^2. The catchments are dominated

by forest (80% in 2005, Figure 4.1g) [Sriwongsitanon et al., 2011], and the landscape is characterized by generally steep mountains. The average annual rainfall between 1988 and 2005 was around 1174 mm/a, and runoff was around 268 mm/a [Taesombat and Sriwongsitanon, 2009]. The climate of this region is tropical savanna (Aw in Köppen–Geiger climate classification), characterized by South Asian Monsoon, with hot wet summers and hot dry winters. Red-yellow podzolic soils, is the dominant soil type (Figure 4.1h), which overlays a complex geology, dominated by quartzite, phyllite, schist, sandstone, shale, tuff, and terrace deposits.

The six study catchments are P.4A, P.20, P.21, P.42, P.76, P.77. Among them, P.4A has steepest slope (Figure 4.1c) and it is mainly covered by evergreen forest (Figure 4.1g), with highest Normalized Difference Vegetation Index (NDVI) in dry seasons (0.773) (Figure 4.1e). P. 42 and P.76 are relatively flat and have larger proportions of wetland and terrace landscapes (Figure 4.1c, d, f). The dominant vegetation cover in P.42 and P.76 are deciduous forest, shrubs and agriculture, with lowest NDVI in dry seasons (0.682 in P.42; 0.671 in P.76). The remaining catchments (P.20, P.21 and P.77) are characterized by steep slopes and denser vegetation cover, i.e. higher NDVI. A detailed summary of catchment characteristics is given in Figure 4.1 and Table 4.1.

Table 4.1: Summary of catchment characteristics. p_W, p_T, and p_H represent proportions of wetlands, terraces and wetlands respectively. Runoff coefficients were computed as the long-term runoff coefficients for the observation period 1995-2005. P and E_0 represent annual precipitation and annual potential evaporation. NDVI was calculated as the long-term average NDVI in dry seasons.

Code	Area (km^2)	Average elevation (m)	Time series	p_W (%)	p_T (%)	p_H (%)	Runoff coefficient	P (mm a^{-1})	E_0 (mm a^{-1})	NDVI
P.4A	1902	1026	1995-2005	5.6	11.5	93.0	0.153	1274	1547	0.773
P.20	1355	777	1995-2005	9.7	17.4	72.9	0.226	1223	1606	0.732
P.21	515	724	1995-2005	10.5	23.0	66.5	0.195	1273	1619	0.759
P.42	315	669	1995-2001	12.2	27.3	60.6	0.106	950	1644	0.682
P.76	1541	582	2000-2005	16.0	41.6	42.4	0.132	980	1655	0.671
P.77	550	637	1999-2005	9.9	19.6	70.6	0.137	1110	1648	0.732

4.2.2. DATA SET

The daily rainfall, runoff and temperature data were collected from the Thailand Meteorological Department and Royal Irrigation Department in Thailand. The daily areal rainfall distribution across the UPRB was generated using 68 stations in and around the UPRB by thin plate spline extrapolation [Taesombat and Sriwongsitanon, 2009]. The potential evaporation (Table 4.1) was calculated using the Hargreaves equation [Hargreaves, 1975], based on daily average, minimum and maximum air temperature from three close-by stations: Chiangmai (18°47'N, 98°59'E), Lamphun (18°34'N, 99°02'E), Maejo (18°55'N, 99°00'E). The Digital Elevation Model (DEM) used in this study is the Shuttle Radar Topography Mission (SRTM) product with a resolution of 90m. NDVI was obtained from the MOD13Q1 product with 250 m spatial and 16 days temporal resolution. Both the DEM and NDVI (2000-2011) data were downloaded from .

Since there is only a limited number of meteorological stations available and due to the marked elevation difference within the UPRB, temperatures for the estimation of the potential evaporation was elevation adjusted using the environmental lapse rate of 0.006

$^{o}Cm^{-1}$.

4.3. METHODOLOGY AND MODEL SET-UPS

To assess the importance of a more complete representation of process and vegetation heterogeneity for the spatial transferability of models, five model set-ups with increasing complexity were tested in this study. As a benchmark, a simple lumped model, hereafter referred to as FLEX^{L}, was tested. Two approaches were tested to consider vegetation information in lumped model set-ups: in the FLEX^{LV} model, the root zone storage capacities ($S_{u,max}$) in the study catchments were estimated by a nonlinear relationship between $S_{u,max}$ and NDVI, while in the FLEX^{LM} model $S_{u,max}$ was estimated with the Mass Curve Technique (MCT), based on climate and vegetation information as recently proposed [Gao et al., 2014b]. Subsequently, guided by topographic information, more process heterogeneity was incorporated in the semi-distributed model set-up FLEX^{T} [Savenije, 2010; Gao et al., 2014a; Gharari et al., 2014; Hrachowitz et al., 2014]. In the most complex model set-up of this study, FLEX^{TM}, we attempted to extend the MCT method from a lumped set-up to different landscape units by an empirical linear relation between $S_{u,max}$ and NDVI of different landscapes. The five model set-ups are in the following described in detail. To evaluate the models' potential for spatial transferability and to assess the relative importance of accounting for topography guided process and vegetation heterogeneity for improving transferability, a "leave-p-out-cross-validation strategy" with p=5 was chosen [Shao, 1993]: from the 6 study catchments, one was chosen as donor catchment to calibrate the 5 models, which were then transferred and tested in the 5 receiver catchments. This procedure was repeated 6 times so that each catchment served once as donor catchment.

4.3.1. FLEX^{L}

The lumped conceptual hydrological model (FLEX^{L}, Figure 4.2) in this study is developed based on the SUPERFLEX modelling framework [Fenicia et al., 2011]. It consists of four reservoirs: the interception reservoir S_i (mm), the unsaturated reservoir S_u (mm), the fast response reservoir S_f (mm), the slow response reservoir S_s (mm) and two lag functions representing the lag time from storm to peak flow ($T_{lag,f}$), and the lag time of recharge from the root zone to the groundwater ($T_{lag,s}$). In total, there are 11 free calibration parameters in FLEX^{L} (see Table 4.2). The relevant model equations and parameter distributions are given in Tables 4.2 and 4.3.

4.3.2. FLEX^{LV}

In a previous study [Gao et al., 2014b], we found strong evidence that the parameter representing the root zone storage capacity $S_{u,max}$ is controlled by climate and vegetation cover. To test the direct influence of vegetation on model transferability, a simple regionalization method [Abdulla and Lettenmaier, 1997; Seibert, 1999; Hundecha and Bárdossy, 2004] was applied to estimate $S_{u,max}$ based on catchment dry seasonal averaged NDVI values, which are expected to reflect ecosystem transpiration during the dry season. The focus was on the dry season because only during this period a correlation between ecosystem evaporation and the buffer it created to overcome the dry season

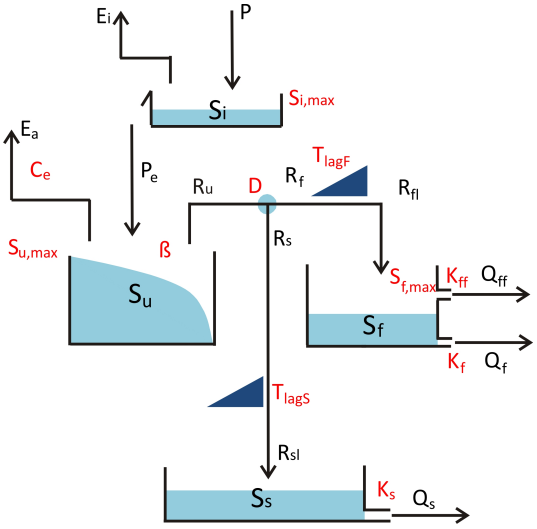

Figure 4.2: Model structure of the FLEX^{L}

Table 4.2: Water balance equations and constitutive equations of each reservoir in the FLEX^{L} model

Reservoirs	Water balance equations	Constitutive equations
Interception reservoir	$\frac{dS_i}{dt} = P - E_i - P_e$ (4.1)	$E_i = \begin{cases} E_0; & S_i > 0 \\ 0; & S_i = 0 \end{cases}$ (4.2) $P_e = \begin{cases} 0; & S_i < S_{i,max} \\ P; & S_i = S_{i,max} \end{cases}$ (4.3)
Unsaturated reservoir	$\frac{dS_u}{dt} = P_e - R_u - E_t$ (4.4)	$\frac{R_u}{P_e} = 1 - \left(1 - \frac{S_u}{(1+\beta)S_{u,max}}\right)^{\beta}$ (4.5) $\frac{E_a}{E_p - E_i} = \frac{S_u}{C_e S_{u,max}}$ (4.6)
Splitter and Lag function		$R_f = R_{uD}$ (4.7); $R_s = R_u(1-D)$ (4.8) $R_{fl}(t) = \sum_{i=1}^{T_{lag,f}} C_f(i) R_f(t-i-1)$ (4.9) $C_f(i) = i / \sum_{u=1}^{T_{lag,f}} u$ (4.10) $R_{sl}(t) = \sum_{i=1}^{T_{lag,s}} C_s(i) R_s(t-i-1)$ (4.11) $C_s(i) = i / \sum_{u=1}^{T_{lag,s}} u$ (4.12)
Fast reservoir	$\frac{dS_f}{dt} = R_{fl} - Q_{ff} - Q_f$ (4.13)	$Q_{ff} = \begin{cases} 0; & S_f \le S_{f,max} \\ (S_f - S_{f,max})/K_{ff}; & S_f > S_{f,max} \end{cases}$ (4.14) $Q_f = S_f / K_f$ (4.15)
Slow reservoir	$\frac{dS_s}{dt} = R_s - Q_s$ (4.16)	$Q_s = S_s / K_s$ (4.17)

(i.e. $S_{u,max}$) is expected [Gao et al., 2014b]. Since the climate is very similar in these adjacent catchments, we linked $S_{u,max}$ directly with dry season (November to April) averaged vegetation index (I_{NDVI}) according to a nonlinear relationship:

$$S_{u,max} = \alpha_{Su} I_{NDVI}^{\beta_{Su}} \tag{4.18}$$

α_{Su} and β_{Su} are two calibration parameters. Besides Equation 4.18, FLEX^{LV} uses the same equations as FLEX^{L}, thus resulting in 12 free calibration parameters. In the absence

Table 4.3: Uniform prior parameter distributions of the FLEX^{L}

Parameter	Range	Parameter	Range
$S_{i,max}$ (mm)	(0.1, 6)	K_{ff} (d)	(1, 9)
$S_{u,max}$ (mm)	(10, 1000)	$T_{lag,f}$ (d)	(0, 5)
β (-)	(0, 2)	$T_{lag,\,s}$ (d)	(0, 5)
C_e (-)	(0.1, 0.9)	K_f (d)	(1, 40)
D (-)	(0, 1)	K_s (d)	(10, 500)
$S_{f,max}$ (mm)	(10, 200)		

of more information, their prior distributions were assumed to be uniform within rather wide limits (α_{Su}=5000-15000, β_{Su}=7-14). The water balance and constitutive functions are kept the same as in FLEX^{L}.

4.3.3. FLEX^{LM}

In this model set-up, $S_{u,max}$ was not estimated by calibration, but it was determined independently using the Mass Curve Technique (MCT), based on the assumption that the root zone is a reservoir that allows ecosystems to overcome droughts with approximately 20 years return periods, as found by Gao et al. [2014b]. Therefore, $S_{u,max}$ was estimated based on observed climate (amount and seasonality of precipitation), and ecosystem transpiration during the dry season (by first estimating the annual average transpiration from the water balance, and subsequently translating this into dry season transpiration by using an NDVI ratio). For details of the MCT approach, the reader is referred to Gao et al. [2014b]. Here we fixed the MCT-derived $S_{u,max}$ to allow the system to overcome drought with 20 years' return period. Using the same equations as FLEX^{L}, FLEX^{LM} therefore has 10 free calibration parameters. Note that until here, all models are lumped.

4.3.4. FLEX^{T}

LANDSCAPES CLASSIFICATION

Based on the recently formalized metric Height Above the Nearest Drainage (HAND), topographic data were used to define landscape classes with different hydrological function [Savenije, 2010; Nobre et al., 2011]. These classes were then associated with individual model structures, that operate in parallel and that generate a combined system of outflows based on the areal proportions of each landscape class. This strategy was found to be valuable for providing more robust representations of the observed system dynamics in a range of previous studies in contrasting environments [Gao et al., 2014a; Gharari et al., 2014; Hrachowitz et al., 2014]. From preliminary terrain analysis, three dominant landscape classes or hydrological response units could be identified for the study catchments: wetlands, terraces and hillslopes. Following the suggestions of Rennó et al. [2008] and [Gharari et al., 2011], the combined use of HAND and local slope allowed the definition of the three HRUs used in this study. Locations with HAND<5m were treated as wetlands, locations with HAND >5m and slope <0.1 were classified as terraces and locations with HAND>5m and slope>0.1 were regarded as hillslopes. The different landscapes proportions of the six catchments are shown in Figure 4.1f and Ta-

ble 4.1.

MODEL STRUCTURE

The model structure of FLEX^{T} is shown in Figure 5.3. The model structures for the three different landscapes operate in parallel. The only connection of these components is the common groundwater reservoir.

The main difference between the three parallel model structures is the architecture of the unsaturated root zone reservoir S_u. To fulfil the contrasting functions of water retention and drainage, hillslopes are often characterized by comparatively large root zone storage capacities ($S_{u,max,H}$), due to deeper ground water and perennial forest cover which buffers for dry periods. The partitioning between drainage and retention is here described by the non-linear reservoir of the Xinanjiang model (Equation 4.5) [Zhao, 1980; Liang et al., 1994]. Water in excess of the storage capacity is split into one part that is routed through the fast reservoir to the channel by subsurface storm flow ($R_{f,H}$) and another part that recharges the groundwater reservoir by preferential flow ($R_{s,H}$).

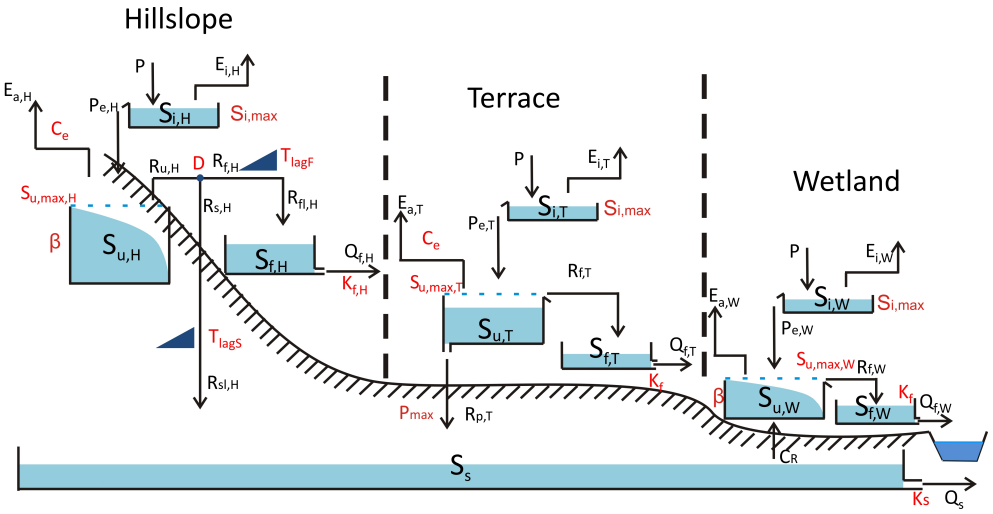

Figure 4.3: Model structure of the FLEX^{T}

In contrast with the largely lateral movement of water on hillslopes, the main direction of water movement on terraces is vertical, due to its flat topography and lower hydraulic gradient. Thus most infiltrating water in terraces is either stored or recharges ($P_{p,T}$) the groundwater reservoir. Only in response to relatively major storm events or extended wet periods, terraces may generate lateral flow ($R_{f,T}$).

On wetlands, the root zone storage capacity ($S_{u,max,W}$) is relatively low due to the shallow groundwater table. As a consequence, wetlands are characterized by higher runoff coefficients than hillslopes, as excess water will be directly and rapidly routed to the stream. In contrast to the other landscape units, wetlands are frequently close to saturation, and transpiration is therefore rather energy limited. The main functions of

Table 4.4: The water balance equations and constitutive equations of each reservoirs in the FLEX^{T} model

Reservoirs	Water balance equations	Constitutive equations
Interception reservoir for hillslope	Same as FLEX^{L}	Same as FLEX^{L}
Unsaturated reservoir for hillslope	Same as FLEX^{L}	Same as FLEX^{L}
Splitter and lag function	Same as FLEX^{L}	Same as FLEX^{L}
Fast reservoir for hillslope	Same as FLEX^{L}	Same as FLEXL
Interception reservoir for terrace	Same as hillslope	Same as hillslope
Unsaturated reservoir	$\frac{dS_{u,T}}{dt} = P_{e,T} - E_{a,T} - R_{p,T} - R_{f,T}$ (4.19)	$R_{f,T} = \begin{cases} 0; & S_{u,T} \le S_{u,max,T} \\ P_{e,T}; & S_{u,T} > S_{u,max,T} \end{cases}$ (4.20) $\frac{E_{a,T}}{E_0 - E_{i,T}} = \frac{S_{u,T}}{C_e S_{u,max,T}}$ (4.21) $R_{p,T} = P_{max}$ (4.22)
Fast reservoir	$\frac{dS_{f,T}}{dt} = R_{f,T} - Q_{f,T}$ (4.23)	$Q_{f,T} = S_{f,T}/K_{f,TW}$ (4.24)
Unsaturated reservoir for wetland	$\frac{dS_{u,W}}{dt} = P_{e,W} + C_R - E_{a,W} - R_{f,W}$ (4.25)	$\frac{R_{f,W}}{P_{e,W}} = 1 - \left(1 - \frac{S_{u,W}}{(1+\beta)S_{u,max,W}}\right)^{\beta}$ (4.26) $E_{a,W} = E_0 - E_{i,W}$ (4.27) $C_R = (p_T/p_W)R_{p,T}$ (4.28)
Fast reservoir for wetland	$\frac{dS_{f,W}}{dt} = R_{f,W} - Q_{f,W}$ (4.29)	$Q_{f,W} = S_{f,W}/K_{f,TW}$ (4.30)
Slow reservoir	$\frac{dS_s}{dt} = p_H R_{sl,H} + p_T R_{f,T} - p_W C_R - Q_s$ (4.31)	$Q_s = S_s/K_s$ (4.32)

Table 4.5: Uniform prior parameter distributions of the FLEX^{T}

Parameter	Range	Parameter	Range
$S_{i,max}$ (mm)	(0.1, 6)	D (-)	(0, 1)
$S_{u,max,H}$ (mm)	(10, 1000)	$K_{f,H}$ (d)	(1, 9)
β (-)	(0, 2)	$T_{lag,f}$ (d)	(0.5, 5)
C_e (-)	(0.1, 0.9)	$T_{lag,s}$ (d)	(1, 90)
P_{max} (-)	(0.1, 0.9)	K_f (d)	(1, 40)
$S_{u,max,T}$ (-)	(0.1, 0.9)	K_s (d)	(10, 400)
$S_{u,max,W}$ (-)	(0.1, 0.9)		

wetlands are thus lateral drainage and transpiration.

The three landscape units described are connected by a common groundwater reservoir, recharged by hillslopes ($R_{sl,H}$) and terraces ($P_{p,T}$), and with capillary rise (C_R) to wetlands. Due to the lack of knowledge and the intention to reduce number of free parameters, it was assumed that the capillary rise from groundwater to wetland in dry seasons is the same amount of water which percolates from terraces.

The transpiration is estimated through different methods. On hillslopes and terraces, we estimated actual transpiration based on soil moisture and potential evaporation, as in the lumped model FLEX^{L}. On wetlands, due to the relatively sufficient water supply, actual transpiration is assumed to occur at potential rates after canopy interception [Mohamed et al., 2012].

There are 13 free calibration parameters in FLEX^{T}. All equations are listed in Table 4.4, and prior parameter distributions are shown in Table 4.5.

4.3.5. FLEX^{TM}

To test the integrated influence of topographic and vegetation information on model performance and model transferability, we extended the FLEX^{T} model into FLEX^{TM}. In FLEX^{TM} , the averaged root zone storage capacity on hillslopes ($S_{u,max,H}$) and on terraces ($S_{u,max,T}$) was calculated based on an estimate of the catchment average $S_{u,max}$ as obtained from the MCT approach and the dry season NDVI in different landscapes ($I_{NDVI,H}$ on hillslopes and $I_{NDVI,T}$ on terraces):

$$S_{u,max,H} = S_{u,max} I_{NDVI,H} / I_{NDVI} \tag{4.33}$$

$$S_{u,max,T} = S_{u,max} I_{NDVI,T} / I_{NDVI} \tag{4.34}$$

In this case, FLEX^{TM} considers both the vegetation and topographic information. The number of free calibration parameters is 11, which is the same as for FLEX^{L}. Note that due to the shallow groundwater level and the potential importance of capillary rise, NDVI is unlikely to reflect $S_{u,max}$ in wetlands. Therefore, the root zone storage capacity of wetlands ($S_{u,max,W}$) is set as a free calibration parameter.

4.4. MODEL EVALUATION

4.4.1. OBJECTIVE FUNCTIONS

To allow for the model to adequately reproduce different aspects of the hydrological response, i.e. high flow, low flow and the flow duration curve, and thereby increase model realism, a multi-objective calibration strategy was adopted in this study. Specifically, the models were calibrated to the Kling-Gupta efficiencies [Gupta et al., 2009] of flows (I_{KGE}), of the logarithm of flows to emphasize low flows (I_{KGL}), and of the flow duration curve (I_{KGF}) to evaluate the modelled flow frequency dynamics.

4.4.2. MODEL CALIBRATION

The MOSCEM-UA algorithm [Vrugt et al., 2003] was used as the calibration algorithm to find the Pareto-optimal solutions defined by the three objective functions. There are three parameters to be set for MOSECEM-UA: the maximum number of iterations, the number of complexes, and the number of random samples that is used to initialize each complex. In order to ensure fair comparisons, we set the parameters of MOSCEM-UA based on number of model parameters. Therefore, the number of complexes is equal to number of free parameters n; the number of random samples is equal to $n * n * 10$; the number of iterations was set to 50000.

4.4.3. EXPERIMENTAL DESIGN OF TRANSFERABILITY TEST

In this study, 5 models (FLEX^{L}, FLEX^{LV}, FLEX^{LM}, FLEX^{T}, FLEX^{TM}) have been used to test model transferability among 6 nested catchments (P.4A, P.20, P.21, P.42, P.76, P.77). Model performance both during calibration and transferability was quantified by three objective functions (I_{KGE}, I_{KGF}, I_{KGL}). The detailed procedure of the experiment is listed as follows:

1) Automatically calibrate one model based on rainfall-runoff data of each catchment using the MOSCEM-UA algorithm. The behavioural parameters are retained;

2) Transfer both, model and behaviour parameter sets to the other 5 catchments, which have different rainfall and potential evaporation as forcing data;

3) Follow the same procedure for all 5 model set-ups.

4) Analyse model transferability in different landscapes by testing the performance of the five model set-ups with regard to: simulated hydrograph, flow duration curve, hydrograph components and water balance of different landscapes.

4.5. RESULTS

4.5.1. THE INFLUENCE OF TOPOGRAPHY AND VEGETATION ON MODEL TRANSFERABILITY

Figure 4.4 illustrates the performance of the five models with respect to their objective functions, both, in the respective donor (calibration) and receiver catchments (transferability). In general the calibration performance of all five models in the donor catchments is similarly good for all objective functions. This indicates that all five models can reproduce the hydrographs and flow duration curves in all six study catchments, as both their model structures and parameters can represent the hydrological characteristic of the calibrated donor catchments to some extent. When transferring the calibrated parameters from the donor to the receiver catchments, the five models exhibit quite distinct potential for transferability.

TRANSFERABILITY OF FLEX^{L}

As shown in Figure 4.4, the model performance of FLEX^{L} deteriorates dramatically in most cases while doing transferability tests, clearly illustrated by the averaged objective functions in the right column of this figure. This is in particular true for transferring the model from P.4A to P.42, P.76, P.77, and from P.42, P.76, P.77 to P.4A, P.20, P.21, especially for I_{KGE} (the representation of the hydrograph) and I_{KGF} (the representation of the flow duration curve). Specifically, when transferring the model from P.4A to P.42, P.76, P.77, I_{KGE} drops to 0.04, 0.23 and 0.41; I_{KGF} drops to 0.11, 0.25 and 0.46. More considerably, transferred from P.42, P.76, P.77 to P.4A, I_{KGE} drops significantly to -0.93, -0.75, -0.28; and I_{KGE} decreases to -0.92, -0.74 and -0.26. The results reveal that some dominant processes may be missed in the FLEX^{L} model, which hindered its transferability among these catchments. For I_{KGL} (representing the baseflow simulation), its deterioration while transferring is not as remarkable as I_{KGE} and I_{KGF}, except transferring from other catchments to P.20. This might be due to the similar recession processes among these catchments except P.20. Interestingly from Figure 4.4, we can also note that FLEX^{L} has certain transferability potential, when transferring from P.20 and P.21 to other catchments. This indicates that the selection of donor catchments is essential if the model does not include catchments' heterogeneity.

For illustrative purposes, the hydrograph and FDC are shown in Figures 4.5 and 4.6 for the receiver catchment P.4A that was modelled with the parameter set obtained from

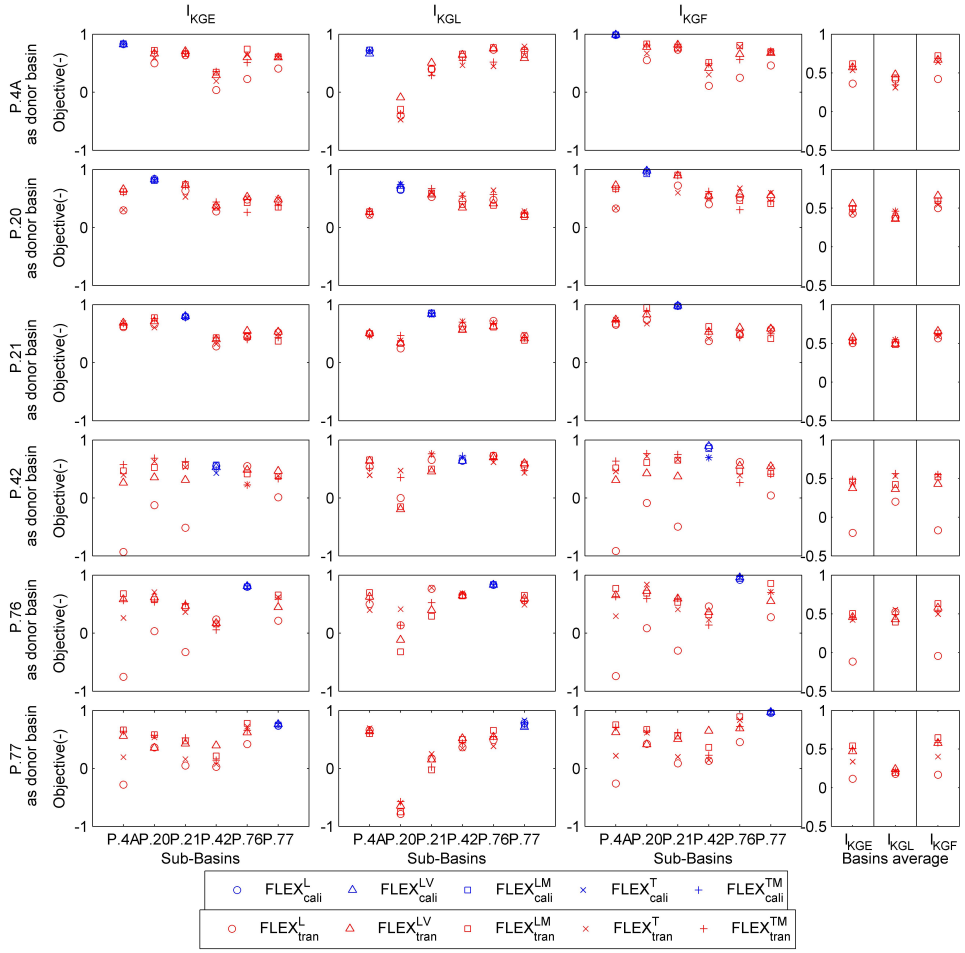

Figure 4.4: The calibration ($FLEX^{L}_{cali}$, $FLEX^{LV}_{cali}$, $FLEX^{LM}_{cali}$, $FLEX^{T}_{cali}$, and $FLEX^{TM}_{cali}$) and transferability ($FLEX^{L}_{tran}$, $FLEX^{LV}_{tran}$, $FLEX^{LM}_{tran}$, $FLEX^{T}_{tran}$, and $FLEX^{TM}_{tran}$) results of four models in six catchments. Three objective functions, in the left three columns, are used to quantify model performance in donor catchments and in receiver catchments. The first column is the performance of I_{KGE}; the second column is the performance of I_{KGL}; and the third column is the performance of I_{KGF}. The first row shows the results of transferring five models and their optimized parameters sets from P.4A as the donor catchment to the other five catchments. The donor catchments are P.20, P.21, P.42, P.76, and P.77 from row 2 to row 6 in turn. Blue symbols represent the calibrated results in donor catchments. Red symbols are the transferred results in receiver catchments. Circles indicate the model performance of $FLEX^{L}$; triangles indicate the model performance of $FLEX^{LV}$; squares indicate the model performance of $FLEX^{LM}$; x-symbols indicate the model performance of $FLEX^{T}$ model; and crosses indicate the model performance of $FLEX^{TM}$ model. The three columns of boxes in the right hand side show the averaged values of three objective functions in five receiver catchments.

the donor catchment P. 42. These catchments have very different landscapes: P.42 is relative flat and has a low vegetation cover, while P.4A is relatively steep and well covered

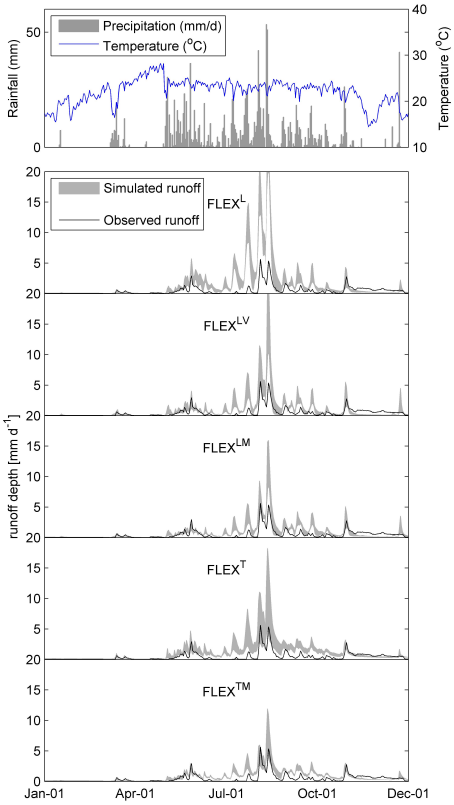

Figure 4.5: Simulated hydrograph of five models in P.4A catchment. The behavioural parameters are calibrated based on rainfall-runoff data in P.42 catchment, and then transferred both model and parameters from P.42 to P.4A.

by forest. Both the hydrograph and the FDC show that FLEX^{L} substantially overestimates flow, most notably during high flow conditions. The results further illustrate that directly transferring parameters obtained from FLEX^{L} without consideration of the differences in hydrological function may result in serious misrepresentations of the system response in the receiver catchments, similarly to what was reported in many previous studies [Heuvelmans et al., 2004; Uhlenbrook et al., 2010; Gao et al., 2014a].

TRANSFERABILITY OF FLEX^{LV}, FLEX^{LM}

In the FLEX^{LV} model formulation, the parameter $S_{u,max}$ was linked to vegetation heterogeneity via dry seasonal NDVI. It was found that prior estimates of $S_{u,max}$ in FLEX^{LV} did little to improve the calibration performance which remained close to the performance of FLEX^{L} for all donor catchments (Figure 4.4). Yet, this piece of information substantially enhanced model transferability for most receiver catchments. This is illustrated in Figure 4.4, where it can be seen that the transferability substantially improved

from P.4A with the densest vegetation cover (NDVI=0.773) to other catchments with less dense vegetation cover P.20 (NDVI=0.732), P.42 (NDVI=0.682), P.76 (NDVI=0.671) and P.77 (NDVI=0.732) for I_{KGE} and I_{KGF}. FLEX^{LV} enhanced model transferability more clearly from catchments with lower NDVI (P.42 and P.76) to catchments with higher NDVI (P.4A, P.20, P.21, P.77). More specifically, when transferring the models from P.42 to P.4A, I_{KGE} increases from -0.93 (FLEX^{L}) to 0.26 (FLEX^{LV}), and I_{KGF} increases from -0.92 to 0.30; while transferring from P.76 to P.4A, the I_{KGE} goes up from -0.75 to 0.58, and I_{KGF} improves from -0.74 to 0.65; and when transferring from P.77 to P.4A, the I_{KGE} improves from -0.28 to 0.55, and I_{KGF} increases from -0.26 to 0.62. However the obvious improvement of FLEX^{LV} performance does not occur when P.20 and P.21 (with intermediate vegetation cover) are used as donor catchments. In those cases FLEX^{L} performs comparatively well. The improvement of FLEX^{LV} performance is not obvious among catchments with similar vegetation cover, i.e. from P.4A to P.21, from P.42 to P.76, and vice versa. When the NDVI values of donor and receiver catchments are similar (such as P.20 and P.77), the transferability of FLEX^{LV} and FLEX^{L} is also similar. This indicates that the NDVI information can increase model transferability when two catchments have different vegetation cover, and especially from sparsely to more densely vegetation covered catchments.

The transferability of FLEX^{LM} is similar to that of FLEX^{LV} in most cases, which is obviously shown from the averaged objective functions shown in the right columns of Figure 4.4. However, when we zoom to specific case studies, their performance is case specific. While transferring from P.42 to P.4A P.20 P.21, the FLEX^{LM} works obviously better than FLEX^{LV}. FLEX^{LV} has better performance when transferring from P.77 to P.42 and from P.42 to P.77.

The results indicate that transferability strongly benefits from inclusion of vegetation information in FLEX^{LV} and FLEX^{LM} model for I_{KGE} and I_{KGF} in most cases. It was further found that the improvement of I_{KGL}, emphasizing the low flow part of the hydrograph, is less pronounced than for I_{KGE} and I_{KGF}. In this study, this can be attributed to two reasons. Firstly, only the root zone storage capacity ($S_{u,max}$) was regionalized, and other parameters were fixed, including the parameters controlling fast and slow recessions. Secondly, this might be influenced by human activity through groundwater abstraction, e.g. for irrigation, that becomes most relevant during dry periods, thus having a proportionally higher influence on base flow than on high flows. The improved high flow performance also becomes apparent in the example given in Figures 4.5 and 4.6 for the transfer of P.42 to P.4A. The results indicate that both the MCT and parameter regionalization techniques, can to some extent reflect the relationship between $S_{u,max}$ and vegetation. The strength of FLEX^{LM} compared with FLEX^{LV} is that the latter has two more free calibration parameters.

TRANSFERABILITY OF FLEX^{T}, FLEX^{TM}

Incorporating topography information, FLEX^{T} increased model transferability significantly as compared to FLEX^{L}, in particular when the donor and the receiver catchments have pronouncedly different topography (Figure 4.1, Table 4.1, Figure 4.4). For example, when transferring the model from P.42 with relatively subdued topography to P4A, a relatively low relief catchment, I_{KGE} improves from -0.93 (FLEX^{L}) to 0.40 (FLEX^{T}), and I_{KGF} improves from -0.92 to 0.46; while transferring P.76 to P.4A, the I_{KGE} of P.4A goes up

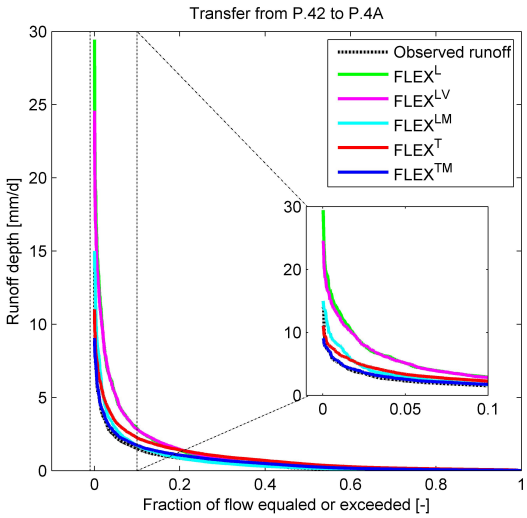

Figure 4.6: The reproduced flow duration curves by five models, when we calibrated the model parameters based on basin P.42, and then transferred both model and parameters to P.4A.

from -0.75 to 0.26, and I_{KGF} increases from -0.74 to 0.30; then the I_{KGE} goes up from -0.28 to 0.20, and I_{KGF} increases from -0.26 to 0.22 when transferring the model from P.77 to P.4A. The better transferability of FLEX^{T} is owed to the fact that it can better describe the contrasting hydrological functions of different landscapes by considering different runoff generation mechanism in these landscape units [Gao et al., 2014a; Gharari et al., 2014]. In only two cases (from P.20 to P.21; from P.42 to P.76), FLEX^{L} performs slightly better than FLEX^{T}, which might due to the more complicated model structure of FLEX^{T} which probably increased model complexity [Pande et al., 2009], and the compensations among internal fluxes.

Compared with FLEX^{LV} model, FLEX^{T} performs almost equally well in transferability tests, except for P.77 as donor catchment. In details, FLEX^{T} outperforms FLEX^{LV} while transferring from P.42 to P.4A P.20 P.21, from P.42 to P.20, from P.76 to P.77, and from P.77 to P.20. On the other hand, FLEX^{LV} performs better while transferring from P.4A to P.42, from P.20 to P.4A, from P.42 to P.76, from P.76 to P.4A, and from P.77 to P.4A P.21 P.42. These diverse results might due to the different dominant roles of topography or vegetation among different catchments, and perhaps uncertainty of both FLEX^{LV} and FLEX^{T}. Similar as FLEX^{LV}, except for P.77 as calibrated catchment, the transferability of FLEX^{T} and FLEX^{LM} are comparable. In some cases, FLEX^{T} works better than FLEX^{LM}, such as transferring from P.42 to P.20, and from P.76 to P.20. And FLEX^{LM} performs better while transferring from P.42 to P.76, from P.76 to P.4A, and P.77 as the donor catchment.

After combing vegetation information into FLEX^{T}, FLEX^{TM} exhibits similar transferability skills compared with FLEX^{LV}, FLEX^{LM} and FLEX^{T}. To avoid redundancy, in the following we thus only compared FLEX^{TM} with FLEX^{LM} and FLEX^{T}. For specific trans-

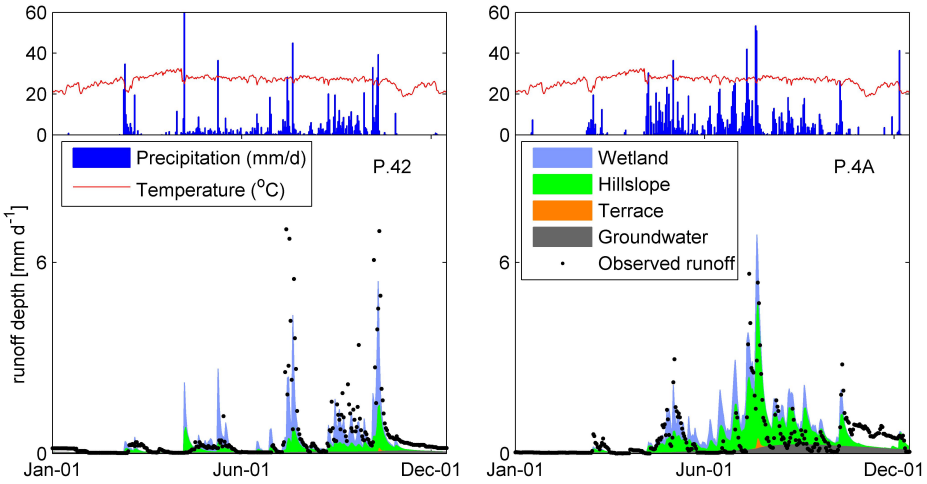

Figure 4.7: The hydrography components obtained by FLEX^{TM}, which are the average values of all simulated hydrographs, while we calibrated the model parameters based on basin P.42, and then transferred both model and parameters to P.4A.

fer cases, the transferability of three models is varying. When transferring from P.42 to P.4A P.20, FLEX^{TM} performs slightly better than FLEX^{LM}. And FLEX^{LM} works better while transferring from P.4A to P.76, from P.20 to P.76, and from P.42 to P.76. In some cases, FLEX^{TM} outperforms FLEX^{T}, such as from P.20 to P.4A, from P.42 to P.4A P.20 P.21, from P.76 to P.4A, and from P.77 to P.4A P.21. Interestingly, in specific cases FLEX^{T} even performs slightly better than FLEX^{TM}, such as transferring from P.4A to P.76, from P.20 to P.76, and from P.42 to P.76. This ambiguous transferability performance compared FLEX^{TM} with FLEX^{LM} and FLEX^{T} is potentially caused by the uncertainty of our transfer functions in FLEX^{TM} from lumped $S_{u,max}$ to $S_{u,max}$ of different landscapes, i.e. hillslopes and terraces (Equation 4.33, 4.34), which needs more investigation.

The reproduced hydrography and FDC of FLEX^{T} and FLEX^{TM} in P.4A, when P.42 performs as donor catchment, are exhibited in Figures 4.5 and 4.6. The figures show that FLEX^{T} can reproduce the observed hydrographs and flow duration curves significantly better than FLEX^{L} and even better than FLEX^{LV} in high flow simulation in this case, although FLEX^{T} exhibits somewhat wider uncertainty intervals. The stepwise improvement of both hydrograph and FDC of these five models, illustrates the importance of vegetation and topography on this model transferability case study. In this transferability test study, both vegetation information and topography data helped us to get more robust model transferability performance step by step. FLEX^{TM}, assisted by vegetation and topography data performed best among all these models.

4.5.2. THE SIMULATED WATER BALANCE OF FLEX^{TM} MODEL

The simulated components of hydrograph from different landscapes for the selected illustrative case (transfer from P.42 to P.4A) are given in Figure 4.7. In the P.42 catchment,

Table 4.6: Simulated water balance of different fluxes in catchment P.4A by calibrated parameter in P.42. Rainfall (P), interception (E_i), simulated runoff (Q_m), and groundwater flow are for the entire catchments. The rest fluxes are for the unit of each landscapes. $E_{a,H}$, $E_{a,T}$, $E_{a,W}$ indicate transpiration from hillslope, terrace and wetland. $Q_{f,H}$, $Q_{f,T}$ and $Q_{f,W}$ indicate subsurface flow from hillslope, and saturated overland flow from terrace and wetland separately. $R_{sl,H}$ indicates preferential flow to groundwater on hillslope; $P_{erc,T}$ indicates the percolation on terrace; C_R indicates the capillary rise from groundwater to unsaturated soil on wetland.

Entire catchment		Hillslope		Terrace		Wetland	
Fluxes	Uncertainty	Fluxes	Uncertainty	Fluxes	Uncertainty	Fluxes	Uncertainty
P (mm a^{-1})	1274	P (mm a^{-1})	1274	P (mm a^{-1})	1274	P (mm a^{-1})	1274
Q_m (mm a^{-1})	(144, 282)	$Q_{f,H}$ (mm a^{-1})	(69, 220)	$Q_{f,T}$ (mm a^{-1})	(0, 50)	$Q_{f,W}$ (mm a^{-1})	(511, 1419)
E_i (mm a^{-1})	(269, 451)	$E_{a,H}$ (mm a^{-1})	(506, 793)	$E_{a,T}$ (mm a^{-1})	(220, 688)	$E_{a,W}$ (mm a^{-1})	(502, 967)
Q_s (mm a^{-1})	(24, 53)	$R_{sl,H}$ (mm a^{-1})	(35, 63)	$P_{erc,T}$ (mm a^{-1})	(130, 708)	C_R (mm a^{-1})	(258, 1411)

firstly, the simulated result clearly shows that, towards the end of dry and the beginning of wet seasons, most runoff is generated from wetlands, although with limited areas (12.1%). Secondly, runoff generation from hillslopes is not comparable with its dominant area proportion (60.6%), especially towards the end of dry seasons. However, with the increase of soil moisture, the proportion of runoff from hillslopes becomes more important during the middle of wet seasons. Thirdly, terraces do not generate direct runoff, except for the end of the wet season, although they cover a considerable area in the catchments (27.3%). P.4A has a similar hydrological characteristic, but due to the dominance of hillslopes (83.0%), a larger amount of runoff is generated from there.

From these two hydrographs, we also note that the recession of wetlands and terraces is faster than hillslopes, because the runoff generation mechanism is mainly saturated overland flow on wetlands and terraces, which is considered faster than the subsurface storm flow on hillslopes. Thus, in the recession periods after flood-peaks, runoff is mainly generated from hillslope, releasing water as shallow subsurface flow. Besides that, we can observe the impact of interception on rainfall-runoff processes and its indispensable role in hydrological models. In Figure 4.7, small rainfall events during dry seasons do not generate any significant amount of flow, in both observed and modelled hydrographs.

In Table 4.6, the uncertainties of all the simulated fluxes for the entire P.4A catchment as well as in its different individual landscapes elements and obtained by calibration of P.42, are given. The results suggest that wetlands generate more runoff (511-1419mm/a, the runoff from each unit area hereinafter) than hillslopes (69-220mm/a), due to their limited storage capacity. Terraces contribute least to storm flow (0-50mm/a) due to their flat slopes and, related to that, the elevated amounts of percolation (130-708mm/a). By comparison, we found that the fast runoff generated from wetlands of each unit is over 3-10 times larger than the runoff generated from each unit of hillslopes, not to mention terraces.

It is worthwhile to check the simulated evaporation from different landscapes as well. The simulated evaporation and transpiration from wetlands (502-967mm/a) is larger than hillslopes (506-793 mm/a), due to relative sufficient soil moisture supplied by the shallow groundwater table and capillary rise (258-1411mm/a). Simultaneously, evaporative fluxes from hillslopes are larger than from terraces (220-688 mm/a). Being less moisture constrained, wetlands not only generate larger proportion of runoff but also

contribute larger proportions of evaporation and transpiration than other landscapes. Although this is not new knowledge in hydrological and land surface modelling, this hillslope scale water-balance realism check is rarely implemented by modellers [Gao et al., 2014a], and is even more rare in model transferability tests.

4.6. DISCUSSION

4.6.1. THE INFLUENCE OF VEGETATION AND TOPOGRAPHY ON MODEL TRANSFERABILITY

The inclusion of vegetation information in the model by adapting $S_{u,max}$ to the observed environmental conditions, both by parameter regionalization and the MCT approach, improved model transferability in all catchments, even if all other model parameters were left unchanged. Our results suggest that the root zone storage capacity $S_{u,max}$ rather than being linked to soil texture, as described for example in the SWAT model [Arnold et al., 1995; Arnold and Fohrer, 2005], relates to climate and vegetation, as suggested in a recent study [Gao et al., 2014b]. For example, due to the less dense vegetation in P.42, a lower root zone storage capacity $S_{u,max}$ is required there than in more densely vegetated P.4A. Thus when using P.42 as donor catchment and directly transferring $S_{u,max}$ to P.4A in FLEX^{L}, the buffer capacity of $S_{u,max}$ is too low, resulting in significant overestimation of peak flows. In contrast, adapting $S_{u,max}$ to the denser vegetation cover and thus higher canopy water demand of P.4A in FLEX^{LV}, the model's ability to moderate high flows significantly increases.

Few examples explicitly studied the influence of topography on model transferability, although numerous hydrological models [Beven and Kirkby, 1979; Reggiani et al., 2000; Savenije, 2010; Hrachowitz et al., 2014] have been developed explicitly based on topographic information. In this study, we classified the entire catchment into different units based on topography information, and then associated different model structures to the individual units. This distribution strategy, especially the discretization of the root zone storage capacity, has improved both model realism and transferability effectively. For example, P.42 has large spatial extent of wetlands and terraces, which are characterized as relatively shallow root zone storage capacity. In contrast, P.4A is dominated by hillslopes, with larger $S_{u,max}$, due to the higher moisture deficit on hillslopes, and more water is needed to establish hydrological connectivity. The FLEX^{T} model takes the proportions of three different landscapes into account, which makes the model suitable to account for the major differences of root storage capacity. This significantly increased the performance in model transferability with respect to the lumped model. The same phenomenon happens in other catchments when transferring from relative flat to steep catchments, such as P.42 to P.20 P.21 P.77, from P.76 to P.4A P.20 P.21 P.77.

The major difference between the lumped model (FLEX^{L}) and the other models (FLEX^{LV}, FLEX^{LM}, FLEX^{T}, and FLEX^{TM}) is the description of the unsaturated root zone reservoir (S_u). FLEX^{LV} and FLEX^{LM} regionalized the storage capacity of S_u ($S_{u,max}$) by vegetation information; FLEX^{T} distributes the $S_{u,max}$ in different landscapes by topography information; while FLEX^{TM} combined both topography and vegetation information together. Therefore, the significant improvement of all these models, compared with FLEX^{L}, indicates that increasing the detailed description of root zone storage capacity is essential to

increase model transfer.

Overall, the models FLEX^{LV} FLEX^{LM} FLEX^{T} and FLEX^{TM} show comparable performance in model transferability, although one may perform better than the other in specific catchments. As topography and vegetation are often correlated [e.g. Savenije, 2010], the similar transferability performance suggests that in many cases and given the incomplete knowledge of the system, only one type of additional information, i.e. topography or vegetation, is sufficient to adequately well account for process heterogeneity in models and to allow for adequate model transferability. For individual catchments, however, the performance of those models differs, which may indicates switches in dominant controls. For example, while in most cases there was no evidence for either vegetation or topography being dominant, one exception was the model transfer from P.77 to the other catchments. For this transfer the importance of vegetation heterogeneity was clearly dominant over the heterogeneity in topography, as FLEX^{TM} and FLEX^{LM} had comparable transfer skills while clearly outperforming FLEX^{T}.

It is worthwhile to remark that as donor catchments P.42 P.76 and P.77 have relatively short time series of data (Table 4.1). This may be a reason why lumped models calibrated on these data cannot have consistent performance when transferred to other catchments. A more consistent model performance could be achieved when considering vegetation or topography heterogeneity. This suggests that if a model together with its parameterization is a more suitable representation of the observed system , it may need less data to obtain a robust and hydrologically consistent calibration.

4.6.2. CONSISTENCY OF MODEL RESULTS

The distributed model FLEX^{TM}, not only has generally better performance than lumped model, but also, and importantly, shows consistent estimates of internal catchment processes. Its complexity, therefore, is necessary to achieve a suitable processes representation.

The parallel structure of this model is supported by field experiments [Zhao, 1984; Pfister, 2006], nearly all catchment isotopic and piezometer experiments showed the different runoff generation mechanism between riparian area and the hillslopes [McGlynn and McDonnell, 2003; Molenat et al., 2008; Detty and McGuire, 2010]. On plateaus or terraces, most proportion of rainfall vertically infiltrates and is stored in root zone and then evaporated or percolated, due to its flat topography and poor drainage condition [Savenije, 2010]. Secondly and more importantly, the dynamics of the individual modelled hydrograph components (Figure 4.7, Section 5.2) and evaporation (Table 4.6) meet the expected system internal dynamics and do not contradict with existing experimental knowledge in hillslope and catchment hydrology [McGlynn and McDonnell, 2003]. Specifically, in the beginning of wet season most peak flows are generated from wetlands. Gradually, more water is discharged from hillslopes as the catchment wets up and the soil moisture deficits on the hillslopes are eventually reduced. During large storm events, terraces become saturated, therefore contributing to runoff to some extent. Thirdly, however due to the more complex model structure, more internal fluxes and larger number of parameters, it is difficult to validate our model by split-sample validation in one specific study site. With the help of transferability test, we can test our proposed model structure by transferring from calibrated donor catchment to receiver

catchments. The good transfer performance further supports our proposed model structure.

4.6.3. THE CO-EVOLUTION OF TOPOGRAPHY, VEGETATION AND SOIL

It is an interesting finding in our results that both vegetation and topography information can help us to improve model transferability almost to the same extent. Our basic assumption of FLEX-Topo type models (FLEX^{T} and FLEX^{TM}) is that topography is an integrated indicator of catchment characteristics, such as climate, vegetation cover, soil texture and geology [Savenije, 2010]. In the catchments investigated in this study, climate is very similar due to their spatial proximity, yet the catchments show significant differences in land cover. In a previous study [Gao et al., 2014a] we showed the feasibility of using topography data to derive the vegetation cover in a large cold-arid catchment. Here, we tested the linkage between topography, vegetation and soil texture.

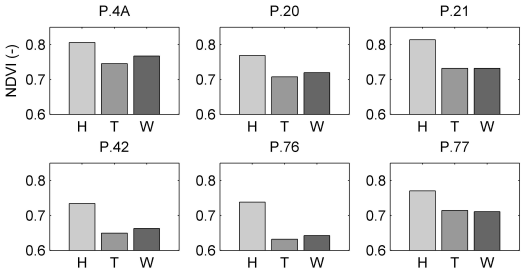

Figure 4.8: Different dry seasonal NDVI values in three different landscapes in 6 catchments. H represents hillslope; T represents terrace; W represents wetland.

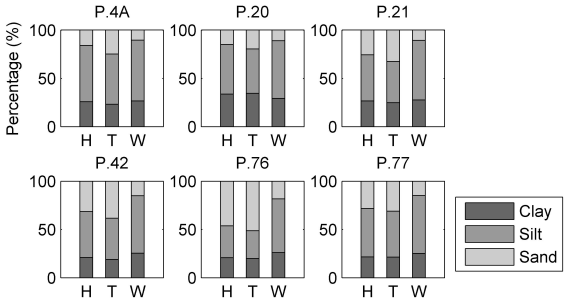

Figure 4.9: Soil textures (proportions of clay, slit and sand) in three different landscapes in 6 catchments. H represents hillslope; T represents terrace; W represents wetland.

Applying spatial analysis, we calculated the different vegetation cover in dry seasons in different landscapes (Figure 4.8), by overlapping the dry seasonal NDVI map (Figure 4.1e) and our landscape classification map (Figure 4.1f). We found that the NDVI on hill-

slope is always the largest one among these three landscapes. Wetlands have larger values than terraces in four (P.4A, P.20, P.42, and P.76) among these six catchments, and almost the same in other two catchments. This means that hillslopes have a higher canopy water demand, which can be associated with a denser vegetation cover, than wetlands and terraces, because hillslopes are mostly covered by forests, and thus requiring larger root zone storage capacities. On terraces, the coarser soil has larger conductivity and easier for percolation. Therefore, in dry periods the terraces in this region are dry and mostly covered by shrubs. Lots of wetlands are close to the river and covered by riparian vegetation, or used as paddy fields. This may cause lower NDVI in wetlands than hillslopes, but larger than terraces.

Similar to the dry seasonal NDVI, we calculated the different soil texture in different landscapes (Figure 4.9). We found that there is a strong pattern between soil texture and topography-based landscapes classification in these six catchments as well. The proportion of sand on terrace soil is always larger than hillslopes, and the sand proportion on hillslopes is larger than wetlands in these six catchments. Wetlands have larger proportion of silt than hillslope, and the silt proportion on hillslopes is larger than terraces. The reason is due to the geomorphological dynamics [Hook and Burke, 2000; Huang and Nanson, 2007; Seibert et al., 2007]. The coarser materials can only be transported and deposited during flood events to the terraces, so coarser sand has larger proportion on terrace than other topographic units. On wetlands, finer soil particles are easier to be transport and deposited in low flow periods. These results are supported by the measured evidence of topography impact on soil texture [Seibert et al., 2007].

These results indicate that topography has strong influence on vegetation and soil texture. The reason is very likely due to the co-evolution of topography, soil, vegetation, geology and climate. These factors are not fully independent. In many cases, we can obtain other factors by easily observable factors. This co-evolution suggests that we do not need to consider all factors in our model to simulate the hydrological processes. In this case, only the topography and vegetation information helped to make our model more realistic. Based on this assumption, we can make our model simpler and dramatically reduce the number of parameters and hence parameter equifinality.

4.7. CONCLUSIONS

Landscapes are essential in determining the dominant runoff generation mechanisms, model structure and parameterization. In this study, we developed five conceptual models with different complexity: a classical lumped model serving as benchmark ($FLEX^{L}$), a lumped model linking root zone storage capacity and NDVI by a nonlinear function ($FLEX^{LV}$), a lumped model with MCT-derived root zone storage capacity ($FLEX^{LM}$), a semi-distributed topography based model ($FLEX^{T}$), and a semi-distributed topography based model with MCT and NDVI derived root zone storage capacity ($FLEX^{TM}$). Six catchments in the upper Ping River basin in Thailand were selected as case study to test the performance of the five model structures, by a calibration and transferability test. The successful calibration indicates that all five models can mimic the hydrological behaviour. But in model transfer to other catchments the performance was quite different. We found that:

1 Accounting for both vegetation and topographic heterogeneity allowed to distinguish catchment characteristics and to increase model transferability.

2 The FLEX-Topo modelling approach is efficient in describing topographic heterogeneity and in identifying different runoff generation mechanisms of different landscapes. The additional realism improves the transferability substantially.

3 Regionalization of root zone parameters based on vegetation indicators also adds to transferability. In this study we merely used NDVI to transfer root zone storage capacity. The improved model transferability demonstrates that these two variables are connected and can help to obtain better understanding of the interaction between ecosystems and hydrology. The MCT-derived root zone parameter did not only reduce the number of free parameters for calibration, but also increased model transferability both in lumped and semi-distributed models. The similar transferability performance of FLEX^{LV} and FLEX^{LM} further showed the feasibility of the MCT approach for root zone estimation and the connection between ecosystem and root zone storage capacity.

5

INTEGRATED GLACIER AND SNOW HYDROLOGICAL MODELLING IN THE URUMQI GLACIER NO.1 CATCHMENT

Glacier and snow melt water from mountainous areas is an essential water resource in northwest China, where the climate is arid. Therefore a hydrologic model including glacier and snow melt simulation is essential for water resources management and prediction under climate change. In this study, the Urumqi Glacier No.1 catchment in northwest China, with 52% of the area covered by glaciers, was selected as the study site. An integrated daily hydrologic model was developed to systematically simulate the hydrograph, separate the discharge into runoff from glacier and non-glacier, and establish the glacier mass balance (GMB), the equilibrium line altitude (ELA), and the snow water equivalent (SWE). Only precipitation and temperature data is required as forcing input. A degree-day model was used to simulate snow and glacier melt. Detailed snow melt processes were included in the model, including water holding capacity of the snow pack, and liquid water refreezing in the snow pack. A traditional rainfall-runoff model (Xinanjiang model) was applied to simulate the rainfall(snowmelt)-runoff process in non-glaciered area. Additionally, the influence of topography on the distribution of temperature and precipitation, and the impact of slope and aspect on snow and glacier melting were considered. The model was validated, not only by long-term observed daily runoff data, but also by intensively observed glacier data (GMB, ELA) and snow data (SWE). Parameter uncertainty and identifiability were analysed in our simulation by generalized likelihood uncertainty estimation (GLUE). Finally, the calibrated model in the Glacier No.1 catchment was capable to be upscaled to a larger catchment, which further verifies our model and parameter sets.

5.1. INTRODUCTION

Glacier and snow melt water, is an essential water resource in arid northwest China [Shi et al., 2000; Qin and Ding, 2010; Yao et al., 2007; Cheng et al., 2014]. It forms the lifeline of millions of downstream residents [Immerzeel et al., 2010; Ding et al., 2006], for agriculture and industry [Li et al., 2013a; Singh and Singh, 2001], and is crucial to maintain downstream ecosystems [Zhao and Cheng, 2002]. On the other hand, glaciers and snow are highly sensitive to climate change [Oerlemans and Fortuin, 1992; Oerlemans, 1994; Yao et al., 2012], including global warming and precipitation change [Liu et al., 2006], which threatens the water security downstream [Immerzeel et al., 2010], and increases the risks of relevant hazards [Moore et al., 2009; Liu et al., 2014].

To systematically understand both the water balance and hydrological processes in this region, it is crucial to integrate the observation data and our knowledge into a hydrological model. Due to the specific environment and landscapes, traditional rainfall-runoff models have great difficulty to simulate hydrological processes in these regions. Therefore there is an urgent need to develop an integrated hydrological model, taking glacier and snow melt into account.

Generally, glacier and snow melt models can be categorized into two classes. One is the energy balance model [Ohmura et al.; Hock, 2005; Blöschl et al., 1991], based on detailed observation and evaluation of surface energy fluxes to calculate the snow and ice melting. It is a physical-based model, which requires distributed detailed and precise measurements, which are hardly accessible in most cases. Alternatively, the temperature-index method [Braithwaite and Olesen, 1989; Hock, 2003; Zhang et al., 2006], which only requires widely accessible temperature data, is extensively applied in practice. Though it is not fully physically-based, as an integrated indicator for the whole energy budget [Hock, 2003], the temperature is sufficient and robust to estimate snow and ice melt [Schaefli et al., 2005].

In past research, glacier melt has been coupled with hydrological models, such as HBV [Konz and Seibert, 2010], and GSM-SOCONT [Schaefli et al., 2005]. And complicated glacier model, coupled with surface runoff, englacial storage and transport, subglacial drainage and flow in a subsurface aquifer, was developed by Flowers and Clarke [2002]. Glacier retreat and area shrinkage was also included in a glacio-hydrological model [Huss et al., 2010; Stahl et al., 2008].

However, most of these models were developed in Europe and North America, where there are long-term glacier observations. But in central Asia, due to the extremely severe environment, the lack of long-term glacier, snow, meteorology and hydrology observations is the bottle neck to develop models and implement systematic validation. Several glacio-hydrological models were implemented in the poorly gauged glacierized catchments in the Himalayas [Fujita et al., 2006; Fujita and Sakai, 2014], such as the TAC^D model [Uhlenbrook et al., 2004; Konz et al., 2007], and SNOWMOD [Singh et al., 2008]. Few previous studies in China also considered the influence of glaciers in their hydrological simulation [Zhao et al., 2013; He et al., 2014; Gao et al., 2012], with short time-series for validation.

From a scientific point of view, a hydrological model is not only an indispensable tool in engineering, but also an approach to systematically understand hydrological behaviour [Fenicia et al., 2008c; Clark et al., 2011a]. However, lack of data to validate simu-

lated results, especially the internal fluxes, is still a great challenge in hydrological model development [Hrachowitz et al., 2013b]. Various components and fluxes create equifinality and uncertainties [Beven and Binley, 1992], especially in subsurface fluxes. In contrast with hardly observable subsurface fluxes, it is relatively easy and reliable to validate our simulated glacier and snow results by measurement. In this case, the glacier and snow data, as important complementary information, provides a unique opportunity to validate our simulated internal fluxes in addition to the hydrograph.

The Urumqi Glacier No.1, as one of the intensively observed glacier and a member of World Glacier Monitoring Service (WGMS, http://www.geo.uzh.ch/microsite/wgms/), located in northwest China has the longest continuous monitoring glacial records in China, from 1959 to present [Ye et al., 2005; Li et al., 2010]. It provides an unique study site to develop and validate an integrated hydrological model incorporating glaciers and snow.

In this study, we extend the newly proposed landscape-based hydrological model, the FLEX-Topo [Savenije, 2010; Hrachowitz et al., 2014; Gharari et al., 2014; Gao et al., 2014b], to a glacierized catchment. The FLEX-Topo modelling framwork, with parallel model structures, is based on landscapes classification. And then different runoff generation mechanisms from different landscapes are considered. In this study, as an isolated landscape, a glacier sub-routine is coupled into the FLEX-Topo, as FLEX^G, which is a tailor-made model for the Urumqi Glacier No.1 catchment. The FLEX^G includes snow and glacier melt in glacierized area, and snow and rainfall-runoff processes in non-glaciered area. The influence of elevation on temperature and precipitation distribution have been considered. The influence of aspect on snow and ice melt is also considered. From this research, except for integrating our long-term observation and accumulated knowledge, we want to further know (1) whether the parsimonious temperature-index model is efficient for both hydrograph, glacier and snow simulation in this region; (2) the proportion of runoff generated from glaciered and non-glaciered area, and their runoff efficiency; (3) whether we can upscale the model to the downstream gauging station.

This paper has four sections: in the study site and data section, the study site and input data are introduced; in the model section, the model is described in detail; in the model evaluation section, several independent model evaluation methods are applied to validate simulation; in the results and discussion, the simulated results are presented and discussed; the results are summarized in the conclusions.

5.2. STUDY SITE AND DATA

5.2.1. STUDY SITE

The Urumqi Glacier No.1 catchment is located in the headwaters of the Urumqi River, in the Xinjiang Uyghur Autonomous Region in northwest China (43°50'N, 86°49'E) (Figure 5.1). Glacier No.1 is a small valley glacier with two branches, the east and west branches [Shi et al., 2000; Ye et al., 2005]. The maps of the Glacier No.1 is obtained from geodesy survey in 2001. The glacier is about 1.84 km^2 and 2.23 km long with elevation between 3740 and 4486 m a.s.l., the average ice thickness measured by radar in 2003 is about 50 m [Sun et al., 2003]. Figure 5.1 shows that the aspect of glacier is mostly facing north, and partly facing east/west. This illustrates the strong influence of topography on the glacier

distribution.

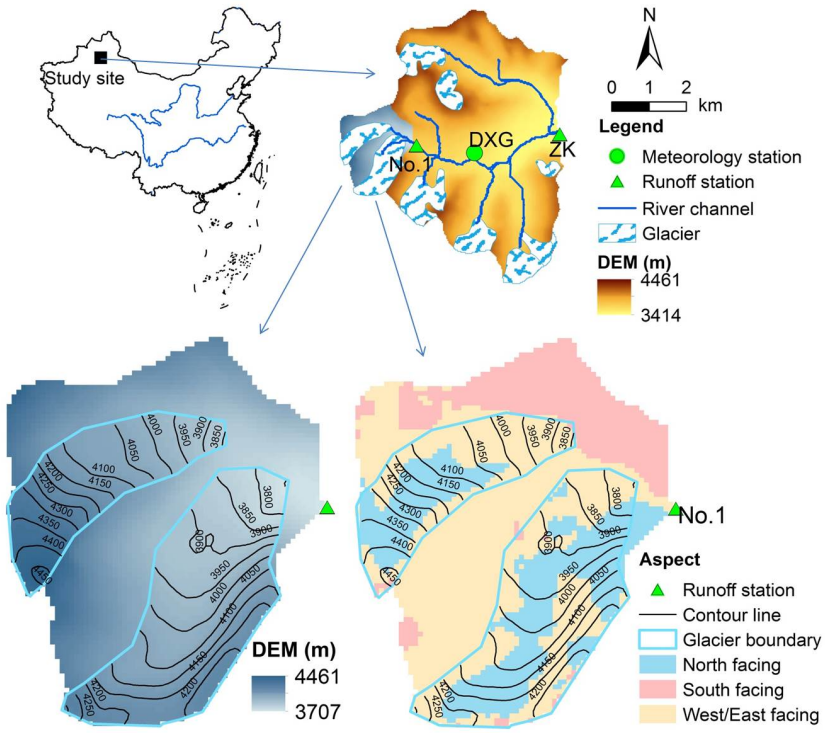

Figure 5.1: Locations of the Glacier No.1 (upper left); the DEM and glaciers cover of the ZK catchment; the detailed DEM and contour lines of the nested Glacier No.1 catchment; and the aspects of the Glacier No.1 catchment.

The glacier observation program at the Tianshan glacier station started in 1959 [Xie and Ge, 1965] and continued up to now. Field observations include glacier accumulation and ablation, meteorological and hydrological data collection. The glacier accumulation and ablation is observed by stake method. There is permanent stake network on the Glacier No1, properly distributed in different elevation zones (about 45–80 stakes in 8–9 rows) and additional snow pits [Ye et al., 2005]. The DXG (Da Xi Gou) is a meteorological station located in the catchment. And runoff is observed by two runoff gauge stations. The No.1 (Urumqi Glacier No. 1) runoff gauge station with a contributing drainage area of 3.34 km^2, has been set up 200 m downstream of the glacier terminus at 3689 m a.s.l, with 52% covered by glacier. Another gauge station, the ZK (Zong Kong), is located in the downstream, which controls an area of 28.9km^2, with 19.4% covered by glaciers. The land cover in non-glacier area is mainly bare soil/rock with sparse grass [Li et al., 2010].

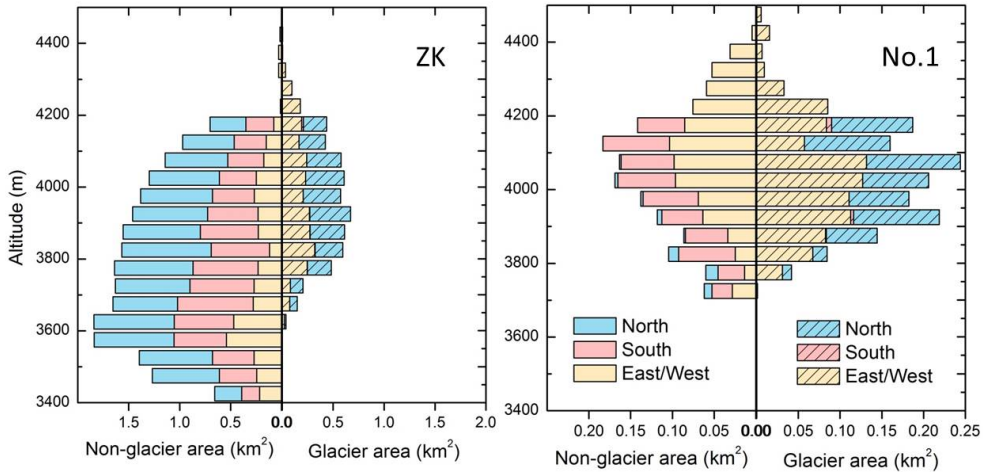

Figure 5.2: Area of different elevation and aspects of the glacierized region and the non-glacierzied region in the ZK catchment and the No1 catchment.

5

5.2.2. GLACIER DATA

Glacier mass balance (GMB) and equilibrium line altitude (ELA) are two essential indicators to quantify the glacier change with climate change [Cuffey and Paterson, 2010]. Both the GMB and ELA are observed by stake method. From the height change of stakes above the ice surface in certain hydrological year (the beginning of October to the end of next September), we can calculate the mass balance of each location in that year. Contributions from several processes determine the GMB at a point:

$$\frac{\mathrm{d}S_\mathrm{g}}{\mathrm{d}t} = P + A_\mathrm{a} + A_\mathrm{w} - Q_\mathrm{s} - E_\mathrm{g} \tag{5.1}$$

representing precipitation (P), avalanche (A_a) and wind deposition (A_w), discharge from glacier (Q_g), and sublimation (E_g) which can be either positive or negative. For the entire glacier in long time series, $\frac{\mathrm{d}S_\mathrm{g}}{\mathrm{d}t} = P - Q_\mathrm{s}$ makes a good approximation to Equation (5.1) [Cuffey and Paterson, 2010]. Based on point observation, subsequently, the GMB of the entire glacier can be calculated by contour maps by accumulation and ablation [Elder et al., 1992].

And we measured the ELA of each hydrological year by measuring stakes as well. The annual ELA is the altitude where the ice accumulation and ablation are equal, in another words it is where the mass balance of that year was zero [Dong et al., 2012].

The annual GMB and ELA are available from 1959 to 1966, and from 1980 to 2006 (Table 5.1) . From 1967 to 1979, the observation was stopped. And the data (1967-1979) was reconstructed based on the relationship between summer air temperature and mass balance during 1959-1966 [Zhang, 1981].

5.2.3. HYDRO-METEOROLOGICAL DATA

Hydrology data

Water level have been observed in two gauge stations during the main melting period (June–August) from 1985 to 2006 (Table 5.1). And flow velocity of the cross section was observed in different flow conditions, covering low flows and high flows. And then rating-curve method was applied to derive the discharge from water level.

Meteorological data

The meteorological data during 1958–2006 (Table 5.1) have been collected at the DXG meteorological station located at 3539 m a.s.l., about 3 km downstream of the glacier (Figure 5.1). The mean annual air temperature is -5.1°C, with -20 °C in winter and over 0 °C from June to August. Annual average precipitation is 450 mm a^{-1} [Ye et al., 2005]. Over 90% of precipitation occurs during April to September. Potential evaporation was calculated by Hamon equation by air temperature [Hamon, 1961].

Snow data

During March 1987 to February 1988, Yang et al. [1992], conducted an intensive snow observation in the DXG meteorological station. Daily snow depth and snow density were measured (Table 5.1). And then the snow water equivalent (SWE, in Figure 5.3) can be derived.

Table 5.1: Observed variables, the periods of observation, and the time step of data

Data	Period of observation	Time step
Discharge in No1	1985-1998, 2001-2004	Daily
Discharge in ZK	1985-1995, 1997-2004	Daily
Temperature	1959-2006	Daily
Precipitation	1959-2006	Daily
Snow water equivalent	1987.3-1988.2	Daily
GMB of Glacier No.1	1959-2006, (1967-1979 was reconstructed)	Annual
ELA of Glacier No.1	1959-2006, (1967-1979 was reconstructed)	Annual

5.3. MODEL DESCRIPTION

Based on FLEX-Topo modelling framework [Savenije, 2010; Hrachowitz et al., 2014; Gharari et al., 2014; Gao et al., 2014b], we extend the landscape-based model into FLEX^{G}, by integrating glacier melt. Due to the distinguishable landscapes and runoff generation mechanisms in glacierized and non-glacierized areas, a parallel model structure was proposed to simulate these two types of hydrological behaviours in two landscapes. Snow accumulation and ablation are considered in both landscapes. Glacier and snow melts are calculated by temperature-index model. A traditional rainfall-runoff model, the Xinanjiang model [Zhao and Liu, 1995], was implemented to simulate the runoff generation processes in the non-glaciered area. The details are shown below.

5.3.1. TOPOGRAPHY DATA PROCESS

Topography has great influence on forcing data distribution and the energy budget, subsequently the ice and snow melt. Elevation and aspect are two substantial factors on forcing data distribution and energy budget. We set 50 meters as the interval to do elevation classification, considering both the accuracy and computational cost simultaneously. Then the Glacier No.1 catchment was classified into 16 elevation zones. And the ZK catchment was classified into 21 elevation zones. Subsequently each elevation was divided into three aspects, including the north south and the east/west facing aspects. With the same air temperature, the south facing aspects get more direct solar radiation, which is the most important energy input for snow/ice melting [Hock, 2005], and leading to more melting water. While the north facing aspects get less direct solar radiation due to the topography shadow impact. The east/west facing aspects get mediate solar radiation and then intermediate amount of melting water. Summarily, considering different elevations and aspects of the glaciered and non-glaciered areas, the Glacier No.1 catchment was classified into 96 classes, and ZK was classified into 126 classes (Figure 5.2).

5.3.2. FORCING DATA DISTRIBUTION

The areal representativeness of point meteorological observation is a pervasive problem in mountainous hydrology [Klemeš, 1990]. Since most meteorological stations are located in low elevated valleys to make maintains easier, but the temperature in bottom valley overestimate the average temperature and the average precipitation is underestimated. Therefore, the impact of elevation was taken into account to correct the observed forcing data to different elevation zones. In this study, linear lapse rate was used to distribute both temperature and precipitation. Temperature lapse rate is set as -0.007°C m^{-1} based on observed data [Li et al., 2013b]. The precipitation lapse is set as 0.05% m^{-1}, obtained from measurement [Yang et al., 1988].

5.3.3. SNOW MODEL

Separate liquid and solid precipitation

Precipitation is simulated to be either snow (P_s) or rain (P_l) depending on whether the daily average air temperature (T) is above or below a threshold temperature, T_t [°C] (Equation 5.2, 5.3).

$$P_s = \begin{cases} P; & T \leq T_t \\ 0; & T > T_t \end{cases} \tag{5.2}$$

$$P_l = \begin{cases} P; & T > T_t \\ 0; & T \leq T_t \end{cases} \tag{5.3}$$

Snowfall correction

Due to systematic errors in measuring, caused by wind wetting and evaporative losses, snowfall is always being dramatically underestimated [Yang et al., 2001; Goodison et al., 1997]. According to field observation in this study site, Yang et al. [1988] concluded that only 76.5% snowfall is captured by observation in this study site. Therefore, we need to multiply 1.3 to correct the biased snowfall observation.

Snowmelt simulation

The snow pack was conceptualized as a porous media which can hold the liquid water from melting/rainfall and where the liquid water could be refrozen into snow/ice. Therefore, the solid snow pack (S_w) and the liquid water inside the snow pack (S_{wl}) were regarded as separate reservoirs. The water balance of the S_w reservoir is shown in Equation 5.4, where R_{rf} (mm d^{-1}) is the refreezing water from liquid storage to solid storage. M_s (mm d^{-1}) indicates the melted snow. Equation 5.5 shows the water balance of liquid water in snow pack, where the P_e (mm d^{-1}) means the generated runoff to soil/ice surface. And the SWE is the sum of solid and liquid water of snow pack. Snowmelt is calculated with the temperature-index approach (Equation 5.6) [Braithwaite and Olesen, 1989; Hock, 2003], which uses a degree-day factor F_{dd} (mm (°C d)$^{-1}$) to calculate melt water by the temperature above the melting threshold temperature T_{tM} (°C). The influence of aspect is taken into account by a multiplier C_a (-), which is larger than 1. The F_{dd} in south facing aspects are multiplied by C_a, and the north facing aspects are multiplied by $1/C_a$, and the east/west facing aspects are kept as F_{dd}. The liquid water in the S_{wl} from meltwater and rainfall is retained within the snowpack until it exceeds a certain fraction, C_{wh} (-), of the solid snow water equivalent (S_w) (Equation 5.7) [Seibert, 1997]. Liquid water within the snowpack refreezes according to Equation 5.8. F_{rr} (-) indicates the correct factor to simulate liquid water refreezing, while temperature is below T_{tM} [Seibert, 1997].

$$\frac{dS_w}{dt} = P_s + R_{rf} - M_s \tag{5.4}$$

$$\frac{dS_{wl}}{dt} = P_l + M_s - R_{rf} - P_e \tag{5.5}$$

$$M_s = \begin{cases} F_{dd} C_a (T - T_{tM}); & T > T_{tM} \\ 0; & T \leq T_t \end{cases} \tag{5.6}$$

$$P_e = \begin{cases} S_{wl} - C_{wh} S_w; & S_{wl} > C_{wh} S_w \\ 0; & S_{wl} \leq C_{wh} S_w \end{cases} \tag{5.7}$$

$$R_{rf} = \begin{cases} F_{dd} C_a F_{rr} (T_{tM} - T); & T_{tM} > T \\ 0; & T_{tM} \leq T \end{cases} \tag{5.8}$$

5.3.4. GLACIER MELTING SIMULATION

If the ice is covered by snow, the energy is first provided to melt snow. If there is no snow cover, the ice starts to melt. The temperature-index method is used to simulate glacier runoff M_g (mm d^{-1}) (Equation 5.9). The degree-day factor of glaciers is larger than snow degree-day factor in the same region [Seibert et al., 2015; Braithwaite and Olesen, 1989], mainly due to the less albedo of ice cover. Therefore we use a multiplier (C_g) to get the glacier degree-day factor by F_{dd}. Additionally, the same as snowmelt simulation, the influence of aspect is also included by a multiplier (C_a). The response routine on ice is different from non-glacierized area. Therefore, we need an independent reservoir $S_{f,g}$ to simulate the response routine on ice (Equation 5.10, 5.11). And a simple linear reservoir, with a recession parameter $K_{f,g}$ (d), is applied to do the simulation. The GMB and ELA

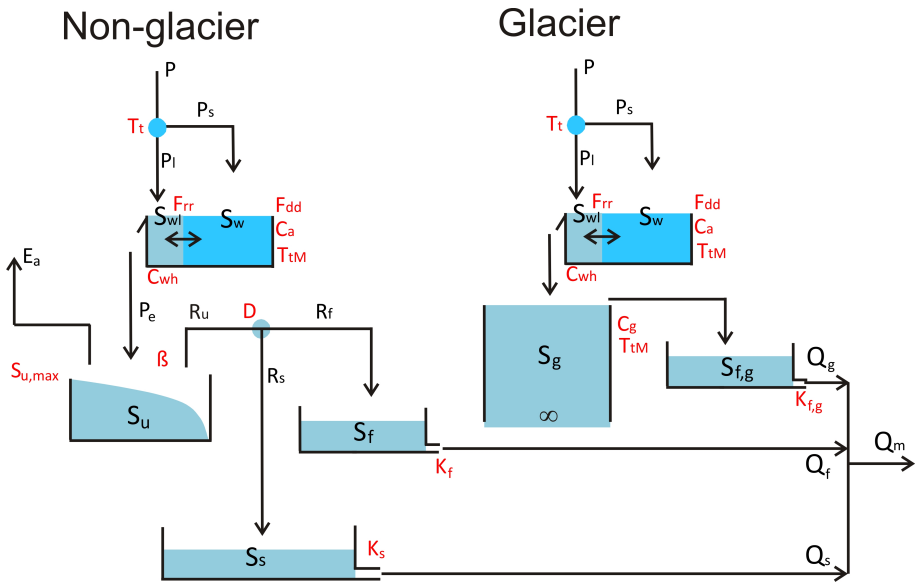

Figure 5.3: Model structure of glacier model. The red words indicate parameters, and black words indicate fluxes.

can be derived from the glacier melt and snow accumulation simulation. It is worthwhile to note that the calculated annual GMB is the water equivalent, which should be transformed to the ice thickness before comparing with measured GMB.

$$M_g = \begin{cases} F_{dd} C_a C_g (T - T_{tM}); & T > T_{tM} \& S_w = 0 \\ 0; & T \le T_{tM} \text{ or } S_w > 0 \end{cases} \tag{5.9}$$

$$\frac{dS_{f,g}}{dt} = P_l + M_g - Q_{f,g} \tag{5.10}$$

$$Q_g = S_{f,g} / K_{f,g} \tag{5.11}$$

5.3.5. MODEL FOR NON-GLACIER AREA

Unsaturated reservoir

The water balance of the unsaturated reservoir (S_u) is

$$\frac{dS_u}{dt} = P_e - E_a - R_u \tag{5.12}$$

Where P_e (mm d^{-1}) is the effective rainfall; E_a (mm d^{-1}) is the actual evaporation, which was assumed to equal to potential evaporation, since energy is the constraint factor for evaporation in this region; and R_u (mm d^{-1}) is the runoff from the unsaturated reservoir (Equation 5.12). Actual evaporation (E_a). Water retention curve of Xinanjiang model (Equation 5.13) [Zhao and Liu, 1995] was used to separate infiltration and runoff

(R_u).

$$\frac{R_u}{P_e} = 1 - \left(1 - \frac{S_u}{(1+\beta)S_{u,max}}\right)^{\beta} \tag{5.13}$$

where $S_{u,max}$ (mm) is the root zone storage capacity and β (-) is the shape parameter.

Response reservoir in non-glacier area

We used two linear reservoirs (S_f and S_s) to represent the response process of subsurface storm flow Q_f (mm d^{-1}) and groundwater runoff Q_s (mm d^{-1}):

$$\frac{dS_f}{dt} = R_f - Q_f \tag{5.14}$$

$$\frac{dS_s}{dt} = R_s - Q_s \tag{5.15}$$

$$Q_f = S_f / K_f \tag{5.16}$$

$$Q_s = S_s / K_s \tag{5.17}$$

Where R_f (mm d^{-1}) is the recharge into fast response reservoir; and R_s (mm d^{-1}) is the recharge into slow response reservoir; K_f (d) is the fast recession parameter; and K_s (d) is the slow recession parameter.

5.4. MODEL CALIBRATION AND EVALUATION

5.4.1. OBJECTIVE FUNCTIONS

The Kling-Gupta efficiencies [Gupta et al., 2009] (I_{KGE}) was used for calibration and evaluation of hydrological models with observed data in melting seasons. The equation is:

$$I_{KGE} = 1 - \sqrt{(r-1)^2 + (\alpha-1)^2 + (\beta-1)^2} \tag{5.18}$$

Where r is the linear correlation coefficient between simulation and observation; α ($\alpha = \sigma_m/\sigma_o$) is a measure of relative variability in the simulated and observed values, where σ_m is the standard deviation of simulated runoff, and σ_o is the standard deviation of observed runoff; β is the ratio between the average value of simulated and observed data.

5.4.2. MODEL CALIBRATION AND UNCERTAINTY

Some parameters are obtained from observation or literature, such as the precipitation lapse rate [Yang et al., 1988], the temperature lapse rate [Li et al., 2013b], and the snowfall correction factor [Yang et al., 1988]. Additionally, there are 13 free parameters to be calibrated. In order to calibrate the model and analysis the model uncertainty, the generalized likelihood uncertainty estimation (GLUE) [Beven and Binley, 1992] was applied. The I_{KGE} is set as the objective function. The prior ranges of parameters are mostly determined by literatures, and shown in Table 5.2. Monte Carlo was applied to sample 20,000 sets of parameters within prior ranges. And then select the best 1% (200 parameter sets) as behavioral parameter sets to do further analysis.

Table 5.2: Model parameters and their prior ranges for Monte Carlo sampling in GLUE method.

Parameter	Description	Unit	Prior Range	Method to estimate
T_t	Threshold temperature to split snowfall and rainfall	$°C^{-1}$	(3, 4)	[Han et al., 2010]
F_{dd}	Degree-day factor of snow	$mm/(d\,°C^{-1})$	(2, 9)	[Zhang et al., 2006] [Yang et al., 2012]
T_{tM}	Threshold temperature to start melting	$°C^{-1}$	(-1, 1)	[Seibert, 1997]
C_g	Factor for ice melt	-	(1, 2)	[Gao et al., 2012]
C_a	Factor for the influence of aspect on melt	-	(1, 2)	[Gao et al., 2012]
C_{wh}	Snow water holding capacity	-	(0, 1)	[Gao et al., 2012]
F_{rr}	Refreezing factor	-	(0, 1)	[Gao et al., 2012]
$K_{f,g}$	Recession coefficient of glacier runoff	d	(1, 10)	Calibration
$S_{u,max}$	Root zone storage capacity	mm	(30, 100)	[Gao et al., 2014b]
β	Shape parameter	-	(0.1, 1)	Calibration
D	The splitter	-	(0.2, 0.8)	Calibration
K_f	Recession coefficient of fast response reservoir	d	(2, 30)	[Gao et al., 2014a]
K_s	Recession coefficient of slow response reservoir	d	(30, 200)	[Gao et al., 2014a]

5.4.3. VALIDATE BY GLACIER AND SNOW OBSERVATION

Except for traditionally used observed hydrograph to validate simulation, we have long-term glacier and snow data to validate the glacier and snow sub-routine. We expect this complementary information to validate the internal fluxes of our simulation, and reduce uncertainty [Konz and Seibert, 2010; Fenicia et al., 2008a].

5.4.4. MODEL UPSCALE TEST

Model transferability is a strong realism test [Refsgaard et al., 2014; Gao et al., 2014a]. In this study, we calibrate the parameters based on Glacier No.1 catchment, and then upscaled the model and optimized parameters to the downstream gauge station (ZK) to test its upscale capability and transferability.

5.5. RESULTS AND DISCUSSION

5.5.1. HYDROGRAPH SIMULATION

Figure 5.4 shows that the hydrograph simulation is quite successful. Most of the observed hydrograph is well reproduced and enveloped by the uncertainty boundary (5/95% limits). And the uncertainty envelope is well constraint. The averaged I_{KGE} of all behavioural parameter sets is 0.77. To understand the hydrological behaviour from glaciered and non-glacierized area, we separated hydrograph of the Glacier No.1 catchment into two components (Figure 5.5). The separated hydrograph shows that the shape of hydro-

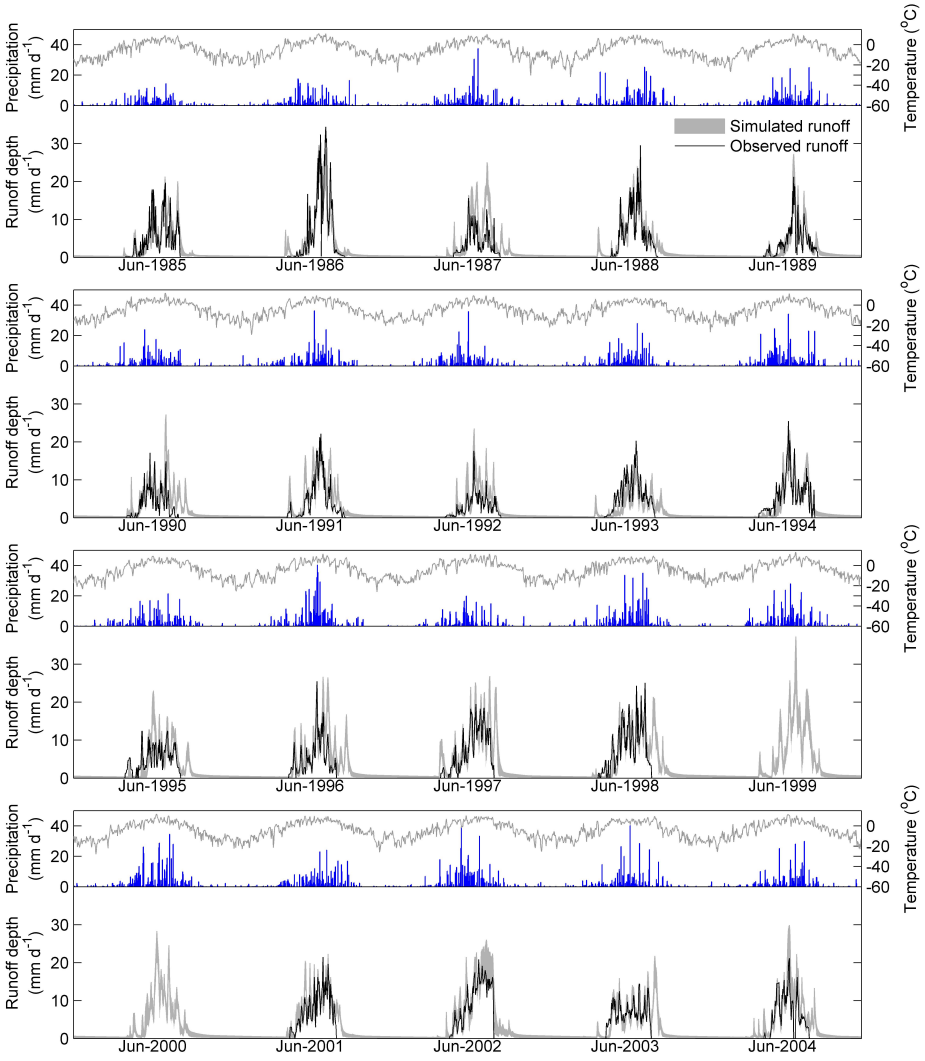

Figure 5.4: The observed daily average air temperature, and daily precipitation; and comparison between the observed daily runoff depth and simulated daily runoff depth (5/95% limits are shown by shadow areas) in the Glacier No.1 catchment.

graph, especially the peak flows, are mainly generated by glacier runoff. And the glacier melt is mainly related to energy input, which is well represented by temperature. This means that the direct precipitation has limited influence on runoff, but temperature has more impact on glacier melt and then runoff. We further quantify these two runoff components. Based on simulation, we conclude that 83% of runoff is generated from glacier-

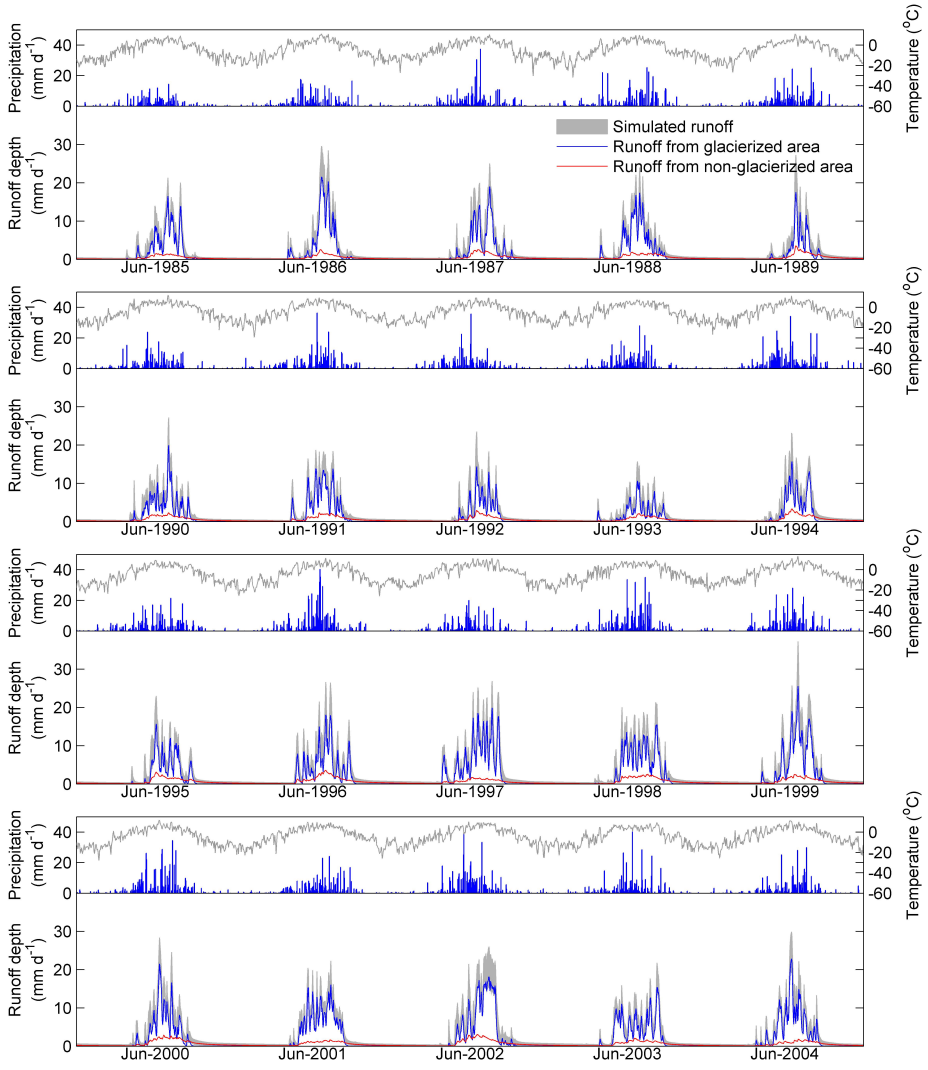

Figure 5.5: The observed daily average air temperature, and daily precipitation; and the simulated daily runoff depth (5/95% limits are shown by shadow areas), runoff generated from glaciered and non-glaciered areas (averaged value from all behavioural parameter sets) in the Glacier No.1 catchment.

ized area; while only 17% of the runoff is generated from non-glaciered area, although they have comparable areas (52% of glacier, and 48% of non-glacier). This indicates that, with the same unit area, the glaciers contribute 4-5 times amount of runoff comparing with non-glaciered area. Additionally, the successful reproducing of flow duration curve (FDC) in Figure 5.6 shows that the FLEX^{G} model can reproduce the flow frequency quite

well.

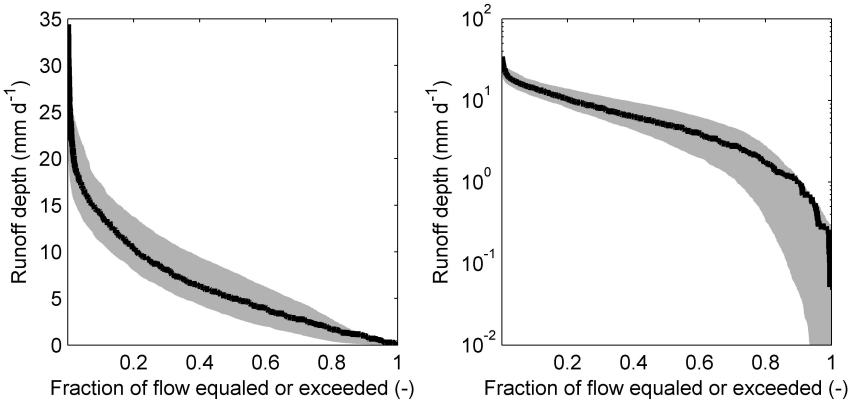

Figure 5.6: Simulated (5/95% limits are shown by shadow areas) and observed (black line) flow duration curve in the Glacier No.1 catchment.

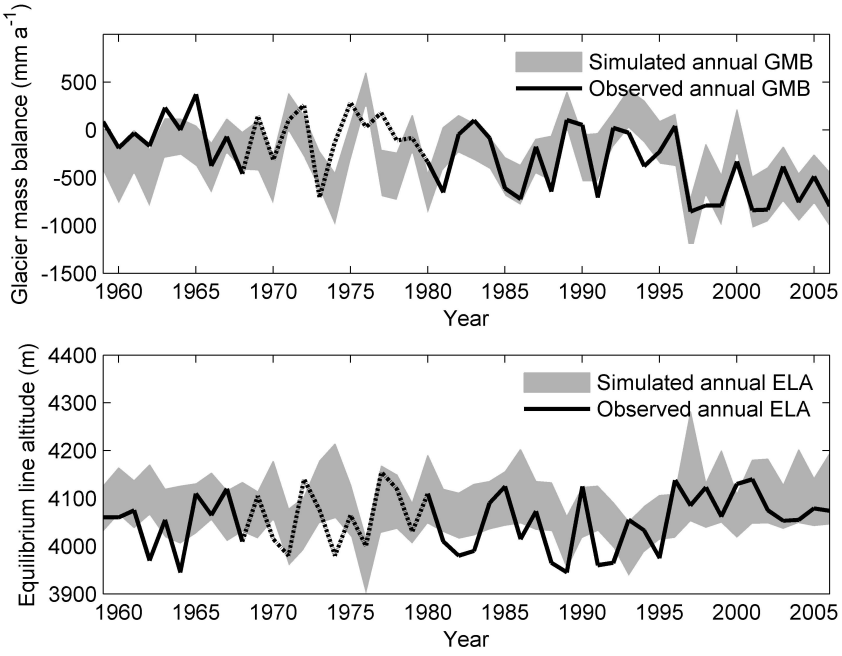

Figure 5.7: Simulated and observed glacier mass balance (GMB), and simulated and observed equilibrium line altitude (ELA). Dash line means the reconstructed GMB and ELA by meteorological data from 1967 to 1979; while 5/95% limits are shown by shadow areas.

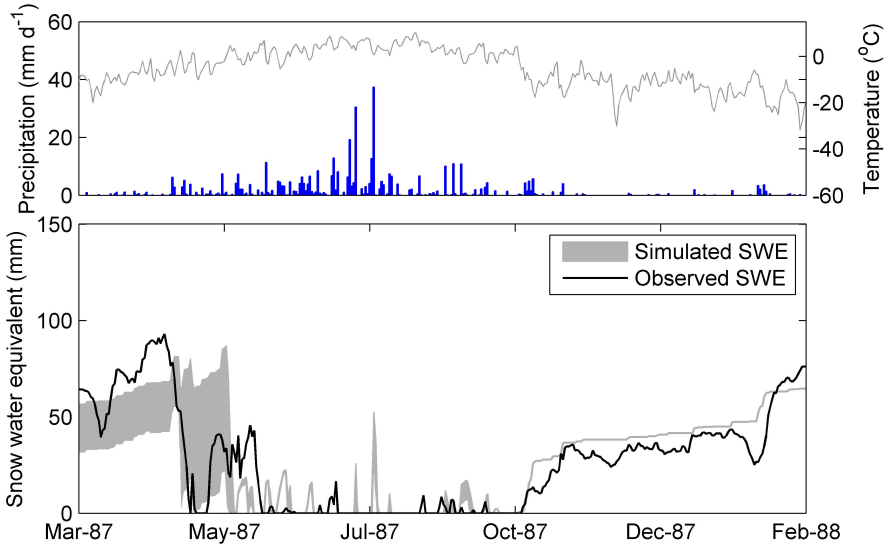

Figure 5.8: The comparison between simulated and observed snow water equivalent from March 1987 to February 1988, and the observed daily average air temperature daily precipitation.

5.5.2. GLACIER SIMULATION

Figure 5.7 shows the comparison between simulated and observed GMB and ELA. We can see that the 5/95% limits of our simulation uncertainty envelops most observation, except for the periods between 1967 and 1979, which were reconstructed by meteorological data. This complementary data indicates that our model has the ability to mimic the dynamic of glacier mass balance. From the observed and simulated GMB, we found that the No.1 Glacier has experienced severe thinning, especially after 1994. Simultaneously the ELA moves upwards. This is in line with the increase of air temperature [Li et al., 2010].

5.5.3. SNOW SIMULATION

The simulated area-averaged SWE, without considering the SWE spatial variability, matches well with measurement, especially in the winter of 1987/1988. This indicates that our snow routine simulation is successful. Interestingly, in the early melting season in 1987, the uncertainty is quite large. This might be due to the influence of threshold temperature. The temperature of precipitation events in the early winter of 1986/1987 was close to the threshold temperature (T_t). Therefore, the different Tt strongly influenced the accumulation of snow pack [Han et al., 2010]. But during the precipitation events in the early winter of 1987/1988, the temperature dropped sharply. Therefore, the uncertainty is limited. Another influence factor of this big uncertainty might be due to snow drift. The wind could redistribute the snow and impact on local snow depth. In addition, the observation is a point observation, which might not represent the averaged SWE [Clark

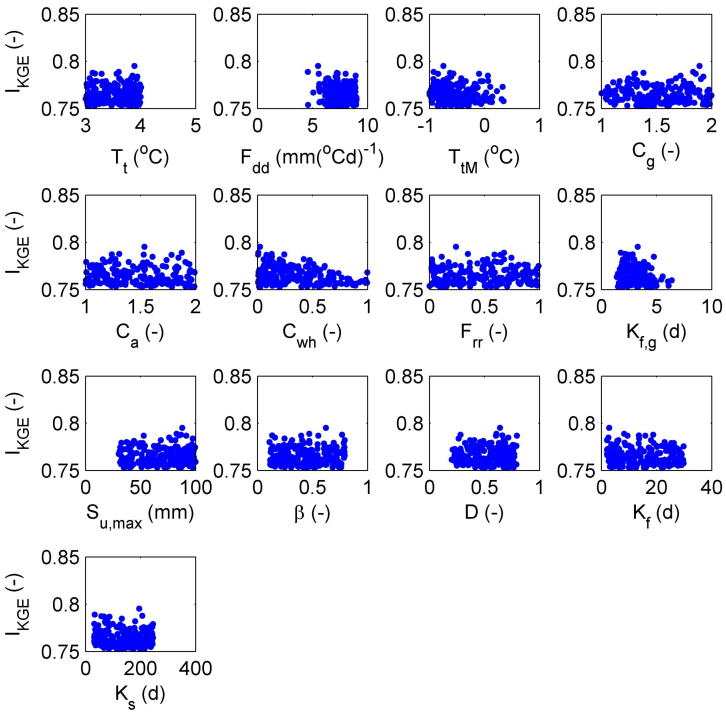

Figure 5.9: Dotty plot of I_{KGE} against parameters.

et al., 2011b].

5.5.4. PARAMETER IDENTITIFICATION

From the dotty plots in the Figure 5.9, we found that several parameters are quite well identified such as, F_{dd}, T_{tM}, C_{wh}, $K_{f,g}$, and K_f. It is interesting to find that the parameters, controlling the snow and glacier melting and recession (F_{dd}, T_{tM}, C_{wh}, $K_{f,g}$), are quite identifiable. This indicates that the hydrograph includes sufficient information from snow and glacier melt. In another word, the snow and glacier melt has great influence on hydrology. In addition, the recession process on glacier and the fast recession in non-glaciered area is quite identifiable. This means their influence on hydrograph is quite noticeable. But other parameters are poorly identified, such as the C_g, C_a, F_{dd}, $S_{u,max}$,β, D and K_s. The poor identifiablity of C_g and C_a indicates that the signal of aspect influence and the quantity difference between snow and glacier melt is not quite clear. And the refreezing process needs more data to identify F_{rr}. The $S_{u,max}$ has been prior constraint by our expert knowledge to a reasonable range. On the other hand, this indicates that the hydrograph signal from non-glaciered area is not as clear as the glacier area, which might explain the poor identifiablity of β as well. The non-identifiablity of D and K_s might be caused by the lack of hydrograph data in the recession period. The field

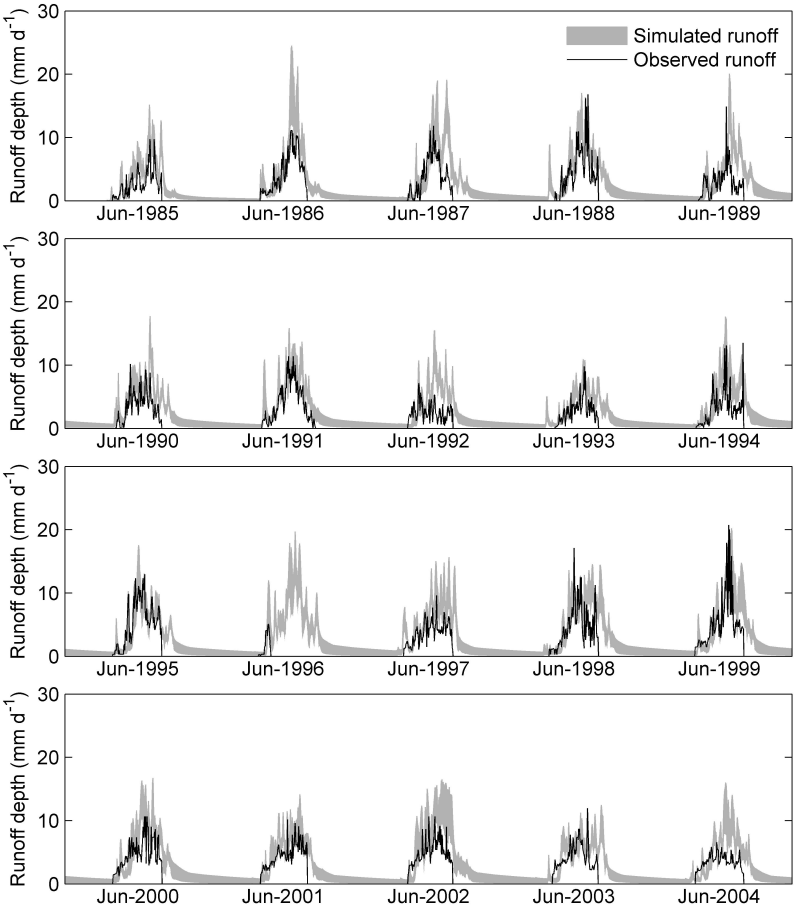

Figure 5.10: Simulated hydrography of the ZK catchment. The behavioural parameters are calibrated based on the Glacier No.1 catchment, and then transferred both model and parameters from the ZK to the Glacier No.1 catchment.

survey on hydrology stopped in the end of August, when there were still quite amount of recession flows. Without sufficient data, the K_s and D cannot be well identified.

5.5.5. MODEL UPSCALE

The simulated hydrograph in the ZK catchment, upscaled from the Glacier No.1 catchment, are shown in Figure 5.10. We found that the simulated hydrograph fits well with observation. The I_{KGE} is 0.51 in the ZK catchment. From the transferability test, we conclude that our model can not only simulate one study site, but also can be upscaled into downstream gauge stations. This indicates that once the model is able to get the heterogeneity of catchment, it can be upscaled/transferred, which is in line with other find-

ings [Gao et al., 2014b; Refsgaard et al., 2014]. The successful model upscaling indicates that the model is powerful to reproduce hydrographs with different proportion of glacier cover. Therefore, it is a robust tool to estimate the influence of glacier retreat/advance on hydrology under climate change.

5.6. SUMMARY

This study is an integrated systematic modelling research in a highly glaciered catchment, the Urumqi Glacier No.1 catchment (52% covered by glacier), with long-term and systematic glacier observation in central Asia. The proposed integrated glacier and snow model is successfully developed and tested. All the important simulated components, including glacier and snow, are validated by long-term observation data. And the model uncertainty is properly limited in an acceptable level. From simulation and observation, we conclude that:

1) The proposed model structure is efficient to simulate hydrograph in highly glacierized catchment, separate glacier runoff component, reproduce annual glacier mass balance (GMB), annual equilibrium line altitude (ELA) and daily snow water equivalent (SWE).

2) The simple temperature-index model is robust to simulate snow and glacier accumulation and melting.

3) The Glacier No.1 experienced server accelerating thinning, from both observation and simulation, especially after 1994.

4) 83% of runoff is generated from glaciered area; while only 17% runoff is generated from non-glaciered area, although they have comparable areas. This indicates that, with the same unit area, the glacier contributes 4-5 times amount of runoff comparing with non-glaciered area.

5) With the proper model structure and optimized parameter sets, we can upscale the calibrated model to the downstream gauge station.

6

CONCLUSIONS AND OUTLOOK

This thesis presents a new landscape-based hydrological model. Topography and land cover were used for landscape classification. Within this landscape-based model, several distinguishable landscapes were included, such as forest hillslopes, grassland hillslopes, bare soil/rock hillslopes, wetlands, terraces and glacierized area. Different model structures were utilized to distinguish different dominant hydrological behavior for different landscapes. The most essential difference among landscapes were their root zone storage capacity, which greatly influenced runoff generation. Besides, we found a strong regional characteristic of the root zone storage capacity which was strongly impacted by climate. With the results presented in previous chapters, the main conclusions and issues for further research are summarized in this chapter.

6.1. CONCLUSIONS

1 Climate controls how ecosystems size the root zone storage capacity at catchment scale. We can derive the root zone storage capacity by hydro-meteorological data without calibration. Ecosystems dynamically and optimally adjust their root systems to their environment in a way that the plant available water storage capacity is controlled by the precipitation regime and canopy water demand (Chapter 2).

2 The FLEX-Topo modelling framework is efficient to explicitly incorporate topography information into hydrology models. Landscape classification based on topography can be implemented to distinguish different runoff generation mechanisms in different landscapes (Chapter 3,4,5).

3 Parameter and process constraints are useful to get rid of unrealistic parameter sets and achieve more robust simulation (Chapter 3).

4 Both vegetation information and topographic information help to get more robust model transferability, especially when we transfer a model to catchments with a different landscape composition (Chapter 4).

5 Regionalization of root zone storage capacity by vegetation information tremendously improves model transferability (Chapter 4).

6 The natural land cover may be identified by topographic information to some extent, because the topography greatly influences the local energy and water budge (Chapter 3).

7 The simple temperature-index method is efficient to simulate daily hydrograph in glacierized catchment, and reproduce the long-term glacier mass balance and snow water equivalent (Chapter 5).

8 Co-evolution of topography vegetation soil and hydrology is valuable for searching a model as simple as possible, but not simpler than that (Chapter 3,4).

6.2. OUTLOOK

We need more catchments to further test the realism of model performance and the transferability of this conceptual landscape-based hydrological model. More importantly, the flexible model structure is an essential tool for us to investigate and understand the hydrological processes at the proper scale.

In this thesis, we only focused on the influence of spatial patterns of climate and landscape on hydrological processes. But the influence of climate and landscape change have not been researched. In a next step, it is interesting to take the influence of landscape and climate change on hydrological behavior into account.

Another interesting point is extending the flexible model to socio-hydrology [Sivapalan et al., 2012]. The purpose of the new scientific decade (2013-2022) of IAHS (International Association of Hydrological Sciences), "Panta Rhei – Everything Flows", is to achieve an improved understanding and interpretation between hydrological system and society [Montanari et al., 2013]. Since human activities are not only external drivers or boundary conditions of hydrological system, but also closely interacted and combined with water cycle in the Anthropocene [Savenije et al., 2014; Di Baldassarre et al., 2015; Sivapalan, 2015]. In this thesis, all catchments are relatively pristine catchments. And the landscapes in our FLEX-Topo model do not include human impacted land cover, such as farmland, urban area, roads, deforestation and reforestation. Including these artificial landscapes into hydrological model is in an urgent need.

REFERENCES

Abbott, M. B. and Refsgaard, J. C.: Distributed Hydrological Modelling, Kluwer Academic Publishers, Dordrecht, 1996.

Abdulla, F. A. and Lettenmaier, D. P.: Development of regional parameter estimation equations for a macroscale hydrologic model, Journal of Hydrology, 197, 230–257, 1997.

Agehara, S. and Warncke, D. D.: Soil Moisture and Temperature Effects on Nitrogen Release from Organic Nitrogen Sources, Soil Sci. Soc. Am. J., 69, 1844–1855, 2005.

Andréassian, V.: Waters and forests: from historical controversy to scientific debate, Journal of Hydrology, 291, 1–27, 2004.

Andréassian, V., Le Moine, N., Mathevet, T., Lerat, J., Berthet, L., and Perrin, C.: The hunting of the hydrological snark, Hydrological Processes, 23, 651–654, 2009.

Arnold, J. G. and Fohrer, N.: SWAT2000: current capabilities and research opportunities in applied watershed modelling, Hydrological Processes, 19, 563–572, 2005.

Arnold, J. G., Srinavasan, R., Muttiah, R. S., and Williams, J. R.: Large-area hydrologic modeling and assessment: Part I. Model development, Journal of the Amercian Water Resources Association, 34, 73–89, 1995.

Bárdossy, A.: Calibration of hydrological model parameters for ungauged catchments, Hydrol. Earth Syst. Sci., 11, 703–710, hESS, 2007.

Barry, R. G.: Mountain Weather and Climate: 2nd edition, Routledge, New York, 2013.

Bastiaanssen, W. G. M., Cheema, M. J. M., Immerzeel, W. W., Miltenburg, I. J., and Pelgrum, H.: Surface energy balance and actual evapotranspiration of the transboundary Indus Basin estimated from satellite measurements and the ETLook model, Water Resour. Res., 48, W11 512, 2012.

Bates, C. G.: First results in the streamflow experiment, Wagon Wheel Gap, Colorado, Jounal of forestry, 19, 402–408, 1921.

Bengtsson, L.: The global atmospheric water cycle, Environmental Research Letters, 5, 2010.

Beven, K.: On landscape space to model space mapping, Hydrological Processes, 15, 323–324, 2001.

Beven, K.: Towards an alternative blueprint for a physically based digitally simulated hydrologic response modelling system, Hydrological Processes, 16, 189–206, 2002.

Beven, K.: Rainfall-Runoff Modelling, 2012.

Beven, K.: So how much of your error is epistemic? Lessons from Japan and Italy, Hydrological Processes, 27, 1677–1680, 2013.

Beven, K. and Binley, A.: The future of distributed models: Model calibration and uncertainty prediction, Hydrological Processes, 6, 279–298, 1992.

Beven, K. and Germann, P.: Macropores and water flow in soils, Water Resources Research, 18, 1311–1325, 1982.

Beven, K. and Kirkby, M. J.: A physically based, variable contributing area model of basin hydrology, Hydrological Sciences-Bulletin, 24, 43–69, 1979.

Blöschl, G.: Scaling in hydrology, Hydrological Processes, 15, 709–711, 2001.

Blöschl, G., Kirnbauer, R., and Gutknecht, D.: Distributed Snowmelt Simulations in an Alpine Catchment: 1. Model Evaluation on the Basis of Snow Cover Patterns, Water Resources Research, 27, 3171–3179, 1991.

Blöschl, G., Sivapalan, M., Wagener, T., Viglione, A., and Savenije, H.: Runoff prediction in ungauged basins: Synthesis across processes, places and scales, Cambridge University Press, Cambridge, 2013.

Bosch, J. M. and Hewlett, J. D.: A review of catchment experiments to determine the effect of vegetation changes on water yield and evapotranspiration, Journal of Hydrology, 55, 3–23, 1982.

Braithwaite, R. and Olesen, O.: Calculation of glacier ablation from air temperature, West Greenland, Glacier fluctuations and climatic change, Kluwer Academic Publisher, Dordrecht, 1989.

Breshears, D. and Barnes, F.: Interrelationships between plant functional types and soil moisture heterogeneity for semiarid landscapes within the grassland/forest continuum: a unified conceptual model, Landscape Ecology, 14, 465–478, 1999.

Briggs, J. M. and Knapp, A. K.: Interannual Variability in Primary Production in Tallgrass Prairie: Climate, Soil Moisture, Topographic Position, and Fire as Determinants of Aboveground Biomass, American Journal of Botany, 82, 1024–1030, 1995.

Budyko, M. I. and Miller, D. H.: Climate and life, vol. 18, Academic Press, London, 1974.

Chen, R. S., Kang, E., Yang, J. P., and Zhang, J. S.: Application of TOPMODEL to simulate runoff from Heihe mainstream mountainous basin, Journal of Desert Research, 23, 428–434, 2003.

Cheng, G., Li, X., Zhao, W., Xu, Z., Feng, Q., Xiao, S., and Xiao, H.: Integrated study of the water–ecosystem–economy in the Heihe River Basin, National Science Review, 2014.

Clark, M. P., Kavetski, D., and Fenicia, F.: Pursuing the method of multiple working hypotheses for hydrological modeling, Water Resour. Res., 47, W09 301, 2011a.

Clark, M. P., McMillan, H. K., Collins, D. B. G., Kavetski, D., and Woods, R. A.: Hydrological field data from a modeller's perspective: Part 2: process-based evaluation of model hypotheses, Hydrological Processes, 25, 523–543, 2011b.

Coenders-Gerrits, A. M. J., van der Ent, R. J., Bogaard, T. A., Wang-Erlandsson, L., Hrachowitz, M., and Savenije, H. H. G.: Uncertainties in transpiration estimates, Nature, 506, E1–E2, 2014.

Costa-Cabral, M. C. and Burges, S. J.: Digital Elevation Model Networks (DEMON): A model of flow over hillslopes for computation of contributing and dispersal areas, Water Resources Research, 30, 1681–1692, 1994.

Cuffey, K. and Paterson, W.: The Physics of Glciers (Fourth Edition), Elsevier, Burlington, USA, 2010.

De Laat, A. T. J. and Maurellis, A. N.: Evidence for influence of anthropogenic surface processes on lower tropospheric and surface temperature trends, International Journal Of Climatology, 26, 897–913, 2006.

Detty, J. and McGuire, K.: Topographic controls on shallow groundwater dynamics: implications of hydrologic connectivity between hillslopes and riparian zones in a till mantled catchment, Hydrological Processes, 24, 2222–2236, 2010.

Di Baldassarre, G., Viglione, A., Carr, G., Kuil, L., Yan, K., Brandimarte, L., and Blöschl, G.: Debates—Perspectives on sociohydrology: Capturing feedbacks between physical and social processes, Water Resources Research, pp. n/a–n/a, 2015.

Ding, Y., Liu, S., Li, J., and Shangguan, D.: The retreat of glaciers in response to recent climate warming in western China, Annals of Glaciology, 43, 97–105, 2006.

Dirmeyer, P. A.: The Hydrologic Feedback Pathway for Land–Climate Coupling, Journal of Hydrometeorology, 7, 857–867, 2006.

Dong, Z., Qin, D., Ren, J., Li, K., and Li, Z.: Variations in the equilibrium line altitude of Urumqi Glacier No.1, Tianshan Mountains, over the past 50 years, Chinese Science Bulletin, 57, 4776–4783, 2012.

Donohue, R. J., Roderick, M. L., and McVicar, T. R.: On the importance of including vegetation dynamics in Budyko's hydrological model, Hydrology and Earth System Sciences, 11, 983–995, 2007.

Donohue, R. J., Roderick, M. L., and McVicar, T. R.: Roots, storms and soil pores: Incorporating key ecohydrological processes into Budyko's hydrological model, Journal of Hydrology, 436–437, 35–50, 2012.

Duan, Z. and Bastiaanssen, W. G. M.: Estimating water volume variations in lakes and reservoirs from four operational satellite altimetry databases and satellite imagery data, Remote Sensing of Environment, 134, 403–416, 2013.

Dunne, T., Zhang, W., and Aubry, B. F.: Effects of Rainfall, Vegetation, and Microtopography on Infiltration and Runoff, Water Resources Research, 27, 2271–2285, 1991.

Eagleson, P. S.: Climate, soil, and vegetation: 6. Dynamics of the annual water balance, Water Resources Research, 14, 749–764, 1978.

Eagleson, P. S.: Ecological optimality in water-limited natural soil-vegetation systems: 1. Theory and hypothesis, Water Resour. Res., 18, 325–340, 1982.

Elder, K., Kattelmann, D., Yang, D., Ushurtev, S., and Chichagov, A.: Differences in mass balance estimation resulting from three alternative measurement techniques, Glacier Number 1, Tian Shan, Xinjiang Province, China, Annals of Glaciology, 16, 198–206, 1992.

Euser, T., Winsemius, H. C., Hrachowitz, M., Fenicia, F., Uhlenbrook, S., and Savenije, H. H. G.: A framework to assess the realism of model structures using hydrological signatures, Hydrol. Earth Syst. Sci., 17, 1893–1912, hESS, 2013.

Euser, T., Hrachowitz, M., Winsemius, H., and Savenije, H.: The effect of forcing and landscape distribution on performance and consistency of model structures, in review., Hydrological Processes, 2014.

Fenicia, F., Savenije, H. H. G., Matgen, P., and Pfister, L.: Is the groundwater reservoir linear? Learning from data in hydrological modelling, Hydrol. Earth Syst. Sci., 10, 139–150, 2006.

Fenicia, F., McDonnell, J. J., and Savenije, H. H. G.: Learning from model improvement: On the contribution of complementary data to process understanding, Water Resour. Res., 44, W06 419, 2008a.

Fenicia, F., Savenije, H. H. G., Matgen, P., and Pfister, L.: Understanding catchment behavior through stepwise model concept improvement, Water Resour. Res., 44, W01 402, 2008b.

Fenicia, F., Savenije, H. H. G., and Winsemius, H. C.: Moving from model calibration towards process understanding, Physics and Chemistry of the Earth, Parts A/B/C, 33, 1057–1060, 2008c.

Fenicia, F., Kavetski, D., and Savenije, H. H. G.: Elements of a flexible approach for conceptual hydrological modeling: 1. Motivation and theoretical development, Water Resour. Res., 47, W11 510, 2011.

Fenicia, F., Kavetski, D., Savenije, H. H. G., Clark, M. P., Schoups, G., Pfister, L., and Freer, J.: Catchment properties, function, and conceptual model representation: is there a correspondence?, Hydrological Processes, 28, 2451–2467, 2014.

Field, C. B., Chapin, F. S., Matson, P. A., and Mooney, H. A.: Responses of terrestrial ecosystems to the changing atmosphere: a resource-based approach, Annual Review of Ecology and Systematics, pp. 201–235, 1992.

Flügel, W.-A.: Hydrological Response Units (HRUs) as modeling entities for hydrological river basin simulation and their methodological potential for modeling complex environmental process systems, Erde, 127, 42–62, 1996.

Flowers, G. E. and Clarke, G. K. C.: A multicomponent coupled model of glacier hydrology 1. Theory and synthetic examples, Journal of Geophysical Research: Solid Earth, 107, 2287, 2002.

Freeze, R. A. and Harlan, R. L.: Blueprint for a physically-based, digitally-simulated hydrologic response model, Journal of Hydrology, 9, 237–258, 1969.

Fuh, B.-p.: On the calculation of the evaporation from land surface, Scientia Atmospherica Sinica, 5, 1981.

Fujita, K. and Sakai, A.: Modelling runoff from a Himalayan debris-covered glacier, Hydrol. Earth Syst. Sci., 18, 2679–2694, hESS, 2014.

Fujita, K., Thompson, L. G., Ageta, Y., Yasunari, T., Kajikawa, Y., Sakai, A., and Takeuchi, N.: Thirty-year history of glacier melting in the Nepal Himalayas, Journal of Geophysical Research: Atmospheres, 111, D03 109, 2006.

Gao, H., He, X., Ye, B., and Pu, J.: Modeling the runoff and glacier mass balance in a small watershed on the Central Tibetan Plateau, China, from 1955 to 2008, Hydrological Processes, 26, 1593–1603, 2012.

Gao, H., Hrachowitz, M., Fenicia, F., Gharari, S., and Savenije, H. H. G.: Testing the realism of a topography-driven model (FLEX-Topo) in the nested catchments of the Upper Heihe, China, Hydrol. Earth Syst. Sci., 18, 1895–1915, hESS, 2014a.

Gao, H., Hrachowitz, M., Schymanski, S. J., Fenicia, F., Sriwongsitanon, N., and Savenije, H. H. G.: Climate controls how ecosystems size the root zone storage capacity at catchment scale, Geophysical Research Letters, p. 2014GL061668, 2014b.

Gentine, P., D'Odorico, P., Lintner, B. R., Sivandran, G., and Salvucci, G.: Interdependence of climate, soil, and vegetation as constrained by the Budyko curve, Geophysical Research Letters, 39, L19 404, 2012.

Gharari, S., Hrachowitz, M., Fenicia, F., and Savenije, H. H. G.: Hydrological landscape classification: investigating the performance of HAND based landscape classifications in a central European meso-scale catchment, Hydrol. Earth Syst. Sci., 15, 3275–3291, 2011.

Gharari, S., Hrachowitz, M., Fenicia, F., Gao, H., Euser, T., and Savenije, H.: FLEX-TOPO: Proof of concept in a central European landscape, Geophysical Research Abstracts, 15, 2013.

Gharari, S., Hrachowitz, M., Fenicia, F., Gao, H., and Savenije, H. H. G.: Using expert knowledge to increase realism in environmental system models can dramatically reduce the need for calibration, Hydrol. Earth Syst. Sci., 18, 4839–4859, hESS, 2014.

Goodison, B., Louie, P., and Yang, D.: The WMO solid precipitation measurement intercomparison, World Meteorological Organization-Publications-WMO TD, pp. 65–70, 1997.

Grayson, R. and Blöschl, G.: Spatial patterns in catchment hydrology: observations and modelling, Cambridge University Press, 2001.

Gumbel, E. J.: Les valeurs extrêmes des distributions statistiques, Annales de l'institut Henri Poincaré, 5, 115–158, 1935.

Gupta, H. V., Wagener, T., and Liu, Y.: Reconciling theory with observations: elements of a diagnostic approach to model evaluation, Hydrological Processes, 22, 3802–3813, 2008.

Gupta, H. V., Kling, H., Yilmaz, K. K., and Martinez, G. F.: Decomposition of the mean squared error and NSE performance criteria: Implications for improving hydrological modelling, Journal of Hydrology, 377, 80–91, 2009.

Gupta, H. V., Perrin, C., Blöschl, G., Montanari, A., Kumar, R., Clark, M., and Andráassian, V.: Large-sample hydrology: a need to balance depth with breadth, Hydrol. Earth Syst. Sci., 18, 463–477, hESS, 2014.

Hamon, W.: Estimating Potential Evapotranspiration, Journal of the Hydraulics Division, ASCE, 87, 107–120, 1961.

Han, C., Chen, R. S., Liu, J., Yang, Y., and Wenwu, Q.: A discuss of separating solid and liquid precipitation, Jounal of Glaciology and Geocryology, 32, 249–256, 2010.

Hansen, M. C., Potapov, P. V., Moore, R., Hancher, M., Turubanova, S. A., Tyukavina, A., Thau, D., Stehman, S. V., Goetz, S. J., Loveland, T. R., Kommareddy, A., Egorov, A., Chini, L., Justice, C. O., and Townshend, J. R. G.: High-Resolution Global Maps of 21st-Century Forest Cover Change, Science, 342, 850–853, 2013.

Hargreaves, G.: Moisture availability and crop production, Trans. Am. Soc. Agric. Eng., 18, 980–984, 1975.

Hargreaves, G. H. and Samani, Z. A.: Estimating Potential Evapotranspiration, Journal of the Irrigation and Drainage Division, 108, 225–230, 1982.

Harman, C. and Troch, P. A.: What makes Darwinian hydrology "Darwinian"? Asking a different kind of question about landscapes, Hydrology and Earth System Sciences, 18, 417–433, 10.5194/hess-18-417-2014, 2014.

Harte, J.: Toward a synthesis of the Newtonian and Darwinian worldviews, Physics Today, 55, 29–34, 2002.

Hartmann, G. and Bárdossy, A.: Investigation of the transferability of hydrological models and a method to improve model calibration, Adv. Geosci., 5, 83–87, aDGEO, 2005.

Hazen, A.: Storage to be provided in impounded reservoirs for municipal water supply, Trans. Amer. Soc. Civil Eng., 77, 1539–1640, 1914.

He, Z. H., Tian, F. Q., Gupta, H. V., Hu, H. C., and Hu, H. P.: Diagnostic calibration of a hydrological model in an alpine area by hydrograph partitioning, Hydrol. Earth Syst. Sci. Discuss., 11, 13 385–13 441, hESSD, 2014.

Heuvelmans, G., Muys, B., and Feyen, J.: Evaluation of hydrological model parameter transferability for simulating the impact of land use on catchment hydrology, Physics and Chemistry of the Earth, Parts A/B/C, 29, 739–747, 2004.

Hock, R.: Temperature index melt modelling in mountain areas, Journal of Hydrology, 282, 104–115, 2003.

Hock, R.: Glacier melt: a review of processes and their modelling, Progress in Physical Geography, 29, 362–391, 2005.

Hook, P. B. and Burke, I. C.: Biogeochemistry in a shortgrass landscape: control by topography, soil texture, and microclimate, Ecology, 81, 2686–2703, 2000.

Horton, R. E.: The Role of infiltration in the hydrologic cycle, Transactions, American Geophysical Union, 14, 446–460, 1933.

Howard, D. M. and Howard, P. J. A.: Relationships between co2 evolution, moisture content and temperature for a range of soil types, Soil Biology and Biochemistry, 25, 1537–1546, 1993.

Hrachowitz, M., Savenije, H., Bogaard, T. A., Tetzlaff, D., and Soulsby, C.: What can flux tracking teach us about water age distribution patterns and their temporal dynamics?, Hydrol. Earth Syst. Sci., 17, 533–564, 2013a.

Hrachowitz, M., Savenije, H. H. G., Blöschl, G., McDonnell, J. J., Sivapalan, M., Pomeroy, J. W., Arheimer, B., Blume, T., Clark, M. P., Ehret, U., Fenicia, F., Freer, J. E., Gelfan, A., Gupta, H. V., Hughes, D. A., Hut, R. W., Montanari, A., Pande, S., Tetzlaff, D., Troch, P. A., Uhlenbrook, S., Wagener, T., Winsemius, H. C., Woods, R. A., Zehe, E., and Cudennec, C.: A decade of Predictions in Ungauged Basins (PUB)—a review, Hydrological Sciences Journal, 58, 1198–1255, 2013b.

Hrachowitz, M., Fovet, O., Ruiz, L., Euser, T., Gharari, S., Nijzink, R., Freer, J., Savenije, H. H. G., and Gascuel-Odoux, C.: Process consistency in models: The importance of system signatures, expert knowledge, and process complexity, Water Resources Research, 50, 7445–7469, 2014.

Huang, H. Q. and Nanson, G. C.: Why some alluvial rivers develop an anabranching pattern, Water Resources Research, 43, W07 441, 2007.

Huang, M., Zhang, L., and Gallichand, J.: Runoff responses to afforestation in a watershed of the Loess Plateau, China, Hydrological Processes, 17, 2599–2609, 2003.

Huang, M., Barbour, S. L., Elshorbagy, A., Zettl, J., and Si, B. C.: Effects of Variably Layered Coarse Textured Soils on Plant Available Water and Forest Productivity, Procedia Environmental Sciences, 19, 148–157, 2013.

Hundecha, Y. and Bárdossy, A.: Modeling of the effect of land use changes on the runoff generation of a river basin through parameter regionalization of a watershed model, Journal of Hydrology, 292, 281–295, 2004.

Huss, M., Jouvet, G., Farinotti, D., and Bauder, A.: Future high-mountain hydrology: a new parameterization of glacier retreat, Hydrol. Earth Syst. Sci., 14, 815–829, hESS, 2010.

Immerzeel, W. W., van Beek, L. P. H., and Bierkens, M. F. P.: Climate Change Will Affect the Asian Water Towers, Science, 328, 1382–1385, 2010.

Jasechko, S., Sharp, Z. D., Gibson, J. J., Birks, S. J., Yi, Y., and Fawcett, P. J.: Terrestrial water fluxes dominated by transpiration, Nature, 496, 347–350, 2013.

Jencso, K. G., McGlynn, B. L., Gooseff, M. N., Wondzell, S. M., Bencala, K. E., and Marshall, L. A.: Hydrologic connectivity between landscapes and streams: Transferring reach- and plot-scale understanding to the catchment scale, Water Resources Research, 45, W04 428, 2009.

Jenerette, G. D., Barron-Gafford, G. A., Guswa, A. J., McDonnell, J. J., and Villegas, J. C.: Organization of complexity in water limited ecohydrology, Ecohydrology, 5, 184–199, 2012.

Jia, Y., Ding, X., Qin, C., and Wang, H.: Distributed modeling of land surface water and energy budgets in the inland Heihe river basin of China, Hydrol. Earth Syst. Sci. Discuss., 6, 2189–2246, 2009.

Jin, X., Wan, L., and Hu, G.: Distribution characteristics of mountain vegetation and the influence factors in upstream of Heihe River Basin, Jounal of Arid Land Resources and Environment, 22, 140–144, 2008.

Kang, E., Cheng, G., Lan, Y., Chen, R. S., and Zhang, J.: Application of a conceptual hydrological model in the runoff forecast of a mountainous watershed, Advance in Earth Sciences, 17, 18–26, 2002.

Kavetski, D. and Kuczera, G.: Model smoothing strategies to remove microscale discontinuities and spurious secondary optima in objective functions in hydrological calibration, Water Resources Research, 43, W03 411, 2007.

Khu, S.-T., Madsen, H., and di Pierro, F.: Incorporating multiple observations for distributed hydrologic model calibration: An approach using a multi-objective evolutionary algorithm and clustering, Advances in Water Resources, 31, 1387–1398, 2008.

Kirchner, J. W.: Getting the right answers for the right reasons: Linking measurements, analyses, and models to advance the science of hydrology, Water Resour. Res., 42, W03S04, 2006.

Kleidon, A.: Global datasets of rooting zone depth inferred from inverse methods, Journal of Climate, 17, 2714–2722, 2004.

Kleidon, A. and Heimann, M.: A method of determining rooting depth from a terrestrial biosphere model and its impacts on the global water and carbon cycle, Global Change Biology, 4, 275–286, 1998.

Klemeš, V.: Dilettantism in hydrology: Transition or destiny?, Water Resources Research, 22, 177S–188S, 1986.

Klemeš, V.: The modelling of mountain hydrology: the ultimate challenge, 1990.

Klemeš, V.: Water storage: source of inspiration and desperation, pp. 286–314, American Geophysical Union, 1997.

Knudsen, J., Thomsen, A., and Refsgaard, J. C.: WATBAL A Semi-Distributed, Physically Based Hydrological Modelling System, Nordic Hydrology, pp. 347–362, 1986.

Kolb, T. E., Steiner, K. C., McCormick, L. H., and Bowersox, T. W.: Growth response of northern red-oak and yellow-poplar seedlings to light, soil moisture and nutrients in relation to ecological strategy, Forest Ecology And Management, 38, 65–78, 1990.

Konz, M. and Seibert, J.: On the value of glacier mass balances for hydrological model calibration, Journal of Hydrology, 385, 238–246, 2010.

Konz, M., Uhlenbrook, S., Braun, L., Shrestha, A., and Demuth, S.: Implementation of a process-based catchment model in a poorly gauged, highly glacierized Himalayan headwater, Hydrol. Earth Syst. Sci., 11, 1323–1339, hESS, 2007.

Kumar, P. and Ruddell, B. L.: Information Driven Ecohydrologic Self-Organization, Entropy, 12, 2085–2096, 2010.

Kumar, R., Livneh, B., and Samaniego, L.: Toward computationally efficient large-scale hydrologic predictions with a multiscale regionalization scheme, Water Resources Research, 49, 5700–5714, 2013.

Kurc, S. A. and Small, E. E.: Soil moisture variations and ecosystem-scale fluxes of water and carbon in semiarid grassland and shrubland, Water Resources Research, 43, W06 416, 2007.

Laaha, G. and Blöschl, G.: A comparison of low flow regionalisation methods—catchment grouping, Journal of Hydrology, 323, 193–214, 2006.

Laio, F., Porporato, A., Ridolfi, L., and Rodriguez-Iturbe, I.: Plants in water-controlled ecosystems: active role in hydrologic processes and response to water stress: II. Probabilistic soil moisture dynamics, Advances in Water Resources, 24, 707–723, 2001.

Legates, D. R., Mahmood, R., Levia, D. F., DeLiberty, T. L., Quiring, S. M., Houser, C., and Nelson, F. E.: Soil moisture: A central and unifying theme in physical geography, Progress In Physical Geography, 2010.

Li, X., Li, X., Li, Z., Ma, M., Wang, J., Xiao, Q., Liu, Q., Che, T., Chen, E., Yan, G., Hu, Z., Zhang, L., Chu, R., Su, P., Liu, Q., Liu, S., Wang, J., Niu, Z., Chen, Y., Jin, R., Wang, W., Ran, Y., Xin, X., and Ren, H.: Watershed Allied Telemetry Experimental Research, J. Geophys. Res., 114, D22 103, 2009.

Li, X., Li, X. W., Roth, K., M.Menenti, and Wagner, W.: Observing and modeling the catchment scale water cycle, Hydrol. Earth Syst. Sci., 15, 597–601, 2011.

Li, X., Cheng, G., Liu, S., Xiao, Q., Ma, M., Jin, R., Che, T., Liu, Q., Wang, W., Qi, Y., Wen, J., Li, H., Zhu, G., Guo, J., Ran, Y., Wang, S., Zhu, Z., Zhou, J., Hu, X., and Xu, Z.: Heihe Watershed Allied Telemetry Experimental Research (HiWATER): Scientific Objectives and Experimental Design, Bulletin of the American Meteorological Society, 94, 1145–1160, 2013a.

Li, X., Wang, L., Chen, D., Yang, K., Xue, B., and Sun, L.: Near-surface air temperature lapse rates in the mainland China during 1962–2011, Journal of Geophysical Research: Atmospheres, 118, 7505–7515, 2013b.

Li, Z., Wang, W., Zhang, M., Wang, F., and Li, H.: Observed changes in streamflow at the headwaters of the Urumqi River, eastern Tianshan, central Asia, Hydrological Processes, 24, 217–224, 2010.

Liang, X., Lettenmaier, D. P., Wood, E. F., and Burges, S. J.: A simple hydrologically based model of land surface water and energy fluxes for general circulation models, Journal of Geophysical Research: Atmospheres, 99, 14 415–14 428, 1994.

Liu, S., Ding, Y., Shangguan, D., Zhang, Y., Li, J., Han, H., Wang, J., and Xie, C.: Glacier retreat as a result of climate warming and increased precipitation in the Tarim river basin, northwest China, Annals of Glaciology, 43, 91–96, 2006.

Liu, S., Shangguan, D., Xu, J., Wang, X., Yao, X., Jiang, Z., Guo, W., Lu, A., Zhang, S., Ye, B., Li, Z., Wei, J., and Wu, L.: Glacier in China and their variations, pp. 583–608, Springer, Heidelberg, 2014.

Lyon, S. W., Nathanson, M., Spans, A., Grabs, T., Laudon, H., Temnerud, J., Bishop, K. H., and Seibert, J.: Specific discharge variability in a boreal landscape, Water Resources Research, 48, W08 506, 2012.

Martinez, G. F. and Gupta, H. V.: Hydrologic consistency as a basis for assessing complexity of monthly water balance models for the continental United States, Water Resources Research, 47, W12 540, 2011.

McGlynn, B. L. and McDonnell, J. J.: Quantifying the relative contributions of riparian and hillslope zones to catchment runoff, Water Resour. Res., 39, 1310, 2003.

Mücher, C. A., Klijn, J. A., Wascher, D. M., and Schaminée, J. H. J.: A new European Landscape Classification (LANMAP): A transparent, flexible and user-oriented methodology to distinguish landscapes, Ecological Indicators, 10, 87–103, 2010.

Merz, R. and Blöschl, G.: Regionalisation of catchment model parameters, Journal of Hydrology, 287, 95–123, 2004.

Milly, P. C. D.: Climate, soil water storage, and the average annual water balance, Water Resources Research, 30, 2143–2156, 1994.

Mohamed, Y. A., Bastiaanssen, W. G. M., Savenije, H. H. G., van den Hurk, B. J. J. M., and Finlayson, C. M.: Wetland versus open water evaporation: An analysis and literature review, Physics and Chemistry of the Earth, Parts A/B/C, 47–48, 114–121, 2012.

Molenat, J., Gascuel-Odoux, C., Ruiz, L., and Gruau, G.: Role of water table dynamics on stream nitrate export and concentration in agricultural headwater catchment (France), Journal of Hydrology, 348, 363–378, 2008.

Montanari, A., Young, G., Savenije, H. H. G., Hughes, D., Wagener, T., Ren, L. L., Koutsoyiannis, D., Cudennec, C., Toth, E., Grimaldi, S., Blöschl, G., Sivapalan, M., Beven, K., Gupta, H., Hipsey, M., Schaefli, B., Arheimer, B., Boegh, E., Schymanski, S. J., Di Baldassarre, G., Yu, B., Hubert, P., Huang, Y., Schumann, A., Post, D. A., Srinivasan, V., Harman, C., Thompson, S., Rogger, M., Viglione, A., McMillan, H., Characklis, G., Pang, Z., and Belyaev, V.: "Panta Rhei—Everything Flows": Change in hydrology and society—The IAHS Scientific Decade 2013–2022, Hydrological Sciences Journal, 58, 1256–1275, 2013.

Moore, R. D. and Wondzell, S.: Physical hydrology and the effects of forest harvesting in the Pacific Northwest: a review, Jounal of the American Water Resources Association, pp. 763–784, 2005.

Moore, R. D., Fleming, S. W., Menounos, B., Wheate, R., Fountain, A., Stahl, K., Holm, K., and Jakob, M.: Glacier change in western North America: influences on hydrology, geomorphic hazards and water quality, Hydrological Processes, 23, 42–61, 2009.

Nash, J. E. and Sutcliffe, J. V.: River flow forecasting through conceptual models part I — A discussion of principles, Journal of Hydrology, 10, 282–290, 1970.

Niu, G.-Y., Yang, Z.-L., Mitchell, K. E., Chen, F., Ek, M. B., Barlage, M., Kumar, A., Manning, K., Niyogi, D., Rosero, E., Tewari, M., and Xia, Y.: The community Noah land surface model with multiparameterization options (Noah-MP): 1. Model description and evaluation with local-scale measurements, Journal of Geophysical Research: Atmospheres, 116, D12 109, 2011.

Nobre, A., Cuartas, L., Hodnett, M., Rennó, C., Rodrigues, G., Silveira, A., Waterloo, M., and Saleska, S.: Height Above the Nearest Drainage–a hydrologically relevant new terrain model, Journal of Hydrology, 404, 13–29, 2011.

Oerlemans, J.: Quantifying Global Warming from the Retreat of Glaciers, Science, 264, 243–245, 1994.

Oerlemans, J. and Fortuin, J. P. F.: Sensitivity of Glaciers and Small Ice Caps to Greenhouse Warming, Science, 258, 115–117, 1992.

Ohmura, A., Konzelmann, T., Rotach, M., Forrer, J., Wild, M., Abe-Ouchi, A., and Toritani, H.: Energy balance for the Greenland ice sheet by observation and model computation, in: Snow and ice covers: interactions with the atmosphere and ecosystems, edited by Jones, H., Davies, T., Ohmura, A., and Morris, E., vol. 223, pp. 163–174, IAHS Publication.

Pande, S., McKee, M., and Bastidas, L. A.: Complexity-based robust hydrologic prediction, Water Resour. Res., 45, W10 406, 2009.

Pastor, J. and Post, W. M.: Influence of climate, soil moisture, and succession on forest carbon and nitrogen cycles, Biogeochemistry, 2, 3–27, 1986.

Pfister, L.: Study of the water cycle components in the Attert River Basin (CYCLEAU), Tech. rep., Fonds Natl. de la Rech., 2006.

Phillips, J. D.: Soils as extended composite phenotypes, Geoderma, 149, 143–151, 2009.

Pokhrel, P. and Gupta, H. V.: On the ability to infer spatial catchment variability using streamflow hydrographs, Water Resources Research, 47, W08 534, 2011.

Porporato, A., Daly, E., and Rodriguez-Iturbe, I.: Soil water balance and ecosystem response to climate change, The American naturalist, 164, 625–632, 2004.

Qin, D. and Ding, Y.: Key Issues on Cryospheric Changes, Trends and Their Impacts, Advances in Climate Change Research, 1, 1–10, 2010.

Qin, J., Ding, Y., Ye, B., Zhou, Z., and Xie, Z.: Regulating effect of mountain landscapes on river runoff in Northwest China, Jounal of Glaciology and Geocryology, 33, 397–404, 2011.

Ray, R. and Jacobs, J.: Relationships among remotely sensed soil moisture, precipitation and landslide events, Natural Hazards, 43, 211–222, 2007.

Refsgaard, J. C. and Knudsen, J.: Operational Validation and Intercomparison of Different Types of Hydrological Models, Water Resources Research, 32, 2189–2202, 1996.

Refsgaard, J. C., Madsen, H., Andréassian, V., Arnbjerg-Nielsen, K., Davidson, T. A., Drews, M., Hamilton, D. P., Jeppesen, E., Kjellström, E., Olesen, J. E., Sonnenborg, T. O., Trolle, D., Willems, P., and Christensen, J. H.: A framework for testing the ability of models to project climate change and its impacts, Climatic Change, 122, 271–282, 2014.

Reggiani, P., Sivapalan, M., and Hassanizadeh, S. M.: Conservation equations governing hillslope responses: Exploring the physical basis of water balance, Water Resources Research, 36, 1845–1863, 2000.

Rennó, C., Nobre, A., Cuartas, L., Soares, J., Hodnett, M., Tomasella, J., and Waterloo, M.: HAND, a new terrain descriptor using SRTM-DEM: Mapping terra-firme rainforest environments in Amazonia, Remote Sensing of Environment, 112, 3469–3481, 2008.

Rippl, W.: The capacity of storage reservoirs for water supply, 1883.

Robinson, M., Gannon, B., and Schuch, M.: A comparison of the hydrology of moorland under natural conditions, agricultural use and forestry, Hydrological Sciences Journal, 36, 565–577, 1991.

Rodríguez-Iturbe, I. and Valdés, J. B.: The geomorphologic structure of hydrologic response, Water Resources Research, 15, 1409–1420, 1979.

Rodriguez-Iturbe, I.: Ecohydrology: A hydrologic perspective of climate-soil-vegetation dynamies, Water Resources Research, 36, 3–9, 2000.

Rodriguez-Iturbe, I., D'Odorico, P., Laio, F., Ridolfi, L., and Tamea, S.: Challenges in humid land ecohydrology: Interactions of water table and unsaturated zone with climate, soil, and vegetation, Water Resources Research, 43, W09 301, 2007.

Sahin, V. and Hall, M. J.: The effects of afforestation and deforestation on water yields, Journal of Hydrology, 178, 293–309, 1996.

Samaniego, L., Kumar, R., and Attinger, S.: Multiscale parameter regionalization of a grid-based hydrologic model at the mesoscale, Water Resources Research, 46, W05 523, 2010.

Savenije, H. H. G.: Determination of evaporation from a catchment water balance at a monthly time scale, Hydrol. Earth Syst. Sci., 1, 93–100, 1997.

Savenije, H. H. G.: The importance of interception and why we should delete the term evapotranspiration from our vocabulary, Hydrological Processes, 18, 1507–1511, 2004.

Savenije, H. H. G.: HESS Opinions "The art of hydrology"*, Hydrol. Earth Syst. Sci., 13, 157–161, 2009.

Savenije, H. H. G.: HESS Opinions "Topography driven conceptual modelling (FLEX-Topo)", Hydrol. Earth Syst. Sci., 14, 2681–2692, 2010.

Savenije, H. H. G., Hoekstra, A. Y., and van der Zaag, P.: Evolving water science in the Anthropocene, Hydrol. Earth Syst. Sci., 18, 319–332, hESS, 2014.

Saxton, K. E. and Rawls, W. J.: Soil Water Characteristic Estimates by Texture and Organic Matter for Hydrologic Solutions, Soil Science Society Of America Journal, 70, 1569–1578, 2006.

Saxton, K. E., Rawls, W. J., Romberger, J. S., and Papendick, R. I.: Estimating Generalized Soil-water Characteristics from Texture1, Soil Sci. Soc. Am. J., 50, 1031–1036, 1986.

Sayama, T., McDonnell, J. J., Dhakal, A., and Sullivan, K.: How much water can a watershed store?, Hydrological Processes, 25, 3899–3908, 2011.

Schaake, J., Cong, S., and Duan, Q.: The US MOPEX data set, IAHS publication, 307, 9, 2006.

Schaefli, B., Hingray, B., Niggli, M., and Musy, A.: A conceptual glacio-hydrological model for high mountainous catchments, Hydrol. Earth Syst. Sci. Discuss., 2, 73–117, hESSD, 2005.

Schenk, H. J.: Vertical vegetation structure below ground: Scaling from root to globe, vol. 66, pp. 341–373, Springer, Heidelberg, 2006.

Schenk, H. J.: The shallowest possible water extraction profile: a null model for global root distributions, Vadose Zone Journal, 7, 1119–1124, 2008.

Schenk, H. J. and Jackson, R. B.: The global biogeography of roots, Ecological Monographs, 72, 311–328, 2002.

Scherrer, S. and Naef, F.: A decision scheme to indicate dominant hydrological flow processes on temperate grassland, Hydrological Processes, 17, 391–401, 2003.

Schymanski, S. J., Sivapalan, M., Roderick, M. L., Beringer, J., and Hutley, L. B.: An optimality-based model of the coupled soil moisture and root dynamics, Hydrol. Earth Syst. Sci., 12, 913–932, hESS, 2008.

Seeger, M., Errea, M. P., Beguería, S., Arnáez, J., Martí, C., and García-Ruiz, J. M.: Catchment soil moisture and rainfall characteristics as determinant factors for discharge/suspended sediment hysteretic loops in a small headwater catchment in the Spanish pyrenees, Journal Of Hydrology, 288, 299–311, 2004.

Seibert, J.: Estimation of parameter uncertainty in the HBV model, Nordic Hydrology, 28, 247–262, 1997.

Seibert, J.: Regionalisation of parameters for a conceptual rainfall-runoff model, Agricultural and Forest Meteorology, 98–99, 279–293, 1999.

Seibert, J. and McDonnell, J.: Gauging the ungauged basin: the relative value of soft and hard data, Jounal of Hydrologic Engineering, 2013.

Seibert, J. and McDonnell, J. J.: On the dialog between experimentalist and modeler in catchment hydrology: Use of soft data for multicriteria model calibration, Water Resour. Res., 38, 1241, 2002.

Seibert, J., Bishop, K., Rodhe, A., and McDonnell, J. J.: Groundwater dynamics along a hillslope: A test of the steady state hypothesis, Water Resour. Res., 39, 1014, 2003.

Seibert, J., Stendahl, J., and Sørensen, R.: Topographical influences on soil properties in boreal forests, Geoderma, 141, 139–148, 2007.

Seibert, J., Jenicek, M., Huss, M., and Ewen, T.: Snow and Ice in the Hydrosphere, pp. 99–130, Elsevier, Amsterdam, 2015.

Seneviratne, S. I., Corti, T., Davin, E. L., Hirschi, M., Jaeger, E. B., Lehner, I., Orlowsky, B., and Teuling, A. J.: Investigating soil moisture–climate interactions in a changing climate: A review, Earth-Science Reviews, 99, 125–161, 2010.

Seneviratne, S. I., Wilhelm, M., Stanelle, T., van den Hurk, B., Hagemann, S., Berg, A., Cheruy, F., Higgins, M. E., Meier, A., Brovkin, V., Claussen, M., Ducharne, A., Dufresne, J.-L., Findell, K. L., Ghattas, J., Lawrence, D. M., Malyshev, S., Rummukainen, M., and Smith, B.: Impact of soil moisture-climate feedbacks on CMIP5 projections: First results from the GLACE-CMIP5 experiment, Geophysical Research Letters, 40, 2013GL057 153, 2013.

Shao, J.: Linear Model Selection by Cross-Validation, Journal of the American Statistical Association, 88, 486–494, 1993.

Shi, Y., Huang, M., and Yao, T.: Glaciers and their environments in China - the present, past and future, vol. 1-410, Scienc Press, Beijing, 2000.

Singh, P. and Singh, V. P.: Snow and glacier hydrology, Kluwer Academic Publishers, Dordrecht, the Netherlands, 2001.

Singh, P., Haritashya, U. K., and Kumar, N.: Modelling and estimation of different components of streamflow for Gangotri Glacier basin, Himalayas, Hydrological Sciences Journal, 53, 309–322, 2008.

Sivapalan, M.: Process complexity at hillslope scale, process simplicity at the watershed scale: is there a connection?, Hydrological Processes, 17, 1037–1041, 2003.

Sivapalan, M.: Pattern, process and function: elements of a unified theory of hydrology at the catchment scale, Encyclopedia of hydrological sciences, 2005.

Sivapalan, M.: Pattern, Process and Function: Elements of a Unified Theory of Hydrology at the Catchment Scale, John Wiley & Sons, Ltd, Hoboken, New Jersey, 2006.

Sivapalan, M.: The secret to 'doing better hydrological science': change the question!, Hydrological Processes, 23, 1391–1396, 2009.

Sivapalan, M.: Debates—Perspectives on sociohydrology: Changing water systems and the "tyranny of small problems"—Sociohydrology, Water Resources Research, pp. n/a–n/a, 2015.

Sivapalan, M. and Kalma, J. D.: Scale problems in hydrology: Contributions of the robertson workshop, Hydrological Processes, 9, 243–250, 1995.

Sivapalan, M., Savenije, H. H. G., and Blöschl, G.: Socio-hydrology: A new science of people and water, Hydrological Processes, 26, 1270–1276, 2012.

Spence, C. and Woo, M.-k.: Hydrology of subarctic Canadian shield: soil-filled valleys, Journal of Hydrology, 279, 151–166, 2003.

Sriwongsitanon, N., Surakit, K., and Thianpopirug, S.: Influence of atmospheric correction and number of sampling points on the accuracy of water clarity assessment using remote sensing application, Journal of Hydrology, 401, 203–220, 2011.

Stahl, K., Moore, R. D., Shea, J. M., Hutchinson, D., and Cannon, A. J.: Coupled modelling of glacier and streamflow response to future climate scenarios, Water Resources Research, 44, W02 422, 2008.

Sun, B., He, M., Zhang, P., Jiao, K., Wen, J., and Li, Y.: Determination of ice thickness, subice topography and ice volume at Glacier No.1 in the Tien Shan, China, by ground penetrating radar, Chinese Journal of Polar Research, 15, 35–44, 2003.

Taesombat, W. and Sriwongsitanon, N.: Areal rainfall estimation using spatial interpolation techniques, ScienceAsia, 35, 268–275, 2009.

Tague, C. and Grant, G. E.: A geological framework for interpreting the low-flow regimes of Cascade streams, Willamette River Basin, Oregon, Water Resources Research, 40, W04 303, 2004.

Tang, Q., Gao, H., Lu, H., and Lettenmaier, D. P.: Remote sensing: hydrology, Progress in Physical Geography, 33, 490–509, 2009.

Thompson, S. E., Harman, C. J., Konings, A. G., Sivapalan, M., Neal, A., and Troch, P. A.: Comparative hydrology across AmeriFlux sites: The variable roles of climate, vegetation, and groundwater, Water Resources Research, 47, W00J07, 2011.

Tian, F., Qiu, G., Yang, Y., Lü, Y., and Xiong, Y.: Estimation of evapotranspiration and its partition based on an extended three-temperature model and MODIS products, Journal of Hydrology, 498, 210–220, 2013.

Trenberth, K. E., Fasullo, J. T., and Kiehl, J.: Earth's Global Energy Budget, Bulletin of the American Meteorological Society, 90, 311–323, 2009.

Troch, P. A., Martinez, G. F., Pauwels, V. R. N., Durcik, M., Sivapalan, M., Harman, C., Brooks, P. D., Gupta, H., and Huxman, T.: Climate and vegetation water use efficiency at catchment scales, Hydrological Processes, 23, 2409–2414, 2009.

Troch, P. A., Berne, A., Bogaart, P., Harman, C., Hilberts, A. G. J., Lyon, S. W., Paniconi, C., Pauwels, V. R. N., Rupp, D. E., Selker, J. S., Teuling, A. J., Uijlenhoet, R., and Verhoest, N. E. C.: The importance of hydraulic groundwater theory in catchment hydrology: The legacy of Wilfried Brutsaert and Jean-Yves Parlange, Water Resources Research, 49, 5099–5116, 2013.

Tromp-van Meerveld, H. J. and McDonnell, J. J.: Threshold relations in subsurface stormflow: 2. The fill and spill hypothesis, Water Resources Research, 42, W02 411, 2006.

Uhlenbrook, S.: Catchment hydrology—a science in which all processes are preferential, Hydrological Processes, 20, 3581–3585, 2006.

Uhlenbrook, S. and Leibundgut, C.: Process-oriented catchment modelling and multiple-response validation, Hydrological Processes, 16, 423–440, 2002.

Uhlenbrook, S., Roser, S., and Tilch, N.: Hydrological process representation at the meso-scale: the potential of a distributed, conceptual catchment model, Journal of Hydrology, 291, 278–296, 2004.

Uhlenbrook, S., Mohamed, Y., and Gragne, A. S.: Analyzing catchment behavior through catchment modeling in the Gilgel Abay, Upper Blue Nile River Basin, Ethiopia, Hydrol. Earth Syst. Sci., 14, 2153–2165, hESS, 2010.

van Breemen, N.: Soils as biotic constructs favouring net primary productivity, Geoderma, 57, 183–211, 1993.

Vrugt, J. A., Gupta, H. V., Bastidas, L. A., Bouten, W., and Sorooshian, S.: Effective and efficient algorithm for multiobjective optimization of hydrologic models, Water Resources Research, 39, 1214, 2003.

Wagener, T., Sivapalan, M., Troch, P., and Woods, R.: Catchment Classification and Hydrologic Similarity, Geography Compass, 1, 901–931, 2007.

Wang, J., Li, H. Y., and Hao, X. H.: Responses of snowmelt runoff to climatic change in an inland river basin, Northwestern China, over the past 50a, Hydrol. Earth Syst. Sci. Discuss., 7, 493–528, 2010.

Wang, K., Wang, P., Li, Z., Cribb, M., and Sparrow, M.: A simple method to estimate actual evapotranspiration from a combination of net radiation, vegetation index, and temperature, Journal of Geophysical Research: Atmospheres, 112, D15 107, 2007.

Wang, N.: Isotope hydrology in Heihe, Chinese Science Bulletin, 54, 2148–2152, 2009.

Wang, P. and Pozdniakov, S. P.: A statistical approach to estimating evapotranspiration from diurnal groundwater level fluctuations, Water Resources Research, 50, 2276–2292, 2014.

Wang, Y., Yu, P., Feger, K., Wei, X., Sun, G., Bonell, M., Xiong, W., Zhang, S., and Xu, L.: Annual runoff and evapotranspiration of forestlands and non-forestlands in selected basins of the Loess Plateau of China, Ecohydrology, 4, 277–287, 2011.

Westerberg, I. K., Guerrero, J. L., Younger, P. M., Beven, K. J., Seibert, J., Halldin, S., Freer, J. E., and Xu, C. Y.: Calibration of hydrological models using flow-duration curves, Hydrol. Earth Syst. Sci., 15, 2205–2227, 2011.

Western, A. W., Grayson, R. B., Blöschl, G., Willgoose, G. R., and McMahon, T. A.: Observed spatial organization of soil moisture and its relation to terrain indices, Water Resour. Res., 35, 797–810, 1999.

Wiken, E., Jimenez Nava, F., and Griffith, G.: North American Terrestrial Ecoregions-Level III, 2011.

Williams, C. A., Reichstein, M., Buchmann, N., Baldocchi, D., Beer, C., Schwalm, C., Wohlfahrt, G., Hasler, N., Bernhofer, C., Foken, T., Papale, D., Schymanski, S., and

Schaefer, K.: Climate and vegetation controls on the surface water balance: Synthesis of evapotranspiration measured across a global network of flux towers, Water Resources Research, 48, W06 523, 2012.

Winsemius, H. C., Schaefli, B., Montanari, A., and Savenije, H. H. G.: On the calibration of hydrological models in ungauged basins: A framework for integrating hard and soft hydrological information, Water Resources Research, 45, W12 422, 2009.

Winter, T. C.: The concept of hydrologic landscapes, JAWRA Journal of the American Water Resources Association, 37, 335–349, 2001.

Xia, J., Wang, G. S., Lv, A. F., and Tan, G.: A research on distributed time variant gain modeling, Acta Geographica Sinica, 58, 789–796, 2003.

Xie, Z. and Ge, G.: Study of accumulation, ablation and mass balance of glacier no. 1 at the headwater of Urumqi River, Tianshan, pp. 14–24, Science Press, Beijing, 1965.

Yang, D., Jiang, T., Zhang, Y., and Kang, E.: Analysis and correction of errors in precipitation measurement at the head of Urumqi River, Tianshan, Journal of Glaciology and Geocryology, 10, 384–400, 1988.

Yang, D., Zhang, Y., and Zhang, Z.: A study on the snow density in the head area of Urumqi River Basin, Acta Geographica Sinica, 47, 260–266, 1992.

Yang, D., Goodison, B., Metcalfe, J., Louie, P., Elomaa, E., Hanson, C., Golubev, V., Gunther, T., Milkovic, J., and Lapin, M.: Compatibility evaluation of national precipitation gage measurements, J. Geophys. Res., 106, 1481–1491, 2001.

Yang, D., Shao, W., Yeh, P. J. F., Yang, H., Kanae, S., and Oki, T.: Impact of vegetation coverage on regional water balance in the nonhumid regions of China, Water Resources Research, 45, W00A14, 2009.

Yang, M., Ye, B., Peng, P., Han, T., Gao, H., Cui, Y., Wang, J., and Gao, M.: HBV model glacier runoff degree-day factor glacier area change glacier volume change, Journal of Glaciology and Geocryology, 34, 130–38, 2012.

Yao, T., Pu, J., Lu, A., Wang, Y., and Yu, W.: Recent Glacial Retreat and Its Impact on Hydrological Processes on the Tibetan Plateau, China, and Surrounding Regions, Arctic, Antarctic, and Alpine Research, 39, 642–650, 2007.

Yao, T., Thompson, L., Yang, W., Yu, W., Gao, Y., Guo, X., Yang, X., Duan, K., Zhao, H., Xu, B., Pu, J., Lu, A., Xiang, Y., Kattel, D. B., and Joswiak, D.: Different glacier status with atmospheric circulations in Tibetan Plateau and surroundings, Nature Clim. Change, 2, 663–667, 10.1038/nclimate1580, 2012.

Ye, B., Yang, D., Jiao, K., Han, T., Jin, Z., Yang, H., and Li, Z.: The Urumqi River source Glacier No. 1, Tianshan, China: Changes over the past 45 years, Geophysical Research Letters, 32, L21 504, 2005.

Yu, P., Krysanova, V., Wang, Y., Xiong, W., Mo, F., Shi, Z., Liu, H., Vetter, T., and Huang, S.: Quantitative estimate of water yield reduction caused by forestation in a water-limited area in northwest China, Geophysical Research Letters, 36, L02 406, 2009.

Zang, C. F., Liu, J., van der Velde, M., and Kraxner, F.: Assessment of spatial and temporal patterns of green and blue water flows under natural conditions in inland river basins in Northwest China, Hydrol. Earth Syst. Sci., 16, 2859–2870, 2012.

Zehe, E., Ehret, U., Pfister, L., Blume, T., Schröder, B., Westhoff, M., Jackisch, C., Schymanski, S. J., Weiler, M., Schulz, K., Allroggen, N., Tronicke, J., van Schaik, L., Dietrich, P., Scherer, U., Eccard, J., Wulfmeyer, V., and Kleidon, A.: HESS Opinions: From response units to functional units: a thermodynamic reinterpretation of the HRU concept to link spatial organization and functioning of intermediate scale catchments, Hydrol. Earth Syst. Sci., 18, 4635–4655, hESS, 2014.

Zhang, G. P. and Savenije, H. H. G.: Rainfall-runoff modelling in a catchment with a complex groundwater flow system: application of the Representative Elementary Watershed (REW) approach, Hydrol. Earth Syst. Sci., 9, 243–261, hESS, 2005.

Zhang, J.: Mass balance studies on Glacier No. 1 in Urumqi River, Tianshan, Jounal of Glaciology and Geocryology, pp. 32–40, 1981.

Zhang, L., Dawes, W. R., and Walker, G. R.: Response of mean annual evapotranspiration to vegetation changes at catchment scale, Water Resources Research, 37, 701–708, 2001.

Zhang, Y., Liu, S., and Ding, Y.: Observed degree-day factors and their spatial variation on glaciers in western China, Annals of Glaciology, 43, 301–306, 2006.

Zhao, N., Zeng, X., and Han, S.: Solar radiation estimation using sunshine hour and air pollution index in China, Energy Conversion and Management, 76, 846–851, 2013.

Zhao, R.-J.: The Xinanjiang model, IAHS report, 135, 371–381, 1980.

Zhao, R.-J.: Watershed Hydrological Modeling——Xinanjiang model and Shanbei model,1984.(in Chinese), Waterpower Press, Beijing, 1984.

Zhao, R.-J.: The Xinanjiang model applied in China, Journal of Hydrology, 135, 371–381, 1992.

Zhao, R. J. and Liu, X. R.: The Xinangjiang model, pp. 215–232, 1995.

Zhao, W. and Cheng, G.: Review of several problems on the study of eco-hydrological processes in arid zones, Chinese Science Bulletin, 47, 353–360, 2002.

Zhou, J., Li, X., Wang, G., Hu, H. C., and Chao, Z. H.: An improved precipitation-runoff model based on MMS and its application in the upstream basin of the Heihe River, Jounal of Natural Resources, 23, 724–736, 2008.

SUMMARY

In this thesis, a novel landscape-based hydrological model is presented that was developed and tested in numerous catchments around the world with various landscapes and climate conditions. A landscape is considered to consist of a topography and an ecosystem living on it.

Firstly, the influence of climate on hydrological process was studied. It was assumed that an ecosystem organizes its root zone storage capacity to overcome droughts with a certain return period to survive, but not larger than needed, so as to save energy and nutrients. It was found that ecosystems organize their root zone storage capacity to overcome droughts with a return period of about 20 years. This indicates that the root zone storage capacity is the optimal result of an ecosystem adjusting to the climate. The size of the root zone storage capacity in turn has great influence on virtually all hydrological processes.

Subsequently, in order to understand the influence of topography on hydrological behavior, we selected a cold-arid catchment in the upper Heihe River in China as the study site. The influence of topography was explicitly considered in the FLEX-Topo model. Firstly, topography data was applied to make a landscape classification. It is interesting to note that also the land cover map can be derived from topography information, indicating the great influence of topography on natural land cover. And then, within the framework of FLEX-Topo modelling approach, we applied a semi-distributed model structure to describe the different runoff generation mechanisms in different landscapes. We found that FLEX-Topo, allowing for catchment heterogeneity, performs much better than lumped models while transferring both model and optimized parameter sets to two nested catchments.

To test the influence of vegetation and topography information on model transferability separately, a stepwise modelling approach was applied in 6 catchments in Thailand. Each model was calibrated on one catchment and then transferred with its optimized parameter sets to the other catchments. During calibration, all models exhibited similar skill to fit the hydrographs in all catchments. However, when transferred, the performance of the lumped model reduced dramatically, because it did not explicitly consider vegetation and topography. It was shown that individually, vegetation and topography helped to improve model transferability, especially in catchments with heterogeneous landscape composition. The likely reason is the co-evolution of topography, vegetation, soil and hydrology.

Finally, a glacier subroutine was added to the FLEX-Topo modelling framework to improve its applicability in glacierized catchments, where glacier melt water is an essential water resource for downstream. The simulated results were not only validated by hydrographs as in other studies, but also by the long-term glacier mass balance and snow water equivalent data. Furthermore, after considering the different proportion of different landscapes, the glacier model could be successfully upscaled and transferred to

a larger catchment. This further validates our proposed modelling concept, the process equations and parameterization.

SAMENVATTING

In dit proefschrift wordt een nieuw landschap-gebaseerd hydrologisch model gepresenteerd dat werd ontwikkeld en getest in een groot aantal stroomgebieden bestaande uit verschillende landschappen en een wijde klimaatvariatie. Een landschap wordt beschouwd te bestaan uit een topografie en een daarop levend ecosysteem.

Allereerst wordt de invloed van het klimaat op hydrologische proces onderzocht. Er is aangenomen dat een ecosysteem de opslagcapaciteit van zijn wortelzone dusdanig organiseert zodat het een droogteperiode kan overwinnen tegen een bepaalde investering, maar deze investering mag niet groter zijn dan nodig, om energie en voedingsstoffen besparen. Het blijkt dat ecosystemen het zo organiseren dat de opslagcapaciteit van de wortelzone groot genoeg is om een droogte te overwinnen met een herhalingstijd van ongeveer 20 jaar. Dit geeft aan dat de wortelzone opslagcapaciteit het optimale resultaat is van een ecosysteem dat zich aanpast aan het klimaat. De grootte van de wortelzone opslagcapaciteit heeft op zijn beurt een grote invloed op vrijwel alle hydrologische processen.

Vervolgens, teneinde de invloed van de topografie op het hydrologische gedrag te onderzoeken is het stroomgebied van de semi-aride Heihe River geselecteerd als onderzoekslocatie. De invloed van topografie is expliciet meegenomen in het FLEX-Topomodel. Eerst werden topografische gegevens gebruikt om een landschapsindeling te maken. Het is interessant op te merken dat ook de landbedekkingskaart kan worden afgeleid uit topografische informatie, wat duidt op de grote invloed van de topografie op de natuurlijke bodembedekking. Vervolgens, gebruikmakend van de FLEX-Topo modelleringsbenadering, is een semi-gedistribueerd modelstructuur toegepast om de verschillende afvoer-genererende mechanismen te beschrijven in de verschillende landschappen. We vonden dat FLEX-Topo, dat rekening houdt met stroomgebied heterogeniteit, veel beter presteert dan gelumpte modellen bij overdracht van zowel modelstructuur als de geoptimaliseerd parametersets naar twee geneste stroomgebieden.

Om de invloed van vegetatie en topografie te testen op de overdraagbaarheid van modellen, zijn 6 stroomgebieden in Thailand afzonderlijk getest, waarbij een stapsgewijze validatie op alle stroomgebieden is toegepast. Elk model is gekalibreerd op een stroomgebied en vervolgens overgebracht met zijn geoptimaliseerd parametersets naar de andere stroomgebieden. Tijdens de kalibratie, lieten alle modellen vergelijkbaar vaardigheid zien om de hydrografen na te bootsen in alle stroomgebieden. Echter, wanneer ze worden overgedragen, wordt de prestatie van gelumpte modellen drastisch verminderd, omdat deze niet expliciet vegetatie en topografie in acht nemen. Er werd aangetoond dat individueel, zowel vegetatie als topografie helpen om model overdraagbaarheid te verbeteren, vooral in stroomgebieden met een heterogene landschapsamenstelling. De reden hiervoor is waarschijnlijk de co-evolutie van topografie, vegetatie, bodem en hydrologie.

Tot slot werd een gletsjer subroutine toegevoegd aan het FLEX-Topo modelkader, om

de toepasbaarheid te testen in gletsjergedomineerde stroomgebieden, waar het smeltwater een essentiële waterbron is. De gesimuleerde resultaten werden niet alleen gevalideerd op het nabootsen van de hydrografen, zoals in vele andere studies, maar ook op tijdseries van de gletsjer massabalans en het watergehalte van de sneeuw. Gebruik makend van de verschillende landschapselementen, kon het gletsjermodel met succes worden opgeschaald en overgebracht naar een groter stroomgebied. Hiermee konden het modelconcept, de procesbeschrijvingen en de parametrisatie verder worden gevalideerd.

CURRICULUM VITÆ

Hongkai Gao was born in Henan Province in China on November 27th, 1984. He studied Geography at the Henan University in Kaifeng in China, and graduated in 2008 with distinction. After that he moved to Lanzhou to pursue a master degree in the Graduation University of Chinese Academy of Sciences (CAS). His research topic at CAS was on glacier and snow hydrology. He was involved in many field surveys on the Tibetan Plateau and several inland river basins in northwest China. He started to publish papers while doing research during his master studies. In 2011, after his graduation he was accepted as a PhD student at Delft University of Technology, supervised by Prof. Savenije and Dr. Hrachowitz, and financially supported by a scholarship from Chinese Scholarship Council (CSC). During his PhD, he majored in landscape-based modelling (FLEX-Topo). Based on this modelling framework, he developed tailor-made rainfall-runoff models for the upper Heihe River basin in China, and the upper Ping River basin in Thailand. Moreover, he found that the root zone storage capacity (Su,max), which is an essential parameter in conceptual hydrological models, is highly related to climate. We can estimate this parameter from observed data without calibration. Based on this research, he published several papers in peer-reviewed journals. Besides that, he developed an interface for the SUPERFLEX hydrological modelling framework programming in C#, to make it user-friendly. He also served as reviewer for a number of scientific journals, such as Hydrology and Earth System Sciences, Journal of Hydrology, Hydrological Processes, Journal of Hydrometeorology, Journal of Glaciology, and Journal of Water and Climate.

List of Publications

Journal articles

Gao, H., Hrachowitz, M., Sriwongsitanon, N., Fenicia, F., Gharari, S., and Savenije, H. H. G.: Towards understanding the influence of vegetation and topography on model transferability, Water Resources Research (under review, 2015).

Liu, Y., Lu, M., Huo, X., Hao, Y., Gao, H., Liu, Y., Fan, Y., Metivier, F.: A Bayesian analysis of Generalized Pareto Distribution of runoff minima, Hydrological Processes (minor revision, 2015)

Wang, Y., Duan, W., Zhang, Z., Gao, H., Lu, Y., Zhao, C.: Spatio-temporal variations of climate extremes during 1961-2008 in North western China associated with elevation and landscapes, Journal of Mountain Science, (under review, 2015)

Gao, H., Hrachowitz, M., Schymanski, S. J., Fenicia, F., Sriwongsitanon, N., and Savenije, H. H. G.: Climate controls how ecosystems size the root zone storage capacity at catchment scale, Geophysical Research Letters, 10.1002/2014GL061668, 2014.

Gao, H., Hrachowitz, M., Fenicia, F., Gharari, S., and Savenije, H. H. G.: Testing the realism of a topography-driven model (flex-topo) in the nested catchments of the upper heihe, china, Hydrology and Earth System Sciences, 18, 1895-1915, 10.5194/hess-18-1895-2014, 2014.

Gao, H., He, X., Ye, B., and Pu, J.: Modeling the runoff and glacier mass balance in a small watershed on the central tibetan plateau, china, from 1955 to 2008, Hydrological Processes, 26, 1593-1603, 10.1002/hyp.8256, 2012.

Gharari, S., M. Hrachowitz, F. Fenicia, H. Gao, and H. H. G. Savenije (2014), Using expert knowledge to increase realism in environmental system models can dramatically reduce the need for calibration, Hydrology and Earth System Sciences, 18(12), 4839-4859.

Conference abstract

Gao, H., Hrachowitz, M., Fenicia, F., Gharari, S., Sriwongsitanon, N., and Savenije, H.: Spatial transferability of landscape-based hydrological models, Geophysical Research Abstracts, 17, 5815, 2015.

Gao, H., Hrachowitz, M., Savenije, H.: Integrated glacier and snow hydrological modelling in the Urumqi No.1 Glacier catchment, Geophysical Research Abstracts, 17, 5861, 2015.

Gao, H., Hrachowitz, M., Schymanski, S., Fenicia, F., Sriwongsitanon, N., and Savenije, H.: Climate controls how ecosystems size the root zone storage capacity at catchment scale, Geophysical Research Abstracts, 17, 5941, 2015.

Wang-Erlandsson, L., Gao, H., Bastiaanssen, W., Jägermeyr, J., Keys, P., Gordon, L., and Savenije, H.: Deriving root zone storage capacity from Earth observation, Geophysical Research Abstracts, 17, 4129, 2015.

Gharari, S., Hrachowitz, M., Fenicia, F., Gao, H., Gupta, H.V., and Savenije, H.H.G.: Progressive evaluation of incorporating information into a model building process: from scratch to FLEX-TOPO, AGU Chapman Conference, Luxembourg, 2014

Gao, H., Fenicia, F., Sriwongsitanon, N., Saengsawang, S., Hrachowitz, M., Gharari, S., and Savenije, H.: Independent determination of the maximum root zone storage (sumax) in conceptual models, Geophysical Research Abstracts, 16, 5305, 2014.

Su, Y., Gao, H., Langhammer, J., and Savenije, H. H. G.: Hydrological response to forest disturbance under a changing climate in experimental headwater basins, central sumava mountains, Geophysical Research Abstracts, 16, 3839, 2014.

Gharari, S., Hrachowitz, M., Fenicia, F., Gao, H., Gupta, H. V., and Savenije, H.: Progressive evaluation of incorporating information into a model building process: From scratch to flex-topo, AGU, San Francisico, 2014

Gao, H., Savenije, H., Hrachowitz, M., Fenicia, F., and Gharari, S.: Realism test of a topography driven conceptual model (flex-topo) in nested catchments of the heihe river basins, china, AGU Fall Meeting Abstracts, 1313, 2013

Gao, H., Savenije, H. H., Hrachowitz, M., Fenicia, F., and Gharari, S.: A topography-driven hydrological model in the heihe river, china, EGU General Assembly Conference Abstracts, 5004, 2013

Gharari, S., Hrachowitz, M., Fenicia, F., Gao, H., Euser, T., and Savenije, H.: Flex-topo: Proof of concept in a central european landscape, Geophysical Research Abstracts, 15, EGU2013-4782, 2013.

Gao, H., Fenicia, F., Kavetski, D., and Savenije, H.: A visual interface for the superflex hydrological modelling framework, EGU General Assembly Conference Abstracts, 4853, 2012

ACKNOWLEDGEMENT

My first and biggest thanks go to my promoter Prof. Dr. Ir. Hubert Savenije for giving me the opportunity to study and work in his prestigious hydrology group . He is always enthusiastic on hydrological sciences. His passion has given me endless inspiration. He always responds very fast to all my concerns and draft manuscripts, which enables me to finalize my thesis on time. This four years' study is a great training for me not only on hydrology but also on thinking clearly and logically. For Prof. Savenije, knowledge is never only for bookshelves, but for practical usage. I was very impressed, during our visit to Lanzhou in China, with his quite precise estimation of the Yellow River discharge after merely walking a quarter of a bridge.

I would like to thank my co-promoter Dr. Markus Hrachowitz. His systematic knowledge on hydrological modelling always improved our manuscripts. And I appreciate very much his great patience on my crappy English and sometimes illogical thinking.

To Fabrizio, your comprehensive and profound insight in hydrology always enlightens me when I am confused. And your sense of humor is great.

To Shervan, your knowledge on parameter calibration has saved me lots of time. And you are really a genius on imitating people's talk.

To Dr. Sriwongsitanon, you are so nice and patient. And your knowledge on remote sensing is always helpful to make our results more convincing.

I would like to also thank my previous supervisor during my master studies, Prof. Baisheng Ye. His constructive suggestions on hydrology and wisdom on life is still guiding me. As a Buddhist, he suffered so much without any complaints while he was alive. I think he must be living happier in heaven.

I also thank Luz Ton-Estrada, Betty Rothfusz and Hanneke de Jong for taking care of all administrative issue and even our daily life, like making an appointment for a doctor and house renting issues.

Many thanks to my other colleagues, Zheng Duan, Huayang Cai, Wim Bastiaanssen, Miriam Coenders-Gerrits, Saket Pande, Ruud van de Ent, Jacqueline I. A. Gisen, Lan Wang, Lingna Wei, Tanja Euser, Remko Nijzink, Sandra Junier, Koen Hilgersom. All your kindly and valuable help makes this dissertation happen. Ali and Hojjat, your everyday greetings make our office warm even in early dark raining morning.

Many thanks to my Chinese friends Xin Gao, Wei Shao, Xin Tian, Jianzhi Dong, Lixia Niu, Zhenpei Wang, Xi Zhang, Yunlong Li, Junchao Shi, Jiangjun Ran, Zongji Yang, Jinglang Feng, Duowa Zhutian, Congli Dong, Le Li, Hualong Luan, Wei Meng, Yingrong Wen, Yang Lv, Yongwei Liu... Your companionship makes every lunch an enjoyable feast.

I am grateful for the Chinese Scholarship Council (CSC). Without its financial support, it was impossible for me to do a PhD in the Netherlands.

This four years oversea study will influence my whole life. It does not only benefit my academic career, but also opened my eyes. Warm-hearted Dutch people made me feel like at home. The different culture and way of thinking used to shock me at first, but

gave me different perspectives for looking at accustomed things from new angles. I love our hydrological modelling group. And I love this beautiful country and the nice people living here.

In the end, I thank Lei Fu for designing the beautiful cover. Thousands thanks go to my parents and grandparents for their unconditional supports! All I ever wanted is to make you proud.

Hongkai Gao
Delft, March 2015